Interfacial bonding between thermoset and thermoplastic polyurethane reinforced textile grade carbon fiber: Structure property relationships

A Dissertation Presented for the

Doctor of Philosophy

Degree

The University of Tennessee, Knoxville

Surbhi S. Kore

December 2021

DEDICATION

I dedicated this work to my parents Shobha and Subhash Kore, uncle Vaijanath Kore, brother Sumeet Kore and sister-in-law Prachi Taklikar for their love, support, encouragement, and guidance throughout the journey. Special thanks to my mother, who always believed in me and supported me.

ACKNOWLEDGEMENT

First and foremost, I would like to express my deepest gratitude to my Ph.D. advisor Dr. Uday Vaidya for the immense support and guidance he has provided me throughout my graduate studies. Dr. Vaidya's extensive knowledge of advanced composites helped me to grow as a researcher in the composites field. I am grateful for his guidance. I would like to thank my committee members, Dr. Chad Duty, Dr. Soydan Ozcan, and Dr. Claudia Rawn, for their valuable advice. Special thanks to Dr. Merlin Theodore from Carbon Fiber Technology Facility (CFTF) at ORNL

Next, I would like to thank Amir Eftekharian, Harsh Baid, and Frank Abdi from Alphastar for sharing their insightful knowledge of computational modeling of composites. The collaboration was highly acknowledged.

I wish to acknowledge all the former and current staff, graduate and undergraduate students of Fiber and Composite Manufacturing Facility (FCMF), UTK research group: Stephen Sheriff, Vanina Ghossein, Hicham Ghossein, Pritesh Yeole, Joe Gausphol, Vidya Hiremath, Ryan Spencer, Alex Stiles, Kaustubh Mungale, Sanjita Wasti, Saurabh Pethe, Vinit Chaudhary and Benjamin Schwartz, Cody Ferree, Molly Mays, Abhi Mistry, and Tyler Sundstrom for their support.

I would like to thank Vinita, Abha, Shalaka, Supriya, Shrish, Mayuri, Shradha and Shruti and all my friends and family for motivating me and being a part of this dream of pursuing a Ph.D.

This work would not be possible without the funding support from the Office of Energy Efficiency and Renewable Energy (EERE), US Department of Energy [grant numbers DE-EE0006926], the Institute of Advanced Composites

Manufacturing Innovation (IACMI), and the Carbon Fiber Technology Facility (CFTF), Oak Ridge National Laboratory (ORNL), TN, USA. I gratefully acknowledge the support by Grant # P42 ES027723-01A1 from the National Institute of Environmental Health Sciences (NIEHS), USA.

ABSTRACT

The research work focused on examining the interfacial adhesion of unsized, epoxy, and urethane-sized textile grade carbon fiber (TCF) reinforced in different classes of polyurethane (PU) thermoplastic (TPU) and thermoset (TSU) polyurethane (PU) through the structure-property relationship. The Carbon Fiber Technology Facility (CFTF) at Oak Ridge National Laboratory (ORNL) has produced TCF to reduce the cost of commercial-grade carbon fiber. The first part of the research examined the fundamental relationships between (a) soft segment thermoplastic polyurethane (S-TPU), (b) hard segment thermoplastic polyurethane (H-TPU), (c) thermoset polyurethane (TSU) and TCF reinforcement's molecular behavior at the interface using the surface and thermal analysis (e.g., atomic force microscopy (AFM), Fourier transform infrared spectroscopy (FTIR), differential scanning calorimetry (DSC), and dynamic mechanical analysis (DMA)). The results showed that S-TPU, H-TPU and TSU could produce strong interaction with urethane sizing TCF through nucleophilic addition reaction.

In the second part of the research, the surface and thermal results obtained from material characterization were used to validate the interfacial adhesion of TCF-TPU and TCF-TSU composites, respectively. The mechanical properties showed that segmented TPU is compatible with epoxy-sized TCF, whereas urethane-sized TCF is compatible with the TSU system. Furthermore, the joining of dissimilar materials is a significant step to produce cost-effective automotive and aircraft components. Hence, the fusion bonding study was conducted using epoxy-sized TCF-TPU and urethane-sized TCF-TSU composites. The lap shear

strength of fusion boded TCF-TSU and TCF-TPU showed 21% improvement compared to PA66/GF and epoxy/CF bonded composites.

The third part of the research studied the effect of sizing thickness on composites' mechanical properties using the Dehomogenized approach. The results showed that increasing sizing thickness from 0.01 to 0.5 enhances the tensile strength by 1200% of TCF-TSU composites. The TCF and TSU properties obtained through reverse engineering mechanism further validated for the cross-ply laminate. The simulations results showed less than 10% variation in the tensile properties than experimental findings. The overall outcome of this work can advance state of the art in TCF polyurethane composites for a range of applications such as aerospace, automotive, sports, and industrial products.

Keywords: Interfacial adhesion of unsized, epoxy and urethane sized TCF, Polyurethane system: soft and hard segment TPU and TSU, surface, thermal and mechanical characterization, FEA model on sizing thickness

Table of Contents

List of Tables

List of Figures

Chapter 1.

INTRODUCTION

1.1 MOTIVATION

Polymer matrix composites (PMC) are a combination of fiber and a matrix, where fibers are reinforced in a polymer and enhance the mechanical, thermal, and environmental properties [1]. PMCs comprises thermoset or thermoplastic polymer (resin), depending on the final applications. Various factors influence properties of PMCs, such as resin chemistry, fiber type, fiber sizing, fiber-matrix interface, and interface thickness. The inter-fiber spacing (interface thickness) typically ranges from 0.1 to 10 μm [micrometer] occupied by the resin, coating on the fiber surface, and the fiber diameter, which is approximately ten μm [micrometer] [2]. Microstructure at the interface can be tailored using various surface treatment techniques. The interface between polymer molecules and reinforcing fibers influences the macro mechanical properties in PMC by increasing the load transfer efficiency between fiber and matrix.

In a thermoset-thermoplastic hybrid composite, bonding of the thermoplastic (TP) with the thermoset (TS) polymer is critical. TP/TS bonded composite materials are widely used in aerospace, transportation, automotive and marine applications [3]. Various laminate bonding approaches in polymer composites include mechanical fastening, adhesive bonding, solvent bonding, and fusion bonding. Among these techniques, fusion-bonding is a promising method. In this approach, the molten thermoplastic composite is adhere to the thermoset composite surface at the required pressure to produce a fusion bonded consolidated panel [4]. Another important aspect in the adhesion theory is an interface thickness between fiber and matrix. The interface thickness is mainly influenced by the polymer coating

concentration (sizing) on fiber surface. Thus, understanding the threshold of sizing concentration on the mechanical properties of the composite through simulation becomes challenging. Hence, the motivation of this work is to first study the interfacial interaction between textile grade carbon fiber (TCF) with thermoplastic polyurethane (TPU) and thermoset polyurethane (TSU) matrix through surface, thermal and mechanical characterization. The second part of the study is to understand the bonding between thermoset-thermoplastic PU composites through fusion bonding technique. Third part is to design a computational model using experimental results of TCF-PU composites to investigate the interface thickness effect on the mechanical properties of TCF-PU composites.

1.2 BACKGROUND

PU has a broad classification of polymers and is produced by chemical reaction of diisocyanate and diol. PU has been used extensively in various applications such as paints, liquid coatings, elastomers, insulators, elastic fibers, foams, integral skins, adhesives, and foams [5]. PU has superior long-term performance with low energy requirements for curing. It shows excellent abrasion resistance, flexibility, chemical resistance, hardness range, gloss and color retention [6]. PU has a broad chemical structure leading to its thermoplastic, thermoset, and biobased forms [7]. The diversity in physical and chemical properties increases its usage in biomedical, civil, automotive, textiles applications.

The chemical structure of PU contains urethane linkage with aliphatic and aromatic hydrocarbons, ester, ether, and urea groups, which contributed to its adhesion efficiency. The change in a stoichiometric ratio of hydroxyl (-OH) and isocyanate (-NCO) PU broadens its classification into thermoplastic, thermoset, waterborne

etc. [5], In this work, aromatic ether-based PU system is used with soft and hard segments of TPU (with different shore hardness from category A) and thermoset PU (shore hardness from category D) have been selected as shown in Figure 1.1 Generally, PU is formed by the chemical reaction of organic isocyanates with active hydrogens from polyol that react to produce a block polymer structure, as shown in Figure 1.2. The average functionality of isocyanate and alcohol should be greater than two to enhance the crosslinking of PU. The PU properties mainly depend on the types of polyol and isocyanate used. The commercially utilized aromatic isocyanates are toluene diisocyanate (TDI) and diphenylmethane diisocyanate (MDI), which are highly reactive compared to aliphatic isocyanate, i.e., hexamethylene diisocyanate (HDI), isophorone diisocyanate (IPDI). The choice of isocyanate influences the rigidity of the polymer segments, which contributes to the strength of the material, and polyol provides the soft segment nature, which enhances the elasticity/flexibility and toughness in PU. The soft PU produces from a long chain polyol has less crosslinking, making them more flexible, and hard segments through rigid polyol have small chains with a superior amount of crosslinking in the backbone structure. The soft segment PU contains higher molecular weight polyol (>1000 units), and the hard segment contains lower molecular weight polyol (~ 100 units). The urethane reaction (-NHCOO-) is highly polar, where the electrophile from the NCO group (produced by the removal of an electron from O or N) attacks the OH group from polyol to produce a covalent bond at the active hydrogen site [8]. The polarities of hard and soft segments change the microstructure of PU. The hard segment possesses superior mechanical properties such as hardness, Young's modulus, and flexural strength at high-temperature. Soft segment provides benefit in terms of low-temperature properties

which is a function of concentration of polyol in the formulations [9]. The R1 and R2 from Figure 1.2 represent aromatic and aliphatic groups from polyether and polyester segments presented in Figure 1.3. Therefore, the hardness of PU can be altered based on R1 and R2.

PU can be produced either from polyester or polyether. The polyether has a (0 to -75°C) lower glass transition temperature (compared to polyester. The key advantage of polyether-based PU is its inherent resistance to hydrolytic attack and microbial performance high moisture resistance and dynamic properties. These are lower in polyester-based PU.

In this research, aromatic polyether-based TPU with shore hardness 74A as a soft segment and shore hardness 85A as a hard segment with thermoset PU (shore hardness 80 D) have been selected for comparative study. These are illustrated in Figure 1.4. The interfacial interaction of polymer composites depends on the properties of the reinforcement, matrix and the interaction between them, which can be studied in the following section [10].

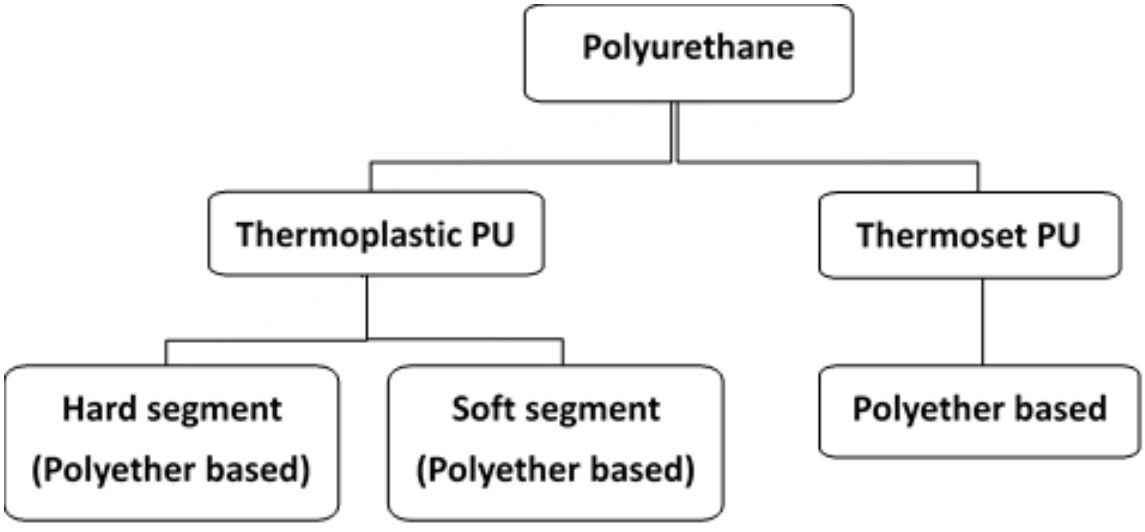

Figure 1.1: Flowchart of classification of polyurethane

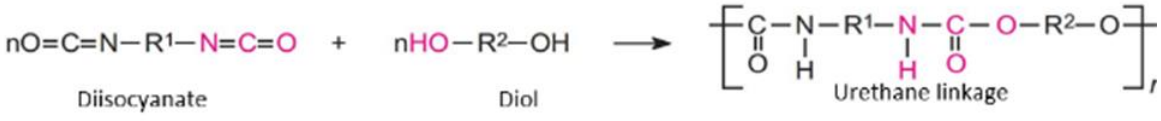

Figure 1.2: Chemical reaction of PU

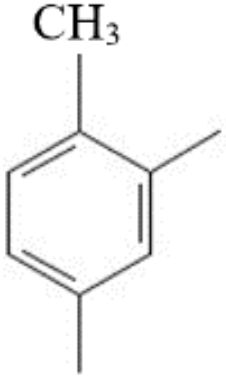

Polyether

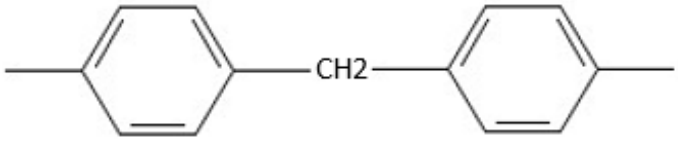

Polyester

Figure 1.3: Chemical structures of polyether and polyester linkage

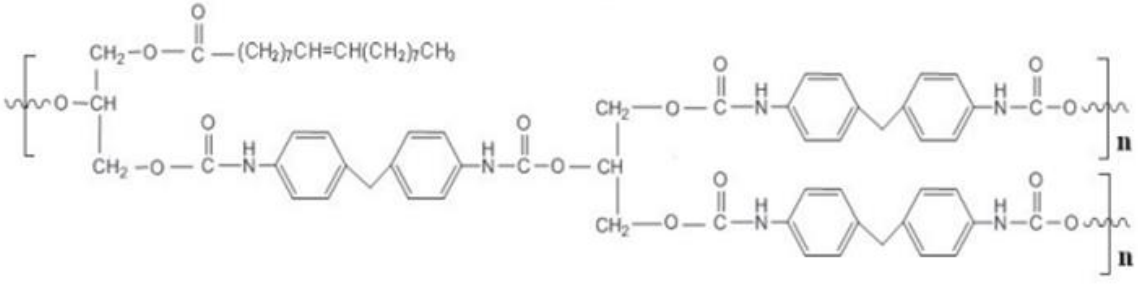

Figure 1.4: Schematic representation of thermoset polyurethane linkage produced from polyester

1.3 Interfacial adhesion chemistry

In general terms, adhesion is defined as an intermolecular interaction between two surfaces with different chemical compositions [11]. The interfacial region, also known as interphase, is formed by the long/short chain of polymer with fiber reinforcement by sharing electrons during interactions (covalent or hydrogen bond). The polymer chain mobility, crystallinity, and degree of cure play a vital role in the interfacial region. The restriction in chain mobility after incorporation of fibers indicates molecular interaction between fiber and matrix whereas the polymer crystallinity enhances the modulus of a polymer by contributing to the interlaminar strength of the composite [12] [13]. The adhesion and cohesion can be achieved by transferring or sharing an electron to form a strong chemical/physical bond at the fiber-matrix interface. The cohesion state contains primary and secondary bonds with a relatively strong polar molecule. However, the energy absorption capacity at the interface is an important parameter to evaluate fiber/ matrix interaction in composites. The interfacial strength influences the mechanical properties of the composite by allowing the load transfer from the matrix to the fiber during the deformation process [14]. The fiber and matrix produce an interlayer that has different physico-chemical properties between them [15]. This physico-chemical interaction involves parameters such as chemical reactions and intermolecular interactions [16]. The chemical interaction achieved from the atomic-scale attraction between matrix and CF active functional group can be explained by the adsorption theory [17].

In the adsorption theory, interatomic and intermolecular forces between two surfaces (TCF and PU) interact in terms of adhesion bonding [18]. These forces

are classified into primary and secondary forces. Primary forces show strong chemical interaction between two surfaces with surface energy in the range of 1000-100 kJ/mol, which is higher than the secondary forces (60-45 kJ/mol). Due to the presence of an active hydrogen group in PU, it forms a primary bond with the substrate [19]. Craton et al. [11] stated that optimal molecular contact between surfaces can restrain maximum energy during bond deformation and cause excellent adhesion. This bond deformation causes chemical or van der Waals bond breakage along with plastic deformation on the interfaces. The fraction of energy required to break the bond is less than the total fraction of energy required to separate two surfaces leads to excellent adhesion [20]. There are few effective methods to improve the adhesion of composites, i.e., mechanical, chemical, and physical bonding.

1.3.1 Physical Bonding between fiber and matrix

The forces created by physical bonding are weaker than secondary or van der Waals forces observe at the interface, presented in Figure 1.5. Physical bonding provides London dispersion, dipole interaction, and hydrogen bonding forces. During composite fabrication, physical bonding produces a closely packed network under applied pressure and temperature, which significantly affects the wettability and shear strength of the fiber-matrix interface. He et al. [21] observed that the highly concentrated multi-wall carbon nanotube (MWNT) bonded to TPU polymer through van der Waals forces, the tensile strength decreased due to agglomeration and insufficient contact between MWNT and TPU, which inadequately transfers the load from fiber to matrix. The bond energy ranges from 8-16 kJ/mol.

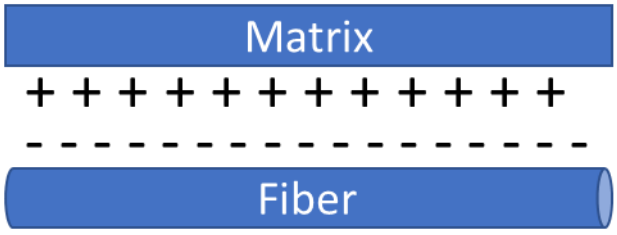

Figure 1.5: Schematics of physical bond formation at the interface of fiber and matrix due to electrostatic forces

1.3.2 Chemical Bonding between fiber-matrix

Chemical bonding involves covalent, ionic, metallic bonds, and the energy produces through primary bonding of a fiber-matrix composite is in the range of 40-400 kJ/mol, presented in Figure 1.6. Most of the polymer composite contains a covalent bond at the interface. Various surface treatment techniques are used to produce chemical networks on the fiber and matrix surfaces to enhance the interface strength of the composites. Krump et al. [22] studied the adhesion strength between plasma-treated polyethylene terephthalate (PET) fibers and the styrene-butadiene rubber (SBR) matrix. The lubricant on the PET surface caused poor adhesion between PET and SBR rubber. Therefore, after removing lubricant from PET surface using acetone, the surface was plasma-treated, and results showed the chemical bond formation (addition of OH group) improved the adhesion strength of composites.

Furthermore, Zhao et al. [23] used the grafting method to improve interfacial bonding between the CF and epoxy matrix. After modification, the grafted polyhedral oligomeric silsesquioxanes (POSS) on the CF surface showed increased surface roughness, wettability, and polar groups. The POSS provides strong chemical bonding between fiber and matrix through reactive groups on the CF surface and the hardener in the matrix. The surface-modified data was further validated through the impact energy characterization, and results showed an 88% increment in the properties by using the grafting polymerization technique. The primary, fundamental, and most simple method for CF surface treatment is sizing. Sizing involves coating a thin layer of specific polymers on the CF surface to improve the fiber-matrix bonding [24,25].

It also improves the cohesive interaction at the interface of CF and PU, which enhances the mechanical properties of composites [26–28]. Guigon et al. [29] used the heat resistant sizing agent, such as thermoplastic polyimide and epoxy sizing on PAN-based CF and observed a 97% improvement in interfacial shear strength (IFSS) compared to unsized fibers. Zhang et al. [30] studied the effect of surface treatment by incorporating methylene diisocyanate (MDI) on the CF surface to improve the interfacial strength between CF and PU matrix. Yue et al. [31] studied the interfacial bonding between surface-modified Kevlar fibers reinforced epoxy matrix. The chemical-treated fibers showed a 60% improvement in the interfacial shear strength due to the mechanical interlocking adhesion mechanism. Karaeva et al. [32] modified the CF surface- by grafting carbon nanotubes (CNT). This modification of the fiber–polymer interface with CNT leads to a drastic increase of IFSS by 144%. However, a decrease in tensile strength was observed compared to unsized CF. Ma et al. [33] have analyzed the strength and toughness of carbon fibers reinforced rigid PU composites with low fiber content. The surface analysis conducted on the carbon fiber through the oxidation treatment showed the appearance of a large amount of hydroxyl group on the CF surface. Hence, both physical and chemical bonding requires good adhesion (wetting) between fiber and matrix to improve the mechanical properties of composites.

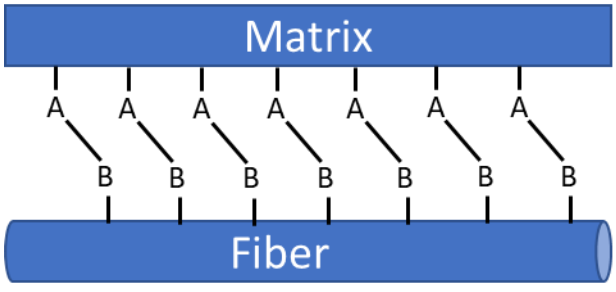

Figure 1.6: Schematic of chemical bond formation at the interface of fiber and matrix due to surface treatment

1.3.3 Mechanical Bonding between fiber matrix interfaces

In mechanical bonding, fiber and polymer surfaces are roughened before interlocking them together, presented in Figure 1.7. The surface roughness produces irregularities on the fiber surface, and the matrix can flow in and around the non-uniformity to form a mechanical bond. Ehrburger et al. suggested that the matrix adherence to the fabrics with difference-shaped yarns is directly proportional to the surface area of fibers. Hence, the increased surface area provides good wettability and eventually enhances the interfacial bond between fiber and matrix [34]. However, the major drawback is trapping the air bubble in the cracks, which acts as stress concentration to build failure at the interface. Lu et al. [35] studied the interfacial adhesion between air plasma treated CF and poly (phthalazinone ether sulfone ketone) (PPESK) composites. The results showed a 13% enhancement in ILSS properties due to surface roughness improvement. Therefore, the properties improved by surface modification and etching process showed mechanical and chemical bonding between fiber and matrix. The author also stated that mechanical bonding has a significant impact on the properties of the composite.

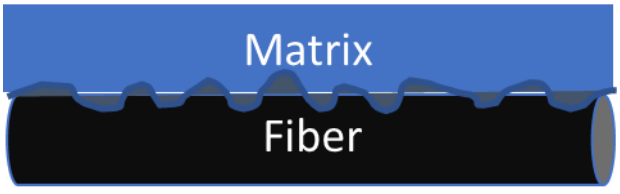

Figure 1.7: Schematics of mechanical bond formation at the interface of fiber and matrix through mechanical interlocking

1.4 RESEARCH OBJETIVES

The research is divided into three objectives

OBJECTIVE 1: INVESTIGATE THE PHYSICO-CHEMICAL INTERACTION OF UNSIZED, EPOXY AND URETHANE SIZED TCF WITH POLYURETHANE SYSTEM

The TCF has an inert surface and cannot produce a chemical interaction with the polymer matrix. Thus, the surface chemistry of soft and hard segmented TPU and unsized, epoxy and urethane sized TCF needs to be evaluated. The surface and thermal characterization techniques include- Fourier transform infrared spectroscopy (FTIR), X-ray photoelectron spectroscopy (XPS), Atomic force microscopy (AFM), Dynamic mechanical analysis (DMA), and Differential scanning calorimetry (DSC). These techniques help to understand the adhesion efficiency and the bonding mechanism through molecular movement, phase separation, hydrogen bonding capability of S-TPU, H-TPU with unsized, epoxy, and urethane sized TCF.

OBJECTIVE 2: INVESTIGATE THE EFFECT OF AHDESION AND COHESION OF UNSIZED, EPOXY AND URETHANE SIZED TCF COMPOSITES REINFORCED IN TPU AND TSU WITH FUSION BOND EFFECIENCY BETWEEN TSU AND TPU COMPOSITES

The hypothesis of this objective is to understand the adhesion and cohesion efficiency between unsized, epoxy and urethane sized TCF and PU system. The proposed theory from objective I that urethane sized TCF is compatible with PU systems will further validated. The surface and thermal characterization performed on TCF reinforced TSU and TPU composites is to understand the effect of

molecular entanglement and the strength of the hydrogen bond at the interface of the composites. The mechanical and microstructural characterization will be conducted on the TCF-TSU and TCF-TPU composites to analyze the fiber-matrix bonding behavior at the interface. The surface energy, flexural, interlaminar, and lap shear strength characterization will be performed on fusion bonded TP/TS and compared to TP and TS composites. The failure modes of the constituents will be analyzed using optical microscopy. The material that provides excellent mechanical properties in thermoplastic and thermoset urethane composites will further explore in Objective 3

OBJECTIVE 3: THE EFFECT OF SIZING THICKNESS OF TEXTILE GRADE CARBON FIBER (TCF) ON THE INTERFACIAL PROPERTIES OF TCF-TSU THROUGH FINITE ELEMENT ANALYSIS

Objective II and III explained the effect of polymer structure, TCF sizing on the interface of TCF-PU composites. In this objective, the sizing thickness effect on the interphase of TCF-PU is evaluated. The mechanical properties of TCF-PU obtained from Objective II are used to design a computational model using the Dehomogenized technique with a reverse engineering mechanism. The effective TCF and PU properties are further used to design a cross-ply laminate, and the simulated properties are compared with experimental results for validation of a model.

REFERENCES

[1] D.K. Rajak, D.D. Pagar, P.L. Menezes, E. Linul, Fiber-reinforced polymer composites: Manufacturing, properties, and applications, Polymers (Basel). 11 (2019) 1667.

[2] F.N. Cogswell, Thermoplastic aromatic polymer composites: a study of the structure, processing and properties of carbon fibre reinforced polyetheretherketone and related materials, Elsevier, 2013.

[3] K.K. Chawla, Carbon fiber composites, in: Compos Mater, Springer, 1998: pp. 252–277.

[4] D.M. Maguire, Joining thermoplastic composites, SAMPE J. 25 (1989) 11–14.

[5] J.O. Akindoyo, M. Beg, S. Ghazali, M.R. Islam, N. Jeyaratnam, A.R. Yuvaraj, Polyurethane types, synthesis and applications--a review, Rsc Adv. 6 (2016) 114453–114482.

[6] Y. Zhang, D.J. Hourston, Rigid interpenetrating polymer network foams prepared from a rosin-based polyurethane and an epoxy resin, J Appl Polym Sci. 69 (1998) 271–281.

[7] M. Heinen, A.E. Gerbase, C.L. Petzhold, Vegetable oil-based rigid polyurethanes and phosphorylated flame-retardants derived from epoxydized soybean oil, Polym Degrad Stab. 108 (2014) 76–86.

[8] M. Szycher, Szycher's handbook of polyurethanes, CRC press, 1999.

[9] D.J. Martin, G.F. Meijs, P.A. Gunatillake, S.J. McCarthy, G.M. Renwick, The effect of average soft segment length on morphology and properties of a series of polyurethane elastomers. II. SAXS-DSC annealing study, J Appl Polym Sci. 64

(1997) 803–817.

[10] N.G. Karsli, C. Ozkan, A. Aytac, V. Deniz, Effects of sizing materials on the properties of carbon fiber-reinforced polyamide 6, 6 composites, Polym Compos. 34 (2013) 1583–1590.

[11] C. Creton, Materials Science of Pressure-Sensitive Adhesives, Mater Sci Technol. (2006).

[12] J. Jordan, K.I. Jacob, R. Tannenbaum, M.A. Sharaf, I. Jasiuk, Experimental trends in polymer nanocomposites﷒a review, Mater Sci Eng A. 393 (2005) 1–11.

[13] H.E. Miltner, G. Van Assche, A. Pozsgay, B. Pukánszky, B. Van Mele, Restricted chain segment mobility in poly (amide) 6/clay nanocomposites evidenced by quasi-isothermal crystallization, Polymer (Guildf). 47 (2006) 826–835.

[14] M.-K. Seo, S.-J. Park, Surface characteristics of carbon fibers modified by direct oxyfluorination, J Colloid Interface Sci. 330 (2009) 237–242.

[15] G.C. Papanicolaou, S.A. Paipetis, P.S. Theocaris, The concept of boundary interphase in composite mechanics, Colloid Polym Sci. 256 (1978) 625–630.

[16] S. Keszei, S. Matkó, G. Bertalan, P. Anna, G. Marosi, A. Tóth, Progress in interface modifications: from compatibilization to adaptive and smart interphases, Eur Polym J. 41 (2005) 697–705.

[17] G. Wu, S. Asai, M. Sumita, H. Yui, Entropy penalty-induced self-assembly in carbon black or carbon fiber filled polymer blends, Macromolecules. 35 (2002) 945–951.

[18] R. Yosomiya, Adhesion and bonding in composites, CRC Press, 2020.

[19] J. Schultz, M. Nardin, A. Pizzi, K. Mittal, Handbook of adhesive technology,

Marcel Dekker, New York. (1994).

[20] H.R. Brown, The adhesion between polymers, Annu Rev Mater Sci. 21 (1991) 463–489.

[21] Z. He, J.-H. Byun, G. Zhou, B.-J. Park, T.-H. Kim, S.-B. Lee, J.-W. Yi, M.-K. Um, T.-W. Chou, Effect of MWCNT content on the mechanical and strain-sensing performance of Thermoplastic Polyurethane composite fibers, Carbon N Y. 146 (2019) 701–708.

[22] H. Krump, M. Šimor, I. Hudec, M. Jaššo, A.S. Luyt, Adhesion strength study between plasma treated polyester fibres and a rubber matrix, Appl Surf Sci. 240 (2005) 268–274.

[23] F. Zhao, Y. Huang, Grafting of polyhedral oligomeric silsesquioxanes on a carbon fiber surface: novel coupling agents for fiber/polymer matrix composites, J Mater Chem. 21 (2011) 3695–3703.

[24] H. Ge, S. Li, H. Liu, D. Wang, J. Chen, Preparation and properties of water-soluble-type sizing agents for carbon fibers, J Appl Polym Sci. 131 (2014).

[25] X. Yuan, B. Zhu, X. Cai, J. Liu, K. Qiao, J. Yu, Improved interfacial adhesion in carbon fiber/epoxy composites through a waterborne epoxy resin sizing agent, J Appl Polym Sci. 134 (2017).

[26] R.L. Zhang, Y.D. Huang, L. Liu, Y.R. Tang, D. Su, L.W. Xu, Effect of emulsifier content of sizing agent on the surface of carbon fibres and interface of its composites, Appl Surf Sci. 257 (2011) 3519–3523.

[27] S.M. Goushegir, J.F. Dos Santos, S.T. Amancio-Filho, Friction spot joining of aluminum AA2024/carbon-fiber reinforced poly (phenylene sulfide) composite single lap joints: microstructure and mechanical performance, Mater Des. 54 (2014) 196–206.

[28] Y.D. Huang, R.L. Zhang, L. Liu, D. Su, A method of preparation the waterborne epoxy resin sizing agent for the carbon fiber, Pat CN 2010103001313. (2010).

[29] M. Guigon, E. Klinklin, The interface and interphase in carbon fibre-reinforced composites, Composites. 25 (1994) 534–539.

[30] Y. Zhang, Y. Zhang, Y. Liu, X. Wang, B. Yang, A novel surface modification of carbon fiber for high-performance thermoplastic polyurethane composites, Appl Surf Sci. 382 (2016) 144–154.

[31] C.Y. Yue, K. Padmanabhan, Interfacial studies on surface modified Kevlar fibre/epoxy matrix composites, Compos Part B Eng. 30 (1999) 205–217.

[32] A.R. Karaeva, N. V Kazennov, V.Z. Mordkovich, S.A. Urvanov, E.A. Zhukova, Carbon Fiber-Reinforced Polyurethane Composites with Modified Carbon--Polymer Interface, in: Proc Sci Conf Res Dev, 2018: pp. 415–420.

[33] R. Ma, W. Li, M. Huang, X. Liu, M. Feng, Enhancing strength and toughness of carbon fibers reinforced rigid polyurethane composites with low fiber content, Polym Test. 71 (2018) 156–162.

[34] P. Ehrburger, Interface in composite materials, Philos Trans R Soc London Ser A, Math Phys Sci. 294 (1980) 495–505.

[35] C. Lu, P. Chen, Q. Yu, Z. Ding, Z. Lin, W. Li, Interfacial adhesion of plasma-treated carbon fiber/poly (phthalazinone ether sulfone ketone) composite, J Appl Polym Sci. 106 (2007) 1733–1741.

[36] K.K. Chee Ho, H. Qian, A. Bismarck, Carbon fiber: surface properties, Wiley Encycl Compos. (2011) 1–11.

[37] S.-J. Park, T.-J. Kim, Studies on surface energetics of glass fabrics in an unsaturated polyester matrix system: effect of sizing treatment on glass fabrics, J

Appl Polym Sci. 80 (2001) 1439–1445.

[38] A. Warrier, A. Godara, O. Rochez, L. Mezzo, F. Luizi, L. Gorbatikh, S. V Lomov, A.W. VanVuure, I. Verpoest, The effect of adding carbon nanotubes to glass/epoxy composites in the fibre sizing and/or the matrix, Compos Part A Appl Sci Manuf. 41 (2010) 532–538.

[39] L. Gao, T.-W. Chou, E.T. Thostenson, Z. Zhang, A comparative study of damage sensing in fiber composites using uniformly and non-uniformly dispersed carbon nanotubes, Carbon N Y. 48 (2010) 3788–3794.

[40] L. Gao, T.-W. Chou, E.T. Thostenson, A. Godara, Z. Zhang, L. Mezzo, Highly conductive polymer composites based on controlled agglomeration of carbon nanotubes, Carbon N Y. 48 (2010) 2649–2651.

[41] N. Dilsiz, J.P. Wightman, Effect of acid--base properties of unsized and sized carbon fibers on fiber/epoxy matrix adhesion, Colloids Surfaces A Physicochem Eng Asp. 164 (2000) 325–336.

Chapter 2.

INVESTIGATE THE PHYSICO-CHEMICAL INTERACTION OF UNSIZED, EPOXY AND URETHANE SIZED TCF WITH POLYURETHANE SYSTEM

ABSTRACT

In polymer composites, the fiber-matrix interface is primarily influenced by the surface treatment of the fibers and polymer morphology, which affects the adhesion at the interface. In this work, the physico chemical interaction between thermoplastic polyurethane (TPU) comprising soft (S-TPU), hard (H-TPU) segment and thermoset polyurethane (TSU) with unsized, epoxy and urethane sized TCF at the interface of composites is investigated. Atomic force microscopy (AFM) results showed 39% improvement in the surface roughness of S-TPU than H-TPU indicating S-TPU can provide a mechanical bond at the interface than H-TPU. For TCF studies, urethane sized TCF showed 276% improvement in the roughness than unsized TCF. X-ray photoelectron spectroscopy (XPS) results revealed 550% increase in C=O content in H-TPU affirming that H-TPU contains multiple hydrogen-bonding network which can produce a chemical bond at the fiber-matrix interface than S-TPU. Dynamic mechanical analysis (DMA) and differential scanning calorimetry (DSC) analysis confirm that the hydrogen bonding network enhanced the crosslinked density by 232% in H-TPU than S-TPU. The surface and thermal results interpret that urethane sized TCF is more compatible with TPU and TSU system than epoxy and unsized TCF due to similar chemical structure present at the backbone.

Keywords: Polyurethane polymer, Textile grade carbon fiber, physico-chemical interaction at the interface, surface characterization, thermal analysis

2.1 INTRODUCTION

As explained in Chapter 1, that fiber-matrix interface is mainly driven by the surface structure of the fiber and the polymer matrix. The carbon fiber (CF) has inert surface created during high temperature carbonization/graphitization steps that reduces the adsorption with polymer systems [1]. Due to the non-polar nature of CF, it undergoes various surface treatments to enhance its surface activity by creating oxygen containing functional groups on its surface [2]. Thus, CF surfaces are coated with a sizing layer either by emulsion or solution technique, which contains polymeric compounds. Conventional sizing method(s) contains film former, emulsifier, antistatic, and coupling agents to improve bonding between fiber surface and polymer matrix [3–6]. Sizing improves the wettability of fibers by adding reactive functional group at the surface. These functional groups roughen the fiber surface to create either chemical or mechanical interlocking between fiber and matrix, which enhances the strength of the composite. Commercially available sizing materials are based on epoxy, polyester, nylon and polyurethane chemistries, to name a few. The key component used for sizing is water as a carrier, coupling agent to improve adhesion between fiber and matrix, lubricants to prevent fiber damage, film former to coat fibers and hold them together, the wetting agent to wet fibers through the resin, cross-linking agent to form a strong bond between fiber and matrix. An antistatic agent decreases the static charges on CF. The literature review showed that the heat resistant sizing agent such as thermoplastic polyimide and epoxy on polyacrylonitrile (PAN) based carbon fiber shows 97% improvement in interfacial shear strength (IFSS) compared to unsized fibers [7]. However, not all sizing types could improve the interfacial adhesion

between fibers and resin matrix [8]. This behavior is observed when sizing is adsorbed onto the fiber surface and cannot dissolve into the matrix during fabrication.

Another important parameter that affects the interface is polymer chemistry. In the polymer chemistry various factors needs to be considered such as the (a) physico-chemical state of polymer, (b) degree of polymerization, (c) chain length of hard and soft segments, (d) chemical structure, and (e) crystallinity of the polymer [9–11]. Tien et al. [12] synthesized the montmorillonite/polyurethane nanocomposites with various ratio of hard segments. Their results showed an improvement in the strength and elongation of nanocomposite properties due to the 20-37% reduction in hydrogen bonding index of polyurethane (PU) than pristine polymer. Liu et al. [13] reported increased tensile properties by 279% after incorporating phenol and formaldehyde in the PU structure. Yazdi et al. [14] observed the phase separation of hard and soft segments after incorporating multi-walled carbon nanotubes (MWCNTs) that improve the tensile strength and modulus of the composites. Pokharel et al. [15] studied the effect of short and long segmental length of PU on the mechanical properties of polyurethane graphene oxide (PU-GO) composites. The increase in the segmental length provided higher tensile strength due to the strong secondary bonding between PU-GO composites during extension. Furthermore, Ciprari et al. [16] stated that the difference in the structure and properties of polymer at the interface can be influenced by the bulk of polymer. The polymer structures contain flexible chains which is divided into adsorbed and unadsorbed monomer segments that can entangle with other chains in their proximity. Hence, the types of chains, its energy adsorption capability,

entanglement of the chain can influence both thermal and surface energy of the polymer. In the interface study, understanding the flexibility and rigidity of the chain is an important aspect to tailor the entanglement of the polymer at the interface.

The physico-chemical interaction of S-TPU, H-TPU, and TSU with unsized, epoxy, and urethane sized TCF on the intermolecular interactions of fiber and matrix is investigated in this work. The surface morphological changes, the hydrogen bonding index, phase separation, and surface segregation behavior of PU and textile grade carbon fiber (TCF) are analyzed through analytical techniques, such as X-ray photoelectron spectroscopy (XPS), atomic force microscopy (AFM), Fourier transform infrared spectroscopy (FTIR), differential scanning calorimetry (DSC) and dynamic mechanical analysis (DMA).

2.2 EXPERIMENTAL

2.2.1 Material and methods

The details of polyurethanes used in this work are summarized in Table 2.1. Unsized, epoxy and urethane sized TCFs were provided by Carbon Fiber Technology Facility (CFTF) at Oak Ridge National Laboratory (ORNL), presented in Table 2.2. The TCF spool contains 450 K filaments in a single tow. TCF has a tensile strength of ≈ 3 GPa and modulus of 275 GPa [17].

Table 2.1: Polyurethane material specifications

Specification	S-TPU	H-TPU	TSU
Product name	DT-7201[1]	LTE-1001[2]	Vitrox[3]
Hardness	75A	85A	80D
Polymer	Aromatic Polyether	Aromatic Polyether	Aromatic Polyether
Tensile Strength (MPa)	25.5	48.2	89.8
Specific Gravity (g/cc)	1.08	1.12	1.23

*1,2. American Polyfilms, Connecticut, USA; 3. Huntsman Corporation, Texas, USA

Table 2.2: TCF sizing nomenclature

Abbreviation	Sizing nomenclature
TCF-UN	Unsized TCF
TCF-E	Epoxy sized TCF
TCF-U	Urethane sized TCF

2.2.2 Atomic force microscopy (AFM)

Atomic force microscopy (AFM) was performed using the MFD-3D infinity microscope with AC/Air topography mode to explore the surface physical structure of S-TPU, H-TPU with unsized, epoxy and urethane sized TCF. A monolithic cantilever (AC240TS-R3 from Oxford instruments) with a force constant of 2 N/m and a resonance frequency of 70 kHz was used with tapping mode at ambient temperature. The maximum scanning image area used was 20 μm× 20 μm, to determine the root-mean-squared roughness (RMS) values of the materials.

2.2.3 X-ray photo-electron spectroscopy (XPS)

XPS techniques performed using the Thermo Scientific Model K-alpha XPS instrument (at the Oak Ridge National Lab, Oak Ridge, Tennessee) to quantify the chemical composition and surface properties of S-TPU, H-TPU with unsized, epoxy and urethane sized TCF. All the spectra were collected by Al Kα X-rays (1486.6 eV) source and a hemispherical electron energy analyzer equipped with a 128 multi-channel electron detection system operated at $2x10^{-9}$ mbar or lower pressure. The S-TPU and H-TPU film size was 4 mm × 4 mm with depth of penetration 5-10 nm. The single point analysis was performed on unsized, epoxy and urethane sized TCF with X-ray spot size of 400 μm diameter. The data analysis was conducted through Thermo Scientific Advantage XPS software package (v 4.61).

2.2.4 Fourier transform infrared spectroscopy (FTIR)

Fourier transform infrared spectroscopy (FTIR) was performed on S-TPU, H-TPU, and TSU to determine the hydrogen bonding efficiency in polymer through functional group analysis of individual constituents. The characterization was conducted using Nicolet iS50 FTIR spectrometer with deuterated triglycine sulfate (DTGS) detector and Mercury Cadmium Telluride (MCT) detector. The aperture diameter was 130 mm, the measurement was made with a spectrum resolution of 4 cm^{-1}, and 64 scans were performed for each material system.

2.2.5 Differential scanning calorimetry (DSC)

DSC was performed on S-TPU and H-TPU using the Q2000 instrument at a temperature range of -100°C to 200°C with a heating rate of 10°C /min under a nitrogen atmosphere to understand the molecular arrangement, crystallinity, and segmental behavior in the PU microstructure. Three samples were tested per each material for statistical analysis, and the average mass used for S-TPU and H-TPU was 4-5 mg respectively.

2.2.6 Dynamic mechanical analysis (DMA)

DMA was performed using a TA Q800 instrument on S-TPU and H-TPU polymer to understand the viscoelastic and morphological behavior of polymer at a molecular level as a function of temperature [18]. According to ASTM D-4065, the dual cantilever configuration with a 0.5 Hz frequency was used. The temperature is ramped from -70 °C to 160 °C (the range determined from DSC section) at a 5 °C/min with a strain rate of 0.1%.

2.3 RESULTS AND DISCUSSION

2.3.1 Atomic force microscopy (AFM)

The AFM technique was used to explore the surface physical structure and quantify the surface roughness of S-TPU, H-TPU with unsized, epoxy and urethane sized TCF, presented in Figure 2.1, Figure 2.2 and Table 2.3. Figure 2.1 shows the presence of extended grooves along the axial direction of the unsized TCF surface [19], after sizing, the groves were substituted by a sizing solution, and height v/s distance plot was analyzed to understand the changes in the depth and width of the groove profile. In Figure 2.2, the various segments of TPU were analyzed through surface hardness measurement. The tabulated surface roughness values are presented in Table 2.3. The grooves depth and width of the fibers and polymers surface, i.e., the spiked profile in Z-direction was analyzed using Gwyddion 2.55 software.

The results indicate that the mean roughness value of TCF-Un, TCF-E, and TCF-U was 163.1 nm, 291.9 nm, and 612.6 nm, respectively. The AFM image of TCF-Un contains a groove structure parallel to the fiber axis, Figure. 2.1. The Z-direction profile showed the smooth surface of TCF-Un, and the two spiked regions in the roughness profile indicate the length of the single fiber filament. In the TCF-E image, the spikes are observed on the edges of TCF due to the presence of bow-shaped structure [20], and smooth surface is observed in the middle section due to grooved structure. This illustrates the non-uniform distribution of epoxy sizing on the TCF surface. A TCF-U image shows the bow-shaped structure throughout the fiber surface, which has revealed in the surface roughness profile where

maximum spikes are observed. No evidence of groove structure indicates that the sizing coated the fiber surface uniformly. Due to these varied patterns, TCF-U shows higher surface roughness values compared to TCF-E and TCF-UN. AFM images of TPU shows the presence of hard and soft segments on the polymer matrix. The roughness in the Z-profile of S-TPU is due to the co-continuous network morphology [21]. A co-continuous network contains more than two interpenetrating networks, supported by soft and hard segment phases [22]. The various microdomains observed on the S-TPU surface may have a significant contribution to the roughness enhancement. H-TPU shows the few large spikes and remaining small spikes. Large spikes indicate the presence of hard segments, and small spikes indicate the soft segments, which improved the overall surface roughness of the H-TPU polymer. Hence, S-TPU has higher surface roughness than H-TPU.

The interfacial adhesion between fiber and matrix depends on the surface roughness values due to the fiber and matrix contact points. As the number of contacts increases (higher surface roughness), the mechanical interlocking increases, which eventually increases the overall strength of the composite. Hence, this work hypothesizes that S-TPU can perform better than H-TPU when mechanical interlocking is present. However, if the chemical bond is present, the H-TPU can produce good interfacial bonding with either urethane or epoxy sized TCF depends on the ultimate chemical structure of composites [23].

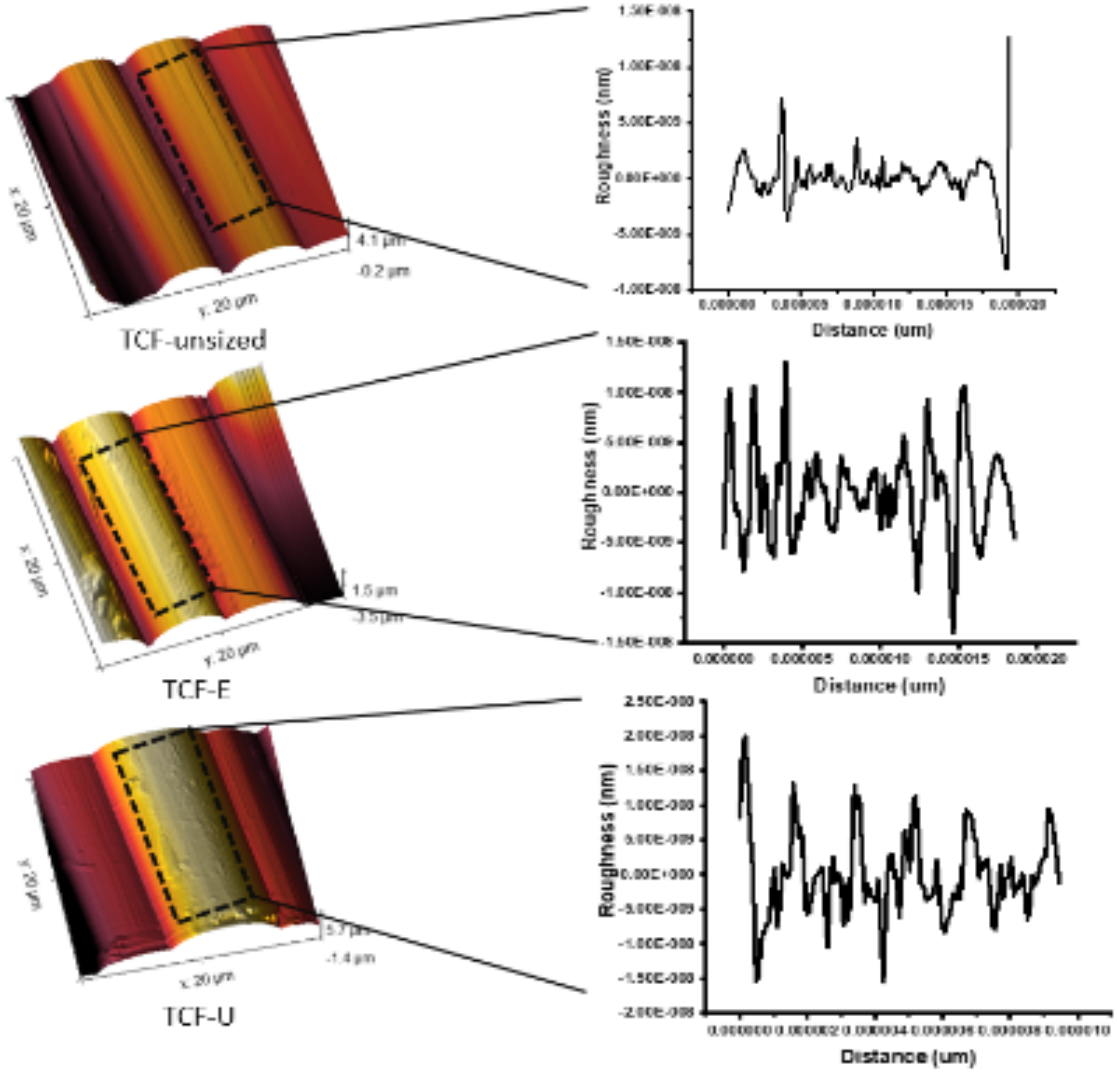

Figure 2.1: Three-dimensional AFM images of unsized (TCF-UN), epoxy sized (TCF-E) and urethane sized (TCF-U) CF with its surface roughness profile image in Z-direction.

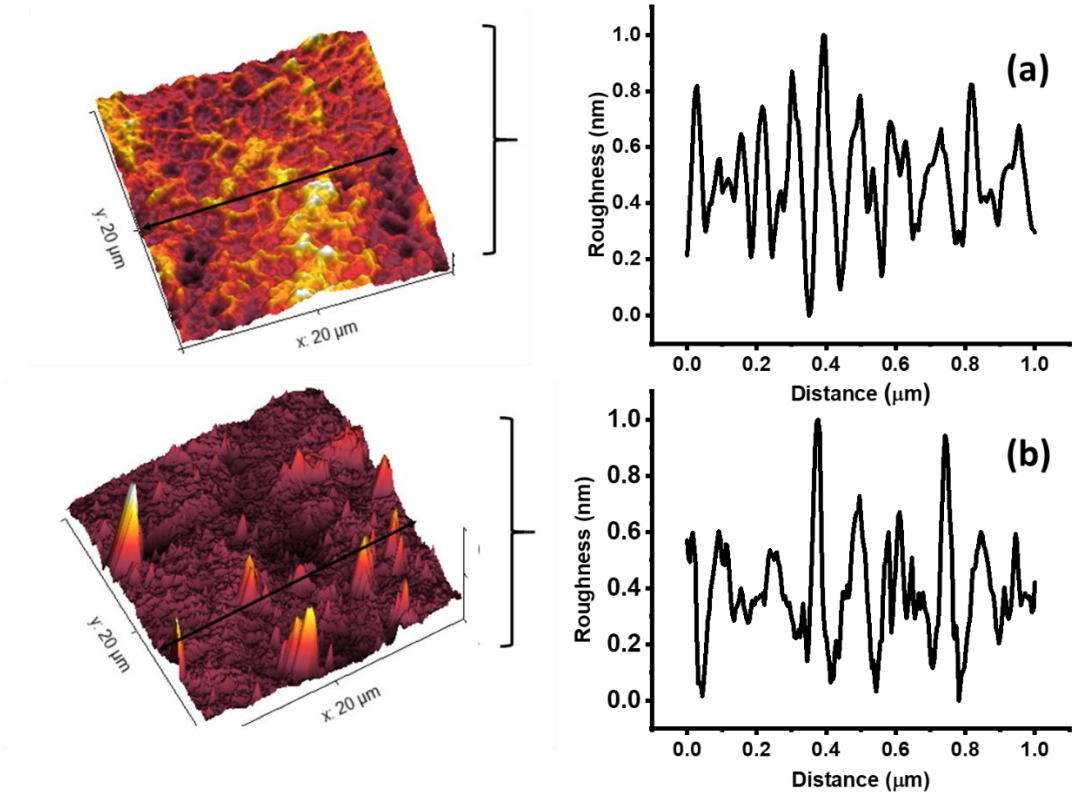

Figure 2.2: Three-dimensional AFM images of (a) S-TPU and (b) H-TPU material with surface roughness profile images in Z direction. The surface roughness increases from H-TPU to S-TPU

Table 2.3: Surface roughness of sized CF and TPU polymer

Specimens	Mean roughness (nm)	Root mean square roughness (nm)
S-TPU	39.38	49.73
H-TPU	15.43	26.19
TCF-Un	120.2	163.1
TCF-E	228.6	291.9
TCF-U	457.6	612.6

2.3.2 X-ray photo-electron spectroscopy (XPS)

XPS technique was used to understand S-TPU, H-TPU, TCF-E, and TCF-U's chemical composition and surface properties. The binding energy determined by the XPS curve depends on the atomic number (Z) of the molecule [24]. The atoms with higher oxidation states show higher binding energy due to coulombic interaction between the photon emitted electron and the ion core. The carbon (C 1s), oxygen (O 1s), and nitrogen (N 1s) are essential components in segmented PU and sized TCF, as shown in the survey spectra of individual constituents, Figure 2.3, Figure 2.4 and Figure 2.5 respectively. The reactive components of segmented TPU and TCF-U are NHCOO and oxirane ring (O-C-O ring) in TCF-E. The atomic concentrations for the respective component (TPU and TCF) are presented in Table 2.4. The common peaks observed for S-TPU and H-TPU in C 1s (at B.E 284 eV), N 1s (at B.E 400 eV) and O 1s (at B.E 530 eV) regions are C-C (284.4 eV), C-O/C/N (286 eV), C=O (287.5 eV), C-O (530.0 eV), C=O (532.0 eV) and C-NH2 (399.5 eV), presented in Figure 2.3 (a), and Figure 2.3 (b). The C 1s, O 1s, and N 1s spectra of S-TPU and H-TPU showed no changes in the peak position; however, H-TPU shows the highest intensity for C-C, C-N, and C-O spectra compared to S-TPU. The difference in the intensities might be due to the maximum concentration of aromatic ring in urethane linkage from PU structure, which explains the Tm trend in the DSC results. The higher C: O ratio observed in S-TPU (17.98) compared to H-TPU (12.91) indicates the presence of more polyol, which enhances the soft segment in the polymer with low Tg. Furthermore, the H-TPU (23.8) shows a higher C: N ratio compared to S-TPU (19.5), which specifies

the existence of the amide group and the hydrogen bonding (NH-COO-), which enhances the crystallinity of polymer.

The XPS peaks observed for TCF-E are C-C, C-O-C, C-O, and C=O at 284.4 eV, 289.1 eV, 534 eV, 532 eV, respectively, Figure 2.4. For TCF-U, C-C, C=O, CH2, C-N, O-CH, O=C-O, C=O, C-O, and N-H at 284.4 eV, 285.1 eV, 285.7 eV, 286.5 eV, 289.1 eV, 531.8 eV, 533.2 eV, and 399.9 eV, respectively, Figure 2.5. The results confirm the presence of epoxy and urethane groups on the TCF surface. The decrease in the atomic concentration of C content by 16% in TCF-E and TCF-U than TCF-Un indicates that the carbon has bonded strongly with sizing chemicals, Table 5. TCF-E (19.6) showed higher oxygen content than TCF-U (15) due to epoxy sizing on TCF. Both TCF-E (0.24) and TCF-U (3.5) show higher N concentration, which we hypothesized due to 1) the carbonization and oxidization process applied to TCF before surface treatment and 2) the N content increased after applying urethane sizing on TCF surface. Furthermore, the C: O ratio has a significant effect on bonding due to the high electronegativity of O [25]. The C:O ratio observed higher in TCF-U than TCF-E, indicating that the O is highly polar, which enhances the reactive groups on the CF surface and eventually affects the interfacial adhesion of composites. Hence, the results interpret that TCF-U may form a strong interfacial bond with TPU compared to TCF-E.

Table 2.4: Chemical composition and atomic ratio of PU and TCF component

Surface Composition (at. %)	C	O	N	C/O	C/N
TCF-E	79.81	19.57	0.24	4.1	NA
TCF-U	81.3	15	3.5	5.42	23.2
TCF-Un	95.7	3.1	1.0	30.87	NA
H-TPU	89.23	6.91	3.75	12.91	23.8
S-TPU	89.9	5.0	4.6	17.98	19.5

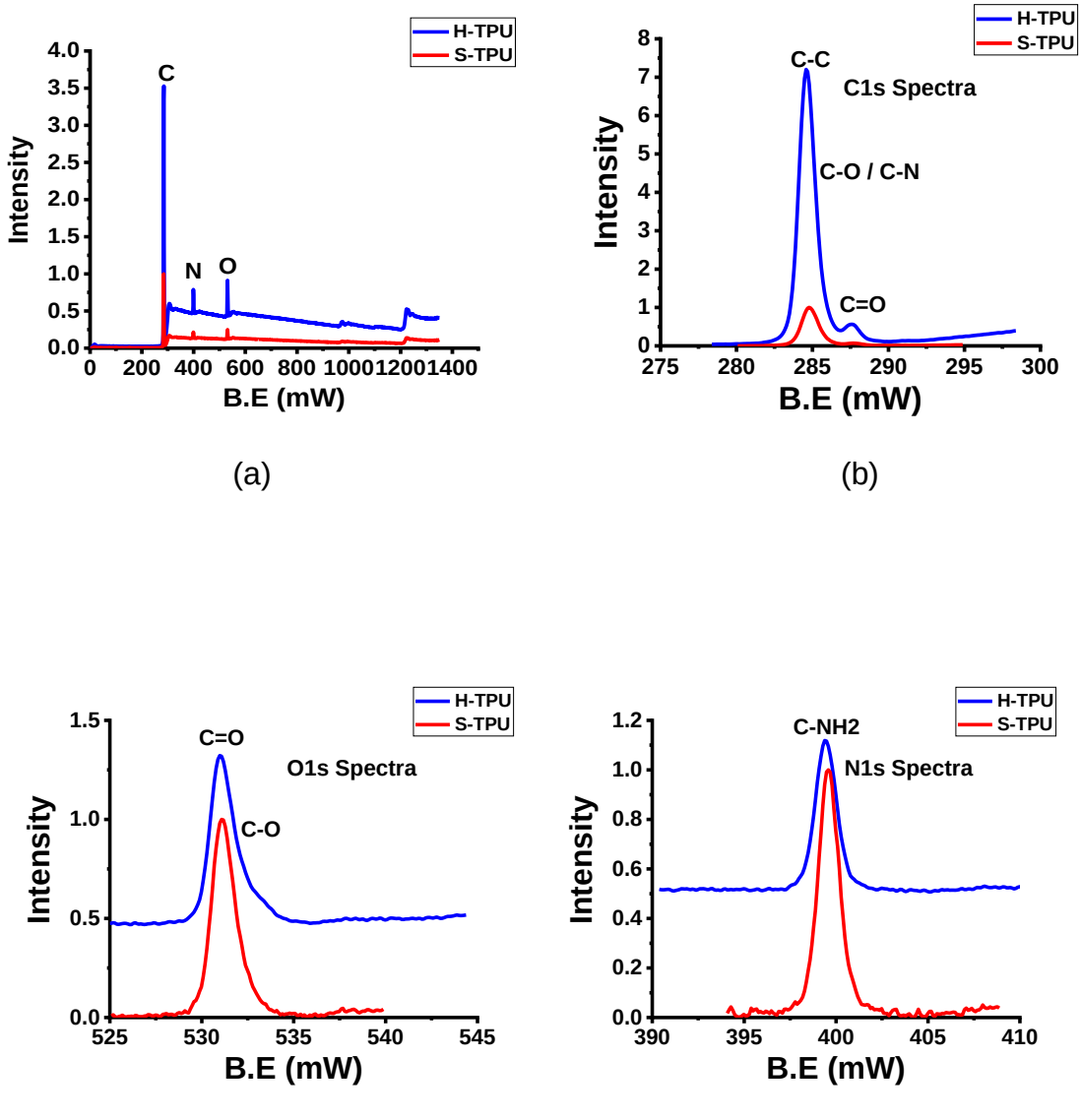

Figure 2.3: (a) XPS survey spectra of S-TPU and H-TPU shows higher concentration of C and O elements, (b) C 1s spectra shows higher C-C concentration in H-TPU than S-TPU structure, (c) O 1s spectra shows the higher concentration of C=O in H-TPU than S-TPU (d) N 1s spectra of S-TPU and H-TPU

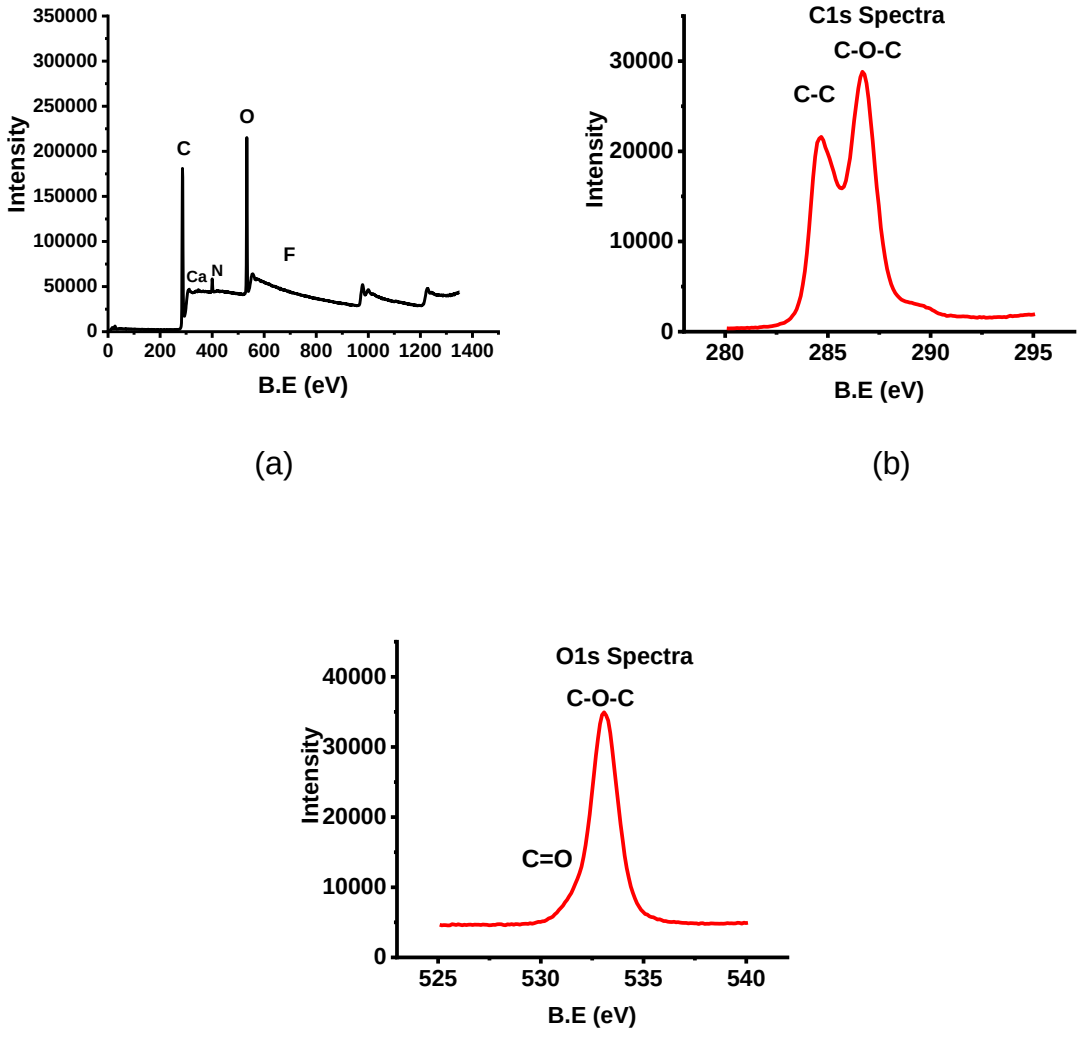

(a) (b)

(c)

Figure 2.4: (a) XPS survey spectra of TCF-E shows higher concentration of C and O elements, (b) C 1s spectra shows C-C bond from TCF structure and C-O-C from sizing, (c) O 1s spectra shows the presence of oxirane structure (C-O-C) from epoxy sizing

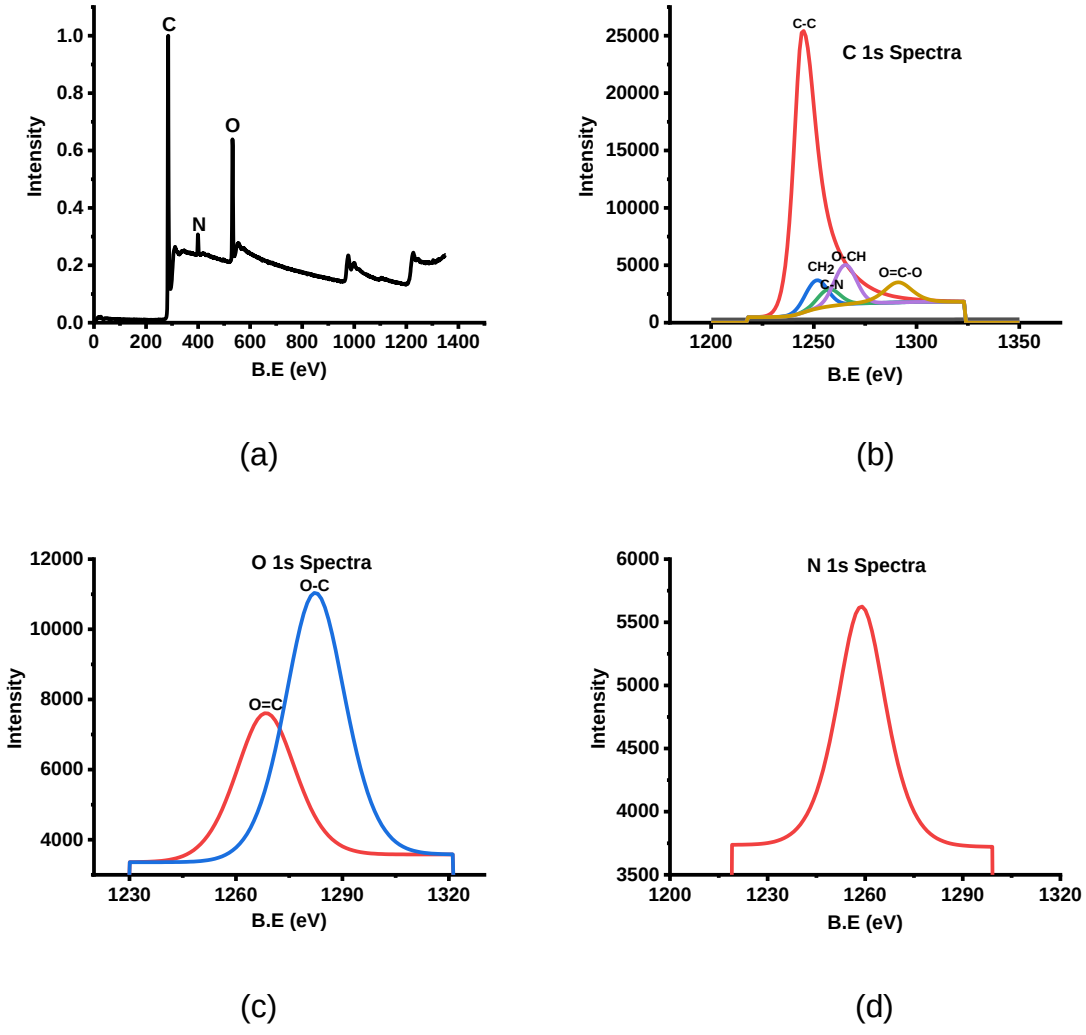

Figure 2.5:(a) XPS survey spectra of TCF-U shows higher concentration of C, O and N elements, (b) C 1s spectra shows C-C from TCF structure, (c) O1s spectra shows C-O and C=O and (d) N 1s spectra shows NH group (NHCOO) structure from urethane sizing

2.3.3 Fourier transform infrared spectroscopy (FTIR)

Fourier transform infrared spectroscopy (FTIR) was performed on S-TPU, H-PTU, and TSU to understand the hydrogen bonding efficiency in polymer through functional group analysis of individual constituents. The essential functional groups in polyether based TPU are N-H (proton donor), carbonyl (C=O), and the ether (C–O–C) groups (proton acceptor). The reactive group's information for individual polymers is presented in Figure 2.6, Figure 2.7 and Figure 2.8. The band that appeared at 3150-3400 cm^{-1} contains NH stretching group, which expresses that the increase in the peak intensities contributes to increase in the NH content in the respective polymer, Figure 2.6. The energy released through intermolecular interaction at the molecular forces (covalent, Van der Waals, and hydrogen bonding forces) provides different peak intensities. These forces restrict the molecular motion and increase the hardness of the polymer by providing the higher peak intensity [26]. Hence, S-TPU shows higher mobility in the structure than H-TPU and TSU due to excess polyol present in the backbone of the polymer. The FTIR spectrum obtained in 1700-1730 cm^{-1} band represents the carbonyl group in urethane structure. Figure 2.7 showed the two frequencies of the C=O group at 1700 cm^{-1} and 1732 cm^{-1} due to the distribution of electrons during chemical bonding formation. The lower frequency (1700 cm^{-1}) indicates the hydrogen bonding between NH and C=O group, and the higher frequency (1732 cm^{-1}) represents free C=O group present in the structure [27]. TSU polymer exhibited bonded C=O at 1700 cm^{-1} spectra and unreacted NCO groups at 2259 cm^{-1}. The data indicate that the isocyanate reaction with polyol might have broadened the C=O peak and enhanced the toughness of the polymer. Hence, the area under the

peak of 1700 cm^{-1} and 1732 cm^{-1} was determined to calculate the hydrogen bonding index (R) of S-TPU and H-TPU. The R-value describes the degree of carbonyl group participated in bonding [12].

$$R = (\text{Area of C=O at 1707 })/(\text{Area of C=O at 1733}) \quad [1]$$

$$DPS = R/ (R+1) \quad [2]$$

$$DPM = 1- DPS \quad [3]$$

The area under the peak calculated using Origin Pro 2019b version 9.6.5.169, and the R-value achieved for H-TPU and S-TPU was 7.6 and 3, respectively. The increase R-value indicates the increasing hardness of the polymer, which correlates with DSC and XPS results. The degree of phase separation (DPS) was measured to evaluate the linkage between a hard segment and a hard segment of polymer, whereas the degree of phase mixing (DPM) calculated the linkage between the hard segment and the soft segment between polymer and fibers. The presence of the amide II group in the range of 1530-1545 cm^{-1} spectra is additional information to validate the R-value results. The amide II peak for S-TPU, H-TPU, and TSU has appeared at 1530 cm^{-1}, 1527 cm^{-1}, and 1508 cm^{-1} spectra, presented in Figure 2.8. The results indicate that the lower the wavenumber of amide II, the stronger the hydrogen bond. Hence the amide II data also provides similar information and shows that the hydrogen bonding enhances in the following order TSU > H-TPU > S-TPU [28].

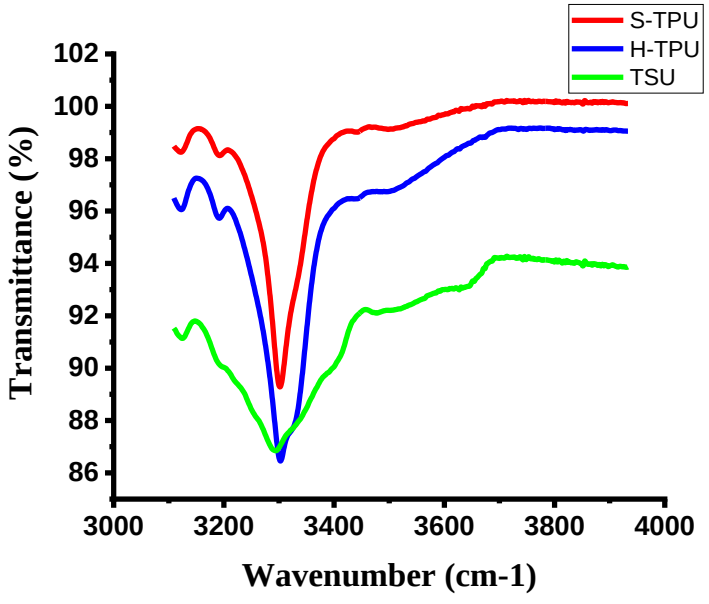

Figure 2.6: The increase in the peak intensity and peak area broadening of NH stretching spectra of S-TPU, H-TPU and TSU

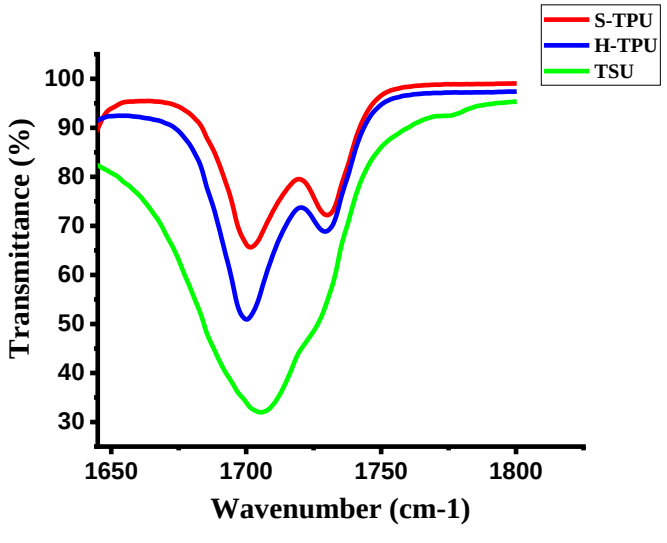

Figure 2.7: Carbonyl spectra at 1700 cm^{-1} (hydrogen bonded C=O) and 1732 cm^{-1} (non-bonded C=O group) in S-TPU, H-TPU and TSU

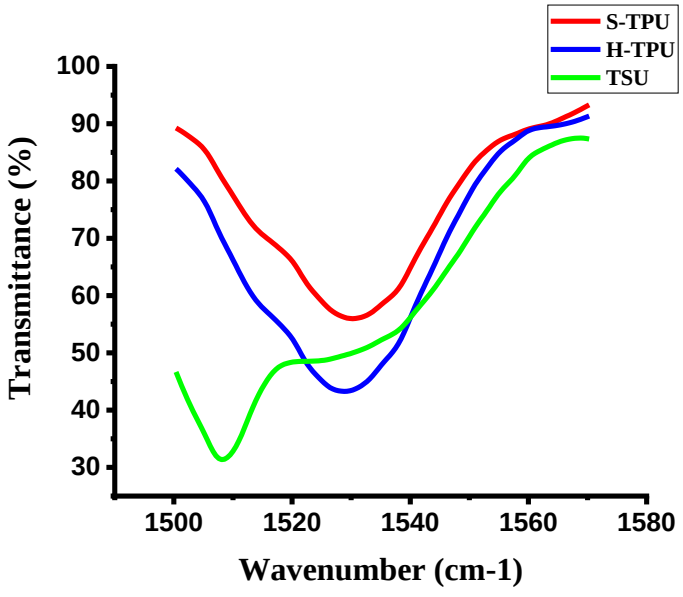

Figure 2.8: Amide II spectra of S-TPU, H-TPU and TSU at 1530 cm^{-1}, 1527 cm^{-1}, and 1508 cm^{-1}, respectively

2.3.4 Differential scanning calorimetry (DSC)

DSC was performed on S-TPU and H-TPU to understand the molecular arrangement, crystallinity, and segmental behavior in the PU microstructure. The analysis started at the temperature -100°C to restrict the molecular movement of TPU and to understand the internal segmental motion after gradually increasing the temperature. Three thermal transitions were observed, such as glass transition, melting, and crystallization temperature of TPU. The glass transition temperature (Tg) of S-TPU is 4.67 °C, and H-TPU is 76.72 °C showed in Figure 2.9. The significant difference in Tg represents the energy absorption capacity of the TPU molecules. The absorbed energy unfolds the molecular orientation by separating the hydrogen bond between N-H and O-C=O in the highly compact crystal structure. The increasing Tg of H-TPU indicates a strong hydrogen-bonded network in the backbone that requires more bond energy than S-TPU [29]. After determining Tg values, the molecular motion is further analyzed with increasing the temperature. The molecular movement at increasing temperature favors arrangements of chains to move in a coordinated manner (depending on the structural regularities).

The melting temperature (Tm) obtained for S-TPU and H-TPU is 162°C and 165°C, with the enthalpy of fusion 0.49 J/g and 1.84 J/g, respectively, Figure 2.10. A nominal difference in Tm and a significant difference in enthalpy of fusion was observed in segmented TPU. The results indicate that both the polymer's molecule melts at the similar temperature. However, the energy absorbed by the individual molecule from H-TPU and S-TPU structure is different due to the variation in the hydrogen bonding content. Hence, the results illustrate that H-TPU may contain

excess amide groups [30], which contributed to the PU reaction for hydrogen bonding formation. In contrast, S-TPU has a significant number of polyol groups, which does not require excess heat for molecular motion [29]. The Tm values of S-TPU and H-TPU will be used to produce the composite laminates.

After reaching melting point, the temperature starts to decrease, and the molecular motion becomes sluggish when it reaches the Tg, and the crystallization rate becomes zero. The crystallization temperature (T_C) for S-TPU and H-TPU is 63.2°C and 82.1°C, respectively, with the enthalpy of crystallization of 1.92 J/g and 7.77 J/g, Figure 2.11. The crystallization temperature mainly depends on the density of the polymer, the closely packed dense structure contains higher molecular arrangement and eventually enhances the T_C. The density of S-TPU and H-TPU is 1.08 g/cc and 1.12 g/cc, as shown in Table 2.1. The density of polymer clarifies the change in the T_C and suggests that the molecular arrangement of H-TPU enhances the mechanical properties of the composite.

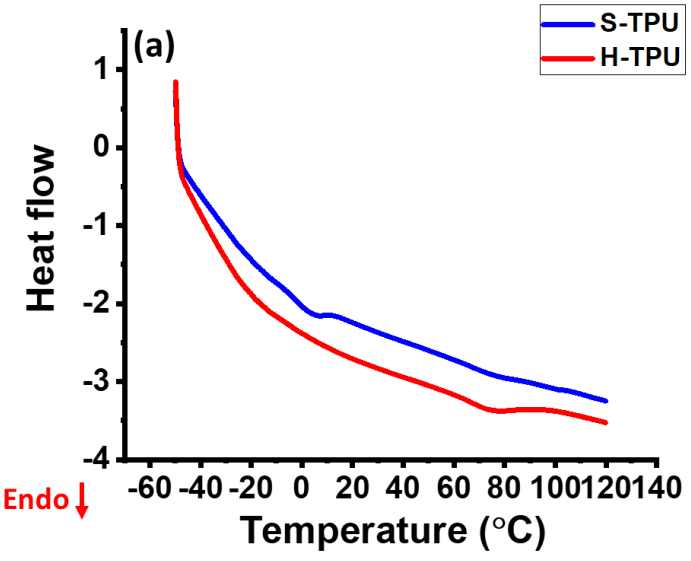

Figure 2.9: Glass transition temperature curve of S-TPU and H-TPU is 4.67 °C, and 76.72 °C respectively.

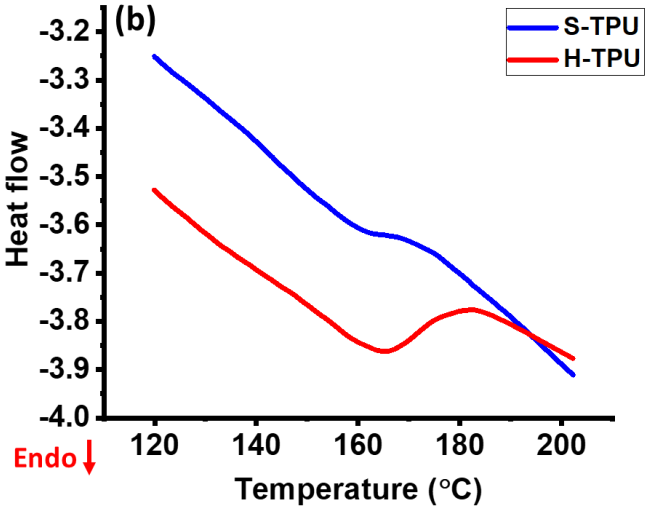

Figure 2.10: Melting temperature curve of S-TPU (162°C) and H-TPU (165°C) with the enthalpy of fusion at 0.49 J/g and 1.84 J/g for S-TPU and H-TPU, respectively

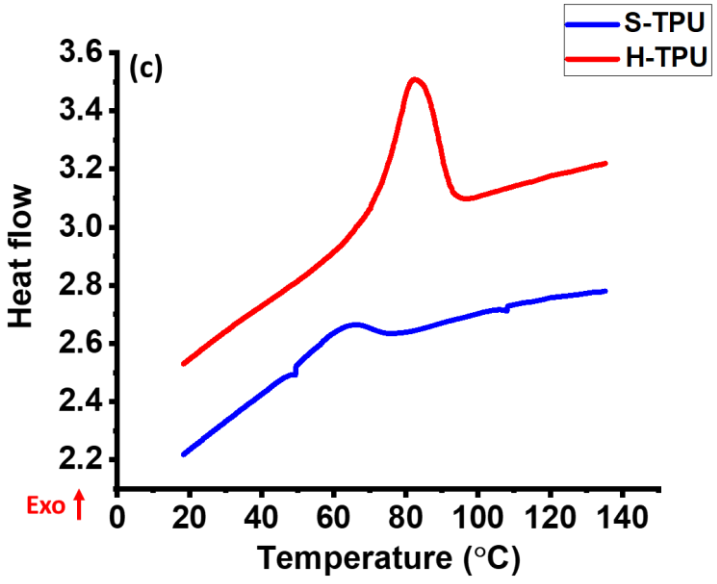

Figure 2.11: Crystallization temperature curve of S-TPU (63.2°C) and H-TPU (82.1°C)

2.3.5 Dynamic mechanical analysis (DMA)

DMA was performed on S-TPU and H-TPU polymer to understand the viscoelastic and morphological behavior of polymer at a molecular level as a function of temperature [18]. The storage modulus (log E') and tan δ curve as a function of the temperature of S-TPU and H-TPU are presented in Figure 2.12 and Table 2.5. The increase in the storage modulus for S-TPU (1078.7 MPa) and H-TPU (1673.8 MPa) observed at -70 °C, indicates that H-TPU has less degree of elasticity compared to S-TPU [31]. After reaching -70 °C, a sudden decrease in the curve was observed due to the alpha transition (Tα) behavior, which indicates the large segmented molecule slippage in the polymer backbone. The Tα of H-TPU and S-TPU is -43°C and -63°C, respectively. The molecular movement of the hard domain was observed at -6.8 °C for S-TPU and 59.7 °C for H-TPU. The difference in the Tα indicates more hydrogen bonding in H-TPU than S-TPU, and the results correlate with DSC findings. For further analysis, the average molecular weight of S-TPU and H-TPU was determined using DMA through high flexibility theory equation, which is as follows

$$Mc = (3 \times \rho \times R \times T)/ET \quad [4]$$

Where,

ρ = density of the individual polymer (g/cm3)

R = Gas constant (8.314 (cm3x MPa)/ (mol × K)

T = The temperature at the inflection points of the viscoelastic transition phase (K)

ET = The storage modulus at the viscoelastic transition (Pa)

Mc = Average molecular weight between entanglement

The results showed a 232% increase in molecular weight of H-TPU compared to S-TPU. The Tg of S-TPU and H-TPU are -29.4 °C and -7.6 °C, respectively. The shift in the tan δ curve affirmed that H-TPU has a higher number of aromatic groups in its backbone chains than S-TPU, which require more energy to break the bond and hence influence the storage modulus and tan δ peak. The Mc value illustrates that more entanglement of molecules presents in the H-TPU polymer than S-TPU, which explains the enhancement of Tg, E' and shift in tan δ curves and eventually enhances the mechanical properties.

In this chapter, amongst S-TPU and H-TPU, the AFM results showed that the S-TPU has higher surface roughness and can provide a strong mechanical bonding with TCF reinforcement. However, FTIR, XPS, DSC, and DMA results illustrate that H-TPU contains a higher R-value that produces more crystalline structure in the polymer backbone and provides a higher storage modulus than S-TPU. In TCF surface studies, the XPS results indicated that NH- group in urethane roughened the surface of TCF than TCF-E, and it can provide a strong either mechanical or chemical interface with PU matrix. The overall results indicate that TCF-U can produce a strong interfacial bonding with H-TPU and TSU than S-TPU.

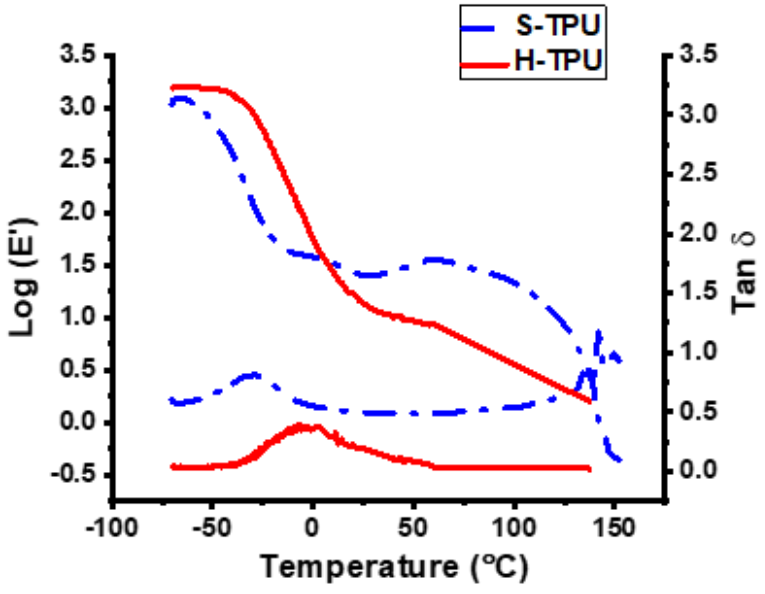

Figure 2.12: DMA results of storage modulus (log E'), loss factor (tan δ) of S-TPU and H-TPU as a function of temperature

Table 2.5: The storage modulus, glass transition temperature, tan δ and average molecular weight of S-TPU and H-TPU

Material	ρ (g/cm3)	Tg (°C)	E' (MPa) at -70 °C	T (K)	tan δ	Mc (g/mol)
S-TPU	1.08	-29.4	1078.7	256.3	-29.4	140
H-TPU	1.12	-7.6	1673.8	317.2	-7.6	465

2.4 CONCLUSIONS

In this objective, the inert surface of TCF is reduced by coating epoxy and urethane polymer on the TCF surface and validated its compatibility with the urethane system. The physico-chemical interaction and adhesion efficiency of S-TPU, H-TPU, and TSU polymer with unsized, epoxy, and urethane sized TCF is investigated through the surface and thermal analysis. The AFM results showed 39% higher surface roughness of S-TPU than H-TPU, indicating S-TPU can provide a mechanical bond at the interface than H-TPU. However, DSC and DMA data showed that the H-TPU contains a closed molecular structure requiring higher thermal energy to separate the bond than S-TPU. The thermal characterization results correlate to the surface analysis and illustrate that H-TPU contains a higher hydrogen bonding index than S-TPU.

Furthermore, XPS and AFM results of TCF-Un, TCF-E, and TCF-U indicate that TCF-U has higher surface roughness than other constituents. Hence, we hypothesized that TCF-U could be more compatible with the polyurethane system and improve the mechanical strength of the composites compared to TCF-E and TCF-Un reinforcements. A detailed understanding and the effect of physico-chemical interaction between TCF and PU systems on the interfacial adhesion will be describe in Chapter 3. Based on the overall analysis, a possible chemical reaction hypothesis is presented in Figure 2.13

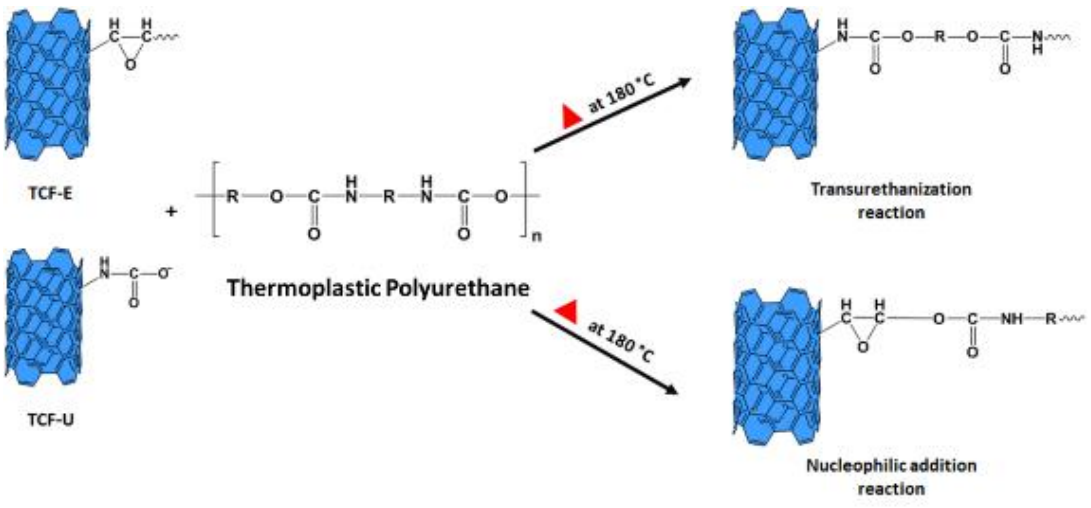

Figure 2.13: Possible reaction mechanism of polyurethane system with epoxy and urethane sized TCF

REFERENCES

[1] M.C. Paiva, C.A. Bernardo, M. Nardin, Mechanical, surface and interfacial characterization of pitch and PAN-based carbon fibres, Carbon N Y. 38 (2000) 1323–1337.

[2] K.K. Chee Ho, H. Qian, A. Bismarck, Carbon fiber: surface properties, Wiley Encycl Compos. (2011) 1–11.

[3] S.-J. Park, T.-J. Kim, Studies on surface energetics of glass fabrics in an unsaturated polyester matrix system: effect of sizing treatment on glass fabrics, J Appl Polym Sci. 80 (2001) 1439–1445.

[4] L. Gao, T.-W. Chou, E.T. Thostenson, Z. Zhang, A comparative study of damage sensing in fiber composites using uniformly and non-uniformly dispersed carbon nanotubes, Carbon N Y. 48 (2010) 3788–3794.

[5] A. Warrier, A. Godara, O. Rochez, L. Mezzo, F. Luizi, L. Gorbatikh, S. V Lomov, A.W. VanVuure, I. Verpoest, The effect of adding carbon nanotubes to glass/epoxy composites in the fibre sizing and/or the matrix, Compos Part A Appl Sci Manuf. 41 (2010) 532–538.

[6] L. Gao, T.-W. Chou, E.T. Thostenson, A. Godara, Z. Zhang, L. Mezzo, Highly conductive polymer composites based on controlled agglomeration of carbon nanotubes, Carbon N Y. 48 (2010) 2649–2651.

[7] M. Guigon, E. Klinklin, The interface and interphase in carbon fibre-reinforced composites, Composites. 25 (1994) 534–539.

[8] N. Dilsiz, J.P. Wightman, Effect of acid--base properties of unsized and sized carbon fibers on fiber/epoxy matrix adhesion, Colloids Surfaces A Physicochem Eng Asp. 164 (2000) 325–336.

[9] G.C. Papanicolaou, P.S. Theocaris, G.D. Spathis, Adhesion efficiency between phases in fibre-reinforced polymers by means of the concept of boundary interphase, Colloid Polym Sci. 258 (1980) 1231–1237.

[10] D.J. Martin, G.F. Meijs, P.A. Gunatillake, S.J. McCarthy, G.M. Renwick, The effect of average soft segment length on morphology and properties of a series of polyurethane elastomers. II. SAXS-DSC annealing study, J Appl Polym Sci. 64 (1997) 803–817.

[11] S.G. Kim, others, Effect of polymerization procedure on thermal and mechanical properties of polyether based thermoplastic polyurethanes, Macromol Res. 10 (2002) 365–368.

[12] Y.I. Tien, K.-H. Wei, Hydrogen bonding and mechanical properties in segmented montmorillonite/polyurethane nanocomposites of different hard segment ratios, Polymer (Guildf). 42 (2001) 3213–3221.

[13] Z. Liu, Y. Tian, S. Kang, X. Zhang, Synthesis and characterization of novel epoxy-modified waterborne polyurethanes and their use in carbon fiber sizing, J Appl Polym Sci. 125 (2012) 3490–3499.

[14] M. Yazdi, V.H. Asl, M. Pourmohammadi, H. Roghani-Mamaqani, Mechanical properties, crystallinity, and self-nucleation of carbon nanotube-polyurethane nanocomposites, Polym Test. 79 (2019) 106011.

[15] P. Pokharel, S. Choi, others, The effect of hard segment length on the thermal and mechanical properties of polyurethane/graphene oxide nanocomposites, Compos Part A Appl Sci Manuf. 69 (2015) 168–177.

[16] D. Ciprari, K. Jacob, R. Tannenbaum, Characterization of polymer nanocomposite interphase and its impact on mechanical properties, Macromolecules. 39 (2006) 6565–6573.

[17] P. Yeole, S. Alwekar, N.K.P. Veluswamy, S. Kore, N. Hiremath, U. Vaidya, M. Theodore, Characterization of textile-grade carbon fiber polypropylene composites, Polym Polym Compos. (2020) 0967391120930109.

[18] S. Ioan, G. Grigorescu, A. Stanciu, Dynamic-mechanical and differential scanning calorimetry measurements on crosslinked poly (ester-siloxane)-urethanes, Polymer (Guildf). 42 (2001) 3633–3639.

[19] Q. Ma, Y. Gu, M. Li, S. Wang, Z. Zhang, Effects of surface treating methods of high-strength carbon fibers on interfacial properties of epoxy resin matrix composite, Appl Surf Sci. 379 (2016) 199–205.

[20] R. Ruan, W. Cao, L. Xu, Quantitative characterization of physical structure on carbon fiber surface based on image technique, Mater Des. 185 (2020) 108225.

[21] I. Javni, O. Bilić, N. Bilić, Z.S. Petrović, E.A. Eastwood, F. Zhang, J. Ilavsk\`y, Thermoplastic polyurethanes with controlled morphology based on methylenediphenyldiisocyanate/isosorbide/butanediol hard segments, Polym Int. 64 (2015) 1607–1616.

[22] D. Carolan, H.M. Chong, A. Ivankovic, A.J. Kinloch, A.C. Taylor, Co-continuous polymer systems: A numerical investigation, Comput Mater Sci. 98 (2015) 24–33.

[23] N. Dilsiz, J.P. Wightman, Surface analysis of unsized and sized carbon fibers, Carbon N Y. 37 (1999) 1105–1114.

[24] V.S. Bagotsky, Fundamentals of electrochemistry, John Wiley & Sons, 2005.

[25] D. Liu, P. Chen, J. Mu, Q. Yu, C. Lu, Improvement and mechanism of interfacial adhesion in PBO fiber/bismaleimide composite by oxygen plasma treatment, Appl Surf Sci. 257 (2011) 6935–6940.

[26] A. Eceiza, M.D. Martin, K. De La Caba, G. Kortaberria, N. Gabilondo, M.A. Corcuera, I. Mondragon, Thermoplastic polyurethane elastomers based on polycarbonate diols with different soft segment molecular weight and chemical structure: mechanical and thermal properties, Polym Eng Sci. 48 (2008) 297–306.

[27] J. Mattia, P. Painter, A Comparison of Hydrogen Bonding and Order in a Polyurethane and Poly (urethane- urea) and Their Blends with Poly (ethylene glycol), Macromolecules. 40 (2007) 1546–1554.

[28] L. Jiang, Z. Ren, W. Zhao, W. Liu, H. Liu, C. Zhu, Synthesis and structure/properties characterizations of four polyurethane model hard segments, R Soc Open Sci. 5 (2018) 180536.

[29] E.J. Woo, G. Farber, R.J. Farris, C.P. Lillya, J.C.W. Chien, Structure-property relationships in thermoplastic elastomers: I. Segmented polyether-polyurethanes, Polym Eng Sci. 25 (1985) 834–840.

[30] R.W. Seymour, S.L. Cooper, Thermal analysis of polyurethane block polymers, Macromolecules. 6 (1973) 48–53.

[31] P. Parcheta, E. Głowińska, J. Datta, Effect of bio-based components on the chemical structure, thermal stability and mechanical properties of green thermoplastic polyurethane elastomers, Eur Polym J. 123 (2020) 109422.

Chapter 3.

INVESTIGATE THE EFFECT OF AHDESION AND COHESION OF UNSIZED, EPOXY AND URETHANE SIZED TCF COMPOSITES REINFORCED IN TPU AND TSU WITH FUSION BOND EFFECIENCY BETWEEN TSU AND TPU COMPOSITES

A version of this chapter is published as a peer-reviewed article.

- Surbhi Kore, Merlin Theodore, and Uday Vaidya*, Effect of the Segmental Structure of Thermoplastic Polyurethane (Hardness) on the Interfacial Adhesion of Textile-Grade Carbon Fiber Composites, ACS Applied Polymer Materials, 2021, DOI: 10.1021/acsapm.1c01001”
- Improvement of interfacial adhesion of unidirectional textile grade carbon fiber (TCF) with unsized, epoxy and urethane sizing reinforced in thermoset urethane composites” in in the Materials Today: Communication journal, Vol.28, 2021

ABSTRACT

The hypothesis proposed in chapter 2 stated that urethane-sized TCF is compatible with thermoplastic and thermoset urethane systems. The adhesion and cohesion between fiber-matrix interfaces and thermoset (TS)-thermoplastic (TP) composite interfaces were investigated in this work through three different studies. The first study was to understand the effect of soft (S-TPU) and hard segments (H-TPU) of TPU with unsized (TCF-Un), epoxy (TCF-E), and urethane sized (TCF-U) TCF composites fabricated via compression molding technique. The results showed that the S-TPU and H-TPU are not compatible with TCF-Un and TCF-U due to the difference in the mobility of molecular chains as a function of temperature. The results showed improved mechanical properties with TCF-E reinforced H-TPU composites. The flexural, impact and tensile properties were 30%, 50%, and 130% higher than S-TPU composites.

The second part of the research explored the bonding efficiency between TCF-Un, TCF-E, and TCF-U with a thermoset urethane (TSU) resin system. The flexural, interlaminar shear strength (ILSS), and impact properties of urethane-sized TCF

increased by 24%, 50%, and 273%, respectively, when compared to unsized TCF. The results demonstrate that the surface and thermal properties correlate with the mechanical properties of TCF-TSU composites, and sizing enhances the wettability of the composite(s).

The third part of the research focused on the fusion bonding between TP and TS composites. H-TPU-TCF-E (TP) and TCF-U-TSU (TS) were used for the fusion bonding study. The results showed 295% and 51% increase in flexural and ILSS properties of TP/TS fusion bonded composite than H-TPU-TCF-E composites. The lap shear strength was 21% higher than studies reported in literature confirming strong interfacial bonding between the TP-TS laminate(s).

Keywords: unsized, epoxy and urethane sized TCF-TPU composites, TCF-TSU composites, fusion bonded TP/TS composites, surface, thermal and mechanical characterization

3.1 INTRODUCTION

The performance of carbon fiber reinforced polymer composites (CFRP) depends on the interatomic and intermolecular contact between the fiber and matrix at the interface that influences adhesion. Sizing of the CF surface delivers chemical groups compatible with the polymer matrix to enhance fiber-matrix bonding. The researcher's study confirms that sizing roughens the CF surface by producing chemical and mechanical interaction with the matrix, thus, improving the mechanical properties of the composite [1–3]. Zhao et al. [4] improved the interfacial bonding by applying polydimethylsiloxane bishydroxylalkyl (PDMSBH) on the CF surface and reinforced in PU matrix. Their results indicate improvement in the mechanical, friction and wear properties of the composite. Liu et al. studied the interfacial adhesion between CF and polysulfone (PES) using graphene oxide. The authors reported that commercial-grade sizing degrades at about 250ºC. Thus, working with high-temperature polymers becomes challenging with thermoplastic polymer due to weak interfacial adhesion at the interface. Gnädinger et al. [5] studied the interfacial shear strength of epoxy, urethane, and polyamide (PA) sized CF with thermosetting urethane and epoxy matrices. A significant improvement (50%) in the interfacial shear strength (IFSS) properties was observed for the similar chemical structure of the sizing agent and polymer.

Understanding the adhesion of the laminates at the macro level is influenced by fiber-matrix bonding at the micro-level. Fusion bonding technique has been widely used in industry for joining two polymer parts through methods such as - surface preparation, heat treatment, pressure, diffusion, and cooling steps. Based on these

methods fusion bonding has been classified into four techniques as illustrated in Figure 3.1.

Among several techniques, bulk heating is an ideal joining method to co-consolidate dissimilar materials using autoclave and/or compression molding techniques [6]. In these methods, no external material or surface treatment is applied to the bond line. The bond strength is dependent on the properties of the composite laminate(s). During the fusion bonding process, two dissimilar laminates are bonded at the melting temperature of the polymer (of the laminate) with adequate pressure to minimize voids at the interface. Weber et al. examined the bond strength between CF/PEEK tape-preforms and CF/PEEK organo sheets using the co-consolidation method. Their results showed that the interlaminar fracture toughness was enhanced by 42% compared to CF-PEEK fabricated in autoclave with a void content of 1.58% [7]. Hou et al. bonded carbon fiber epoxy prepreg with thermoplastic film using the interpenetrating polymer network (IPN) mechanism with the co-consolidation technique in the presence of heat and pressure. Their results showed 45% improvement in single lap shear strength properties [8]. Most research has been conducted on thermoplastic and thermoset bonding using resistance welding, vibrational welding, and ultrasonic welding [9–12].

The widely used polymer systems for fusion bonding techniques are- poly(phenylene oxide) (PPO), poly(ethylene oxide) (PEO), phenoxy, poly(methylmethacrylate) (PMMA), poly(vinylpyrrolidone) (PVP), poly (ether ether ketone) (PEEK), polystyrene (PS), polycarbonate (PC)., Polyamide (PA), Polyetherimide (PEI), Polyethersulfone (PES), Polysulfone (PSU) with epoxy resin [13]. However, literature on fusion bonding of the thermoplastic urethane (TPU)

composites and thermoset urethane (TSU) composites is very limited. This work attempts to fill this gap in literature. The work is divided into three subcategories:-

a) Study of the effect different segments of TPU with unsized, epoxy and urethane sized TCF through compression molding technique.
b) Investigation of the molecular interaction at the interface of TSU with unsized, epoxy and urethane sized TCF using hand-layup method followed by the compression molding technique.
c) Evaluation of fusion bonding between TPU composites and TSU composites using compression molding technique.

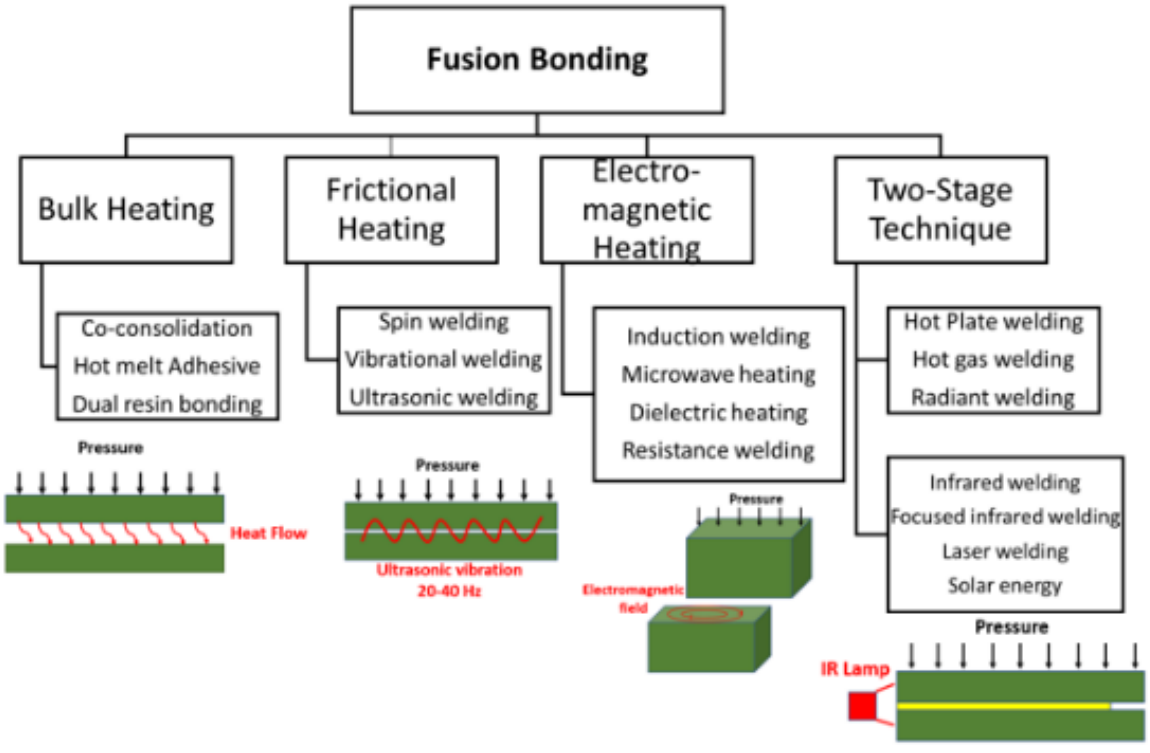

Figure 3.1: Classification of fusion bonding techniques used for laminate bonding [6]

a) Study the effect different segments of TPU with unsized, epoxy and urethane sized TCF through compression molding technique.

3.2 (a) EXPERIMENTAL

3.2.1 (a) Fabrication of TPU-TCF using compression molding

TCF-Un, TCF-E, and TCF-U were reinforced in S-TPU and H-TPU composite panels fabricated using the film stacking compression molding technique, explained in Figure 3.2. TCF-E was in non-crimped form, whereas TCF-U and TCF-UN were in tow forms. Eight layers of TCF mats were sandwiched between TPU films to produce a 3 mm thick panel. The sandwiched layup was placed in a 152 mm × 152 mm (6" × 6") tool (mold), and the assembly was placed in a Carver hot press (Model 3895). The panels were processed as follows. S-TPU at 160 °C and H-TPU at 170 °C under 4.2 MPa (611 Psi) pressure. Initially, the panel was dwelled for 120 mins at 0.2 MPa (28 Psi) to allow the resin to flow and penetrate through the TCF filaments. The pressure was applied at a 0.2 MPa/mins rate of up to 4.2 MPa and the dwell cycle was for 60 mins to improve the interfacial adhesion between TCF and TPU. Six panels were fabricated for each sizing system of TCF reinforcement (unsized, epoxy and urethane sizing) with two polymer systems such as S-TPU and H-TPU polymer for detailed analysis. Each panels nomenclature is described in Table 3.1.

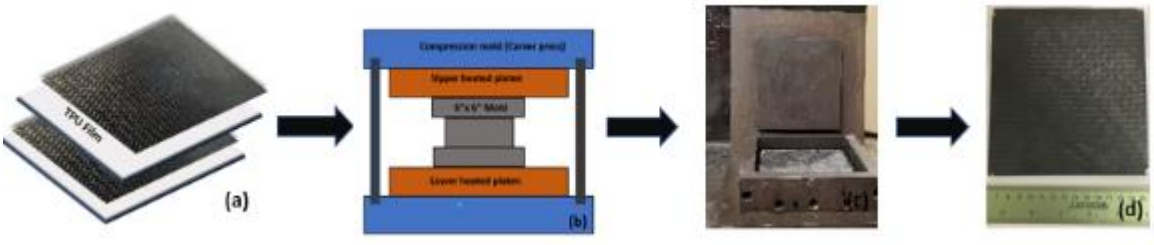

Figure 3.2: Schematic of fabrication of TCF-TPU laminates. (a) sandwiched TCF sheets and TPU films, (b) compression molding, (c) fabricated panel, (d) consolidated panel

Table 3.1: TPU composite panel nomenclature specifications

Nomenclature	Explanation
S-TPU-TCF-UN	S-TPU polymer reinforced in unsized TCF
S-TPU-TCF-E	S-TPU polymer reinforced in epoxy sized TCF
S-TPU-TCF-U	S-TPU polymer reinforced in urethane sized TCF
H-TPU-TCF-UN	H-TPU polymer reinforced in unsized TCF
H-TPU-TCF-E	H-TPU polymer reinforced in epoxy sized TCF
H-TPU-TCF-U	H-TPU polymer reinforced in urethane sized TCF

Characterization techniques:

Surface and thermal characterization techniques used in this work were explained in Chapter 2. The mechanical testing parameters are as follows:

3.2.2 Flexural testing

The flexural specimens were prepared according to ASTM D790-17 [14] and the testing was conducted using Test Resources Universal Testing Machine (UTM) machine (Model 313 series frame, MN) with a 50 kN load cell. The fixture had a 6 mm diameter loading nose and supports with a crosshead speed of 1.14-1.18 mm/ minute.

3.2.3 Impact testing

The Izod impact was performed according to ASTM D-256 [15] using Tinius Olsen (Model Impact 104) with loading capacity 22.6 J and 37 N pendulum weight to understand the material absorption capacity under impact loading. Five specimens for each formulation with dimensions 65 mm x 12.7 mm x 3 mm were prepared using a notch type A with a radius of 0.25 mm and notch angle of 45°. The average impact strength was calculated.

3.2.4 Tensile testing

Tensile specimens were prepared and tested according to ASTM D 3039-17. A servo hydraulic load frame with 22 kN load cell capacity was used. An extensometer (MST 634.11E-125) was mounted on each specimen. A crosshead speed of 2 mm/min was used.

3.2.5 Interlaminar shear strength

The interlaminar shear strength test was conducted according to ASTM D-2344 [16]. Five specimens were tested with a cross-head rate of 1 mm/minute on the Test Resources Universal Testing Machine (UTM) machine (Model 313 series frame, MN) equipped with a 50 kN load cell.

3.2.6 Contact angle measurement

The surface wettability of TCF-Un, TCF-E, TCF-U, and TSU resin was measured using the sessile drop method [17][31] at room temperature with a Glycerol ($\gamma d = 34$ mN/m, $\gamma p = 30$ mN/m) as a single liquid system. The size of the liquid droplet was 5 µL. The measurement was aided by the Image J software, and video-based contact angle instrument and software (VHX 600E, Keyence). Six specimens were tested per sample by mounting the fiber and matrix on a glass slab. The surface energy was evaluated by thermodynamic model of adhesion with Antonov's empirical rule. Equation 5 represents contact angle where Θ = equilibrium contact angle; surface energy of solid (mN/m); and = surface energy of the liquid (mN/m) [18].

$$\text{Cos}\ \Theta = (2\gamma_S/\ \gamma_L) - 1 \qquad [5]$$

3.2.7 Scanning electron microscopy (SEM)

Zeiss Auriga electron microscope was performed on the fracture surfaces of composites to evaluate the bonding mechanism. The fractured samples were coated with gold (SPI-MODULETM sputter coater, PA, USA) for 30 sec to improve the resolution of the micrographs. SEM was operated at 5 kV to characterize the interfacial adhesion of TCF surface.

3.3 (a) RESULTS AND DISCUSSION

3.3.1 Fourier transform infrared spectroscopy (FTIR)

The hydrogen bonding index (R) has been calculated for S-TPU and H-TPU composites with various sized TCF reinforcement. The percentage reactivity of hydrogen bonds between fiber and matrix is presented in Figure 3.3. The degree of phase separation (DPS) (equation 2 presented in chapter 2) is determined to evaluate the linkage between a two hard segments in the polymer. The degree of phase mixing (DPM) calculated the linkage between the hard and the soft segment within the polymers.

The R-value was found to increase with the hard segment content from 3 (S-TPU) to 7.6 (H-TPU), as shown in Figure 3.3, and Table 3.2. The DPS of H-TPU (0.88) is 17% higher than the S-TPU (0.75), indicating a large number of hard segment linkages in the H-TPU backbone. After the addition of TCF reinforcements, the hydrogen bonding indices of S-TPU-TCF-UN (3.48), S-TPU-TCF-E (3.55), H-TPU-TCF-E (7.9), and H-TPU-TCF-U (7.8) have increased significantly compared to pristine TPU. Dong et al. [19] stated that the molecular interaction at the fiber-matrix interface improves the R-value, contributing towards the enhancement of the mechanical performance. However, S-TPU-TCF-U and H-TPU-TCF-UN showed no changes in the R-value, indicating mechanical interlocking and no chemical bonding between the fiber and matrix. The R value of TCF-E, regardless of their hard and soft segment presence, increased by 18% and 4% in S-TPU and H-TPU, respectively. The higher R values for TCF-E composites explain the presence of a strong bonding between oxirane and urethane groups that may provide higher mechanical properties compared to TCF-UN and TCF-U.

Table 3.2: The hydrogen bonding index (R), degree of phase separation (DPS) and degree of phase mixing (DPM) of S-TPU and H-TPU reinforced in different sized TCF

Material	R value	DPS	DPM
S-TPU	3.0	0.75	0.25
S-TPU-TCF-UN	3.48	0.77	0.23
S-TPU-TCF-E	3.55	0.78	0.22
S-TPU-TCF-U	3.0	0.75	0.25
H-TPU	7.6	0.884	0.12
H-TPU-TCF-UN	7.60	0.884	0.12
H-TPU-TCF-E	7.90	0.888	0.11
H-TPU-TCF-U	7.80	0.886	0.12

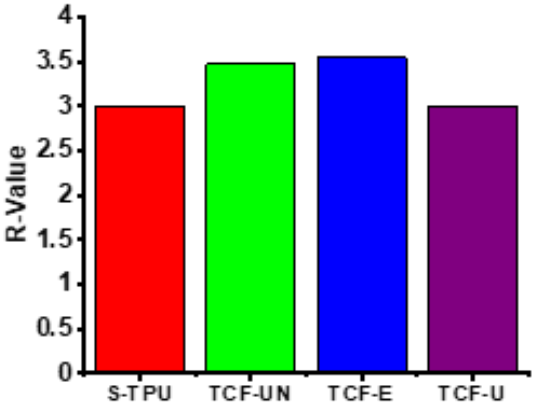

(a)

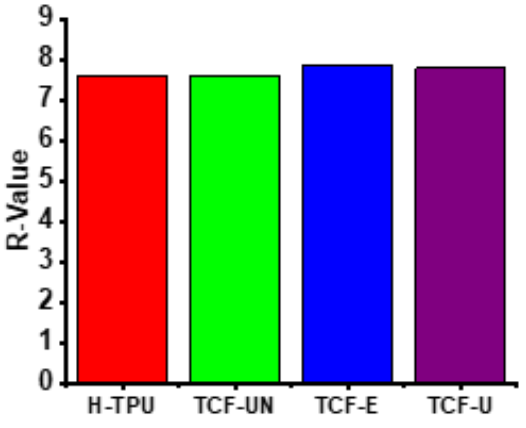

(b)

Figure 3.3: Hydrogen bonding index (R) of unsized (TCF-UN), epoxy sized (TCF-E) and urethane sized (TCF-U) TCF reinforced in (a) S-TPU and (b) H-TPU polymer. R value is increased with TCF-E reinforcement for S-TPU and H-TPU polymer

3.3.2 Dynamic mechanical analysis (DMA)

DMA was performed to understand the interfacial adhesion at the molecular level between various sized TCF and segmented TPU. The DMA data was evaluated in terms of storage modulus (E'), and tan δ. The E' at the glassy region (-100 °C) and tan δ of S-TPU and H-TPU composites are shown in Figures 3.4 and Figure 3.5. The glassy region temperature was used to understand the cross-link density (closed packed structure) of the polymer at the fiber interface, which directly relates to the storage and loss modulus. It can be observed that the E' of S-TPU and H-TPU increased for sized TCF. However, epoxy sized TCF reinforcement in both hard and soft segmented TPU showed a significant increment in stiffness compared to unsized and urethane sized TCF composites. The increase in the storage modulus of S-TPU-TCF-E (from 1.1 GPa to 89 GPa) compared to H-TPU-TCF-E (from 1.7 GPa to 4.3 GPa) was attributed to enhancing molecular interaction at the fiber and matrix interface by improving the stress transferability (stiffness) of the composite. As shown in Figure 3.5, there is no change in Tg observed after the addition of TCF. However, a noticeable reduction in the height of tanδ was noticed. The remarkable drop of tan δ was for S-TPU-TCF-E (from 0.44 to 0.33) and H-TPU-TCF-E (from 0.36 to 0.17) by 25% and 53%, respectively. Hassan et al. [20] stated that the decrease in tanδ peak height illustrates the strong fiber-matrix interaction at the interface. Hence, based on the authors analysis, epoxy sized TCF was interpreted to form a strong interface with segmented TPU. The DMA results correlate with the FTIR findings, where R value of epoxy-sized TCF with TPU (section 3.3.1) is higher than that of unsized and urethane-sized TCF reinforcements. Though the urethane-sized TCF has a similar chemical

structure with segmented TPU, it did not provide a strong fiber-matrix bond because the bond activation temperature requires for urethane sizing was 182°C, and the S-TPU and H-TPU panels processed <180°C. Increasing the processing temperature made it challenging to control the fiber orientation and matrix flow, which causes a reduction in the DMA and FTIR properties. Therefore, the mechanical characterization was performed on the epoxy-sized TCF and segmented TPU to validate the hypothesis further.

As shown in Figure 3.5, there is no change in Tg observed after the addition of TCF. However, a noticeable reduction in the height of tanδ was noticed. The remarkable drop of tan δ was for S-TPU-TCF-E (from 0.44 to 0.33) and H-TPU-TCF-E (from 0.36 to 0.17) by 25% and 53%, respectively.

Hassan et al. [20] stated that the decrease in tanδ peak height illustrates the strong fiber-matrix interaction at the interface. Hence, based on the authors analysis, epoxy sized TCF was interpreted to form a strong interface with segmented TPU. The DMA results correlate with the FTIR findings, where R value of epoxy-sized TCF with TPU (section 3.3.1) is higher than that of unsized and urethane-sized TCF reinforcements. Though the urethane-sized TCF has a similar chemical structure with segmented TPU, it did not provide a strong fiber-matrix bond because the bond activation temperature requires for urethane sizing was 182°C, and the S-TPU and H-TPU panels processed <180°C. Increasing the processing temperature made it challenging to control the fiber orientation and matrix flow, which causes a reduction in the DMA and FTIR properties. Therefore, the mechanical characterization was performed on the epoxy-sized TCF and segmented TPU to validate the hypothesis further.

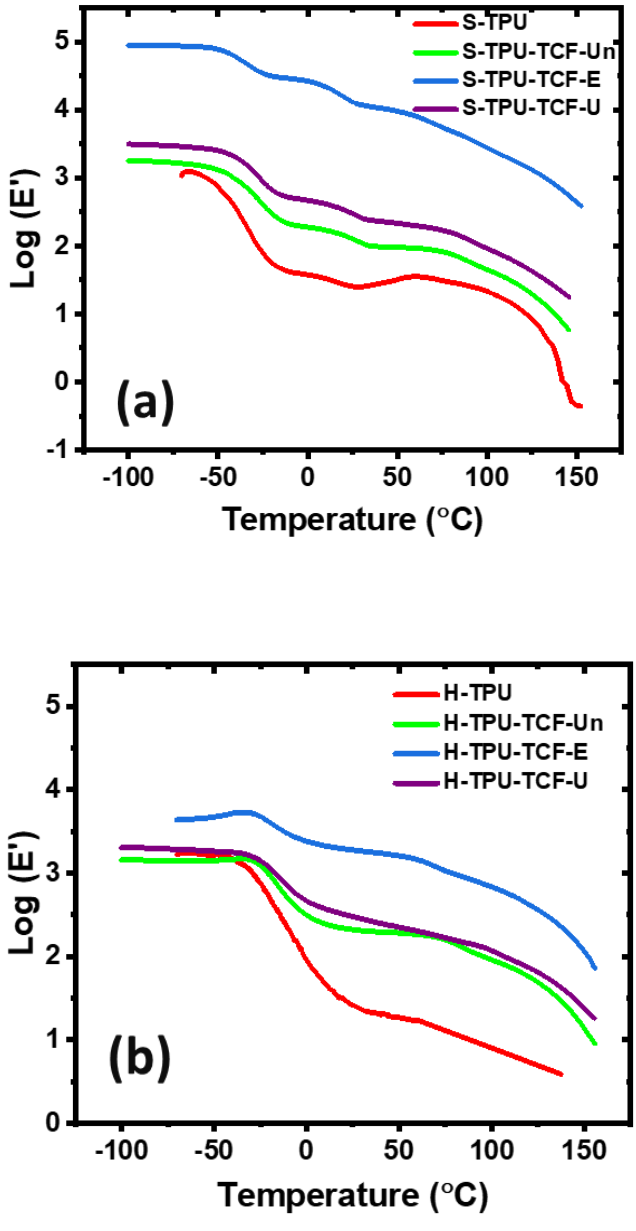

Figure 3.4: Storage modulus (E') of (a) TCF-Un, TCF-E and TCF-U reinforced in S-TPU, (b) TCF-Un, TCF-E and TCF-U reinforced in H-TPU at -100 °C as a function of temperature. Both S-TPU and H-TPU provided higher storage modulus with TCF-E reinforcement

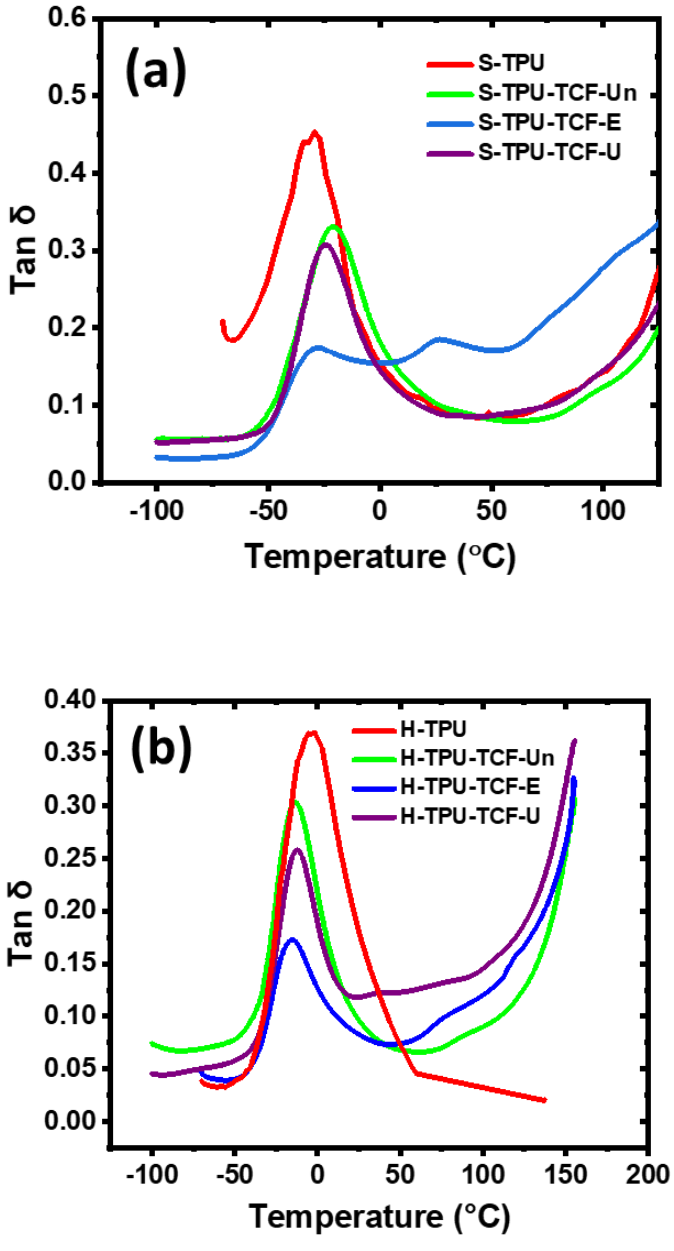

Figure 3.5: Tan δ of (a) TCF-Un, TCF-E and TCF-U reinforced in S-TPU, (b) TCF-Un, TCF-E and TCF-U reinforced in H-TPU at -100 °C as a function of temperature. Both S-TPU and H-TPU provided lowest Tan δ with TCF-E reinforcement with strong adhesion at the interface

Mechanical Characterization of TCF-TPU composites

3.3.3 Flexural properties

Flexural properties of epoxy-sized TCF reinforced in S-TPU, and H-TPU composites are presented in Figure 3.6. The typical stress-strain curve and the micrographs of the urethane composites are shown in Figure 3.7. The surface and thermal characterizations results obtained from XPS and DMA infer that the entanglement in the urethane segments significantly affects the flexural performance of TCF-TPU composites. The flexural strength increased by 30% from 69.72 ± 5.76 MPa to 90.86 ± 2.87 MPa. The stress-strain curve shows a notable difference in the failure behavior of TCF-PU composites that refers to the transition of elastic (S-TPU) to the rigid matrix (H-TPU). Also, the difference in the first failure for S-TPU (64.7 MPa) and H-TPU (85.2 MPa) is due to the cross-linked structure in the backbone, enhancing the load absorbing capacity of S-TPU composites. The improvement in the flexural strength indicates a high degree of interfacial adhesion between fiber and matrix. The flexural strength and modulus show a linear relationship with the molecular weight of TPU. The modulus showed a similar trend where H-TPU (9.8 ± 0.16 GPa) has higher stiffness than S-TPU (3.5 ± 0.9 GPa) composites. The failure modes of soft and hard segment composites showed a good wetting, strong interaction at the interface, and improved load transfer efficiency between fiber and matrix. Hence, it can be inferred that strong interface interaction increases failure resistance, and the results correlate with the XPS and DMA findings. Husic et al. observed the difference in the flexural properties for two-segmented TPU composites and explained that the higher CLD of the polymer provides higher flexural properties [46].

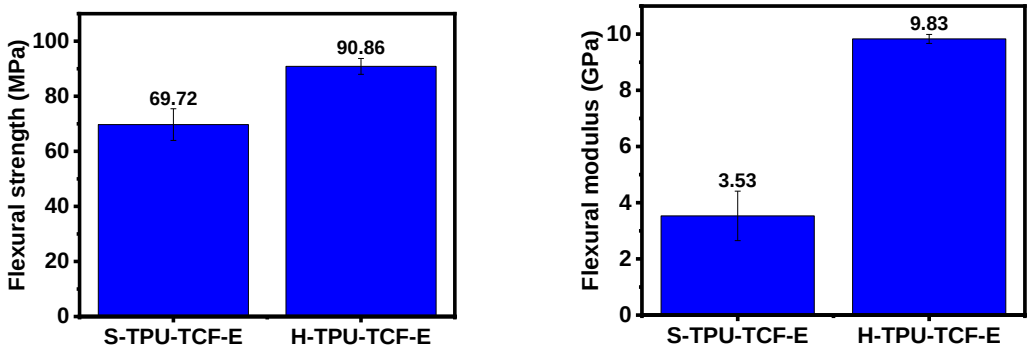

Figure 3.6: Flexural strength and modulus of TCF-TPU composites for S-TPU and H-TPU with TCF-E reinforcement

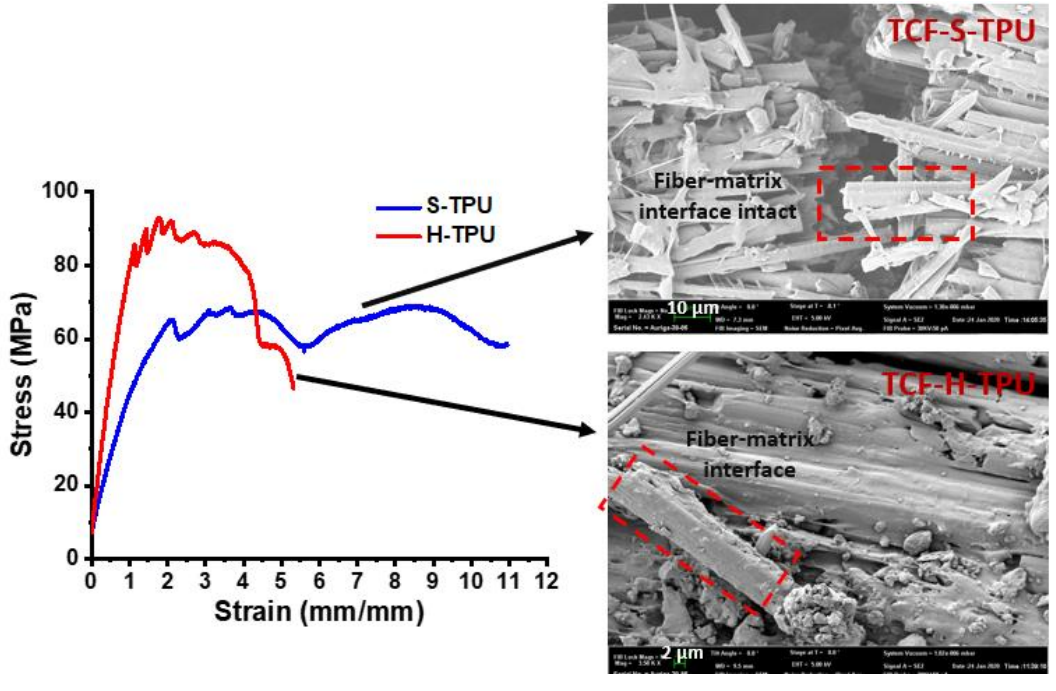

Figure 3.7 Stress-strain curve and SEM micrographs of fractured surface morphologies of TCF-S-TPU and TCF-H-TPU composites with 2 µm and 10 µm magnifications (right), demonstrating the interfacial adhesion of fiber and matrix

3.3.4 Impact properties

The effect of segmental chain difference on the dissipation energy of S-TPU and H-TPU composite is presented in Figure 3.8 [21]. The impact strength is generally correlated with flexural modulus; it measures the total impact energy absorbed during the flexural failure. Therefore, the trend of the impact strength is consistent with flexural properties. As shown in Figure 3.8, the impact strength results have increased by 50% from 107.4 ± 10.7 J/m (TCF-S-TPU) to 161.5 ± 17.9 J/m (TCF-H-TPU). The increase in the impact strength explains that H-TPU contains more polar groups in the urethane linkage that can absorb more energy by altering the structure and providing space for molecular movement in the network. These polar groups produced strong intermolecular interaction with epoxy-sized TCF through a covalent bond, which provides strong intermolecular forces and increases the impact strength of the composites. Hence the XPS data shows that H-TPU composites have a higher C=O content than S-TPU composites, enhancing the hydrogen bonding efficiency and significantly improving the impact strength of TCF-TPU composites [22].

3.3.5 Tensile properties

The tensile test on S-TPU and H-TPU composites was conducted using ASTM D 3039 to understand the effect of segmental motion in TCF-TPU composites. The trend of tensile properties is similar to the flexural and impact properties. The S-TPU and H-TPU showed improvement in the tensile properties after incorporating TCF that proves efficient load transfer between the fiber and matrix. As shown in Figure 3.9. the tensile strength of the TCF-H-TPU improved by 131% (from 61.2 ± 2 MPa to 141.4 ± 12.3MPa), and modulus increased by 313% (from 11.3 ± 2.4

GPa to 46.7 ± 8.2 GPa) than TCF-S-TPU composites. The tensile strength is driven by the fiber-matrix interaction and matrix stretching (strain hardening) [23]. Yang et al. [22] stated that hydrogen bonding contributes to enhancing tensile properties. Hence, H-TPU has a more hydrogen-bonded network, which helps to improve the tensile properties of the composites. The tensile properties of TCF-TPU are higher than the reported results [47–49]. Hence, the improvement of mechanical properties of H-TPU composites has a significant influence due to the multiple hydrogen bonding network between TCF and TPU.

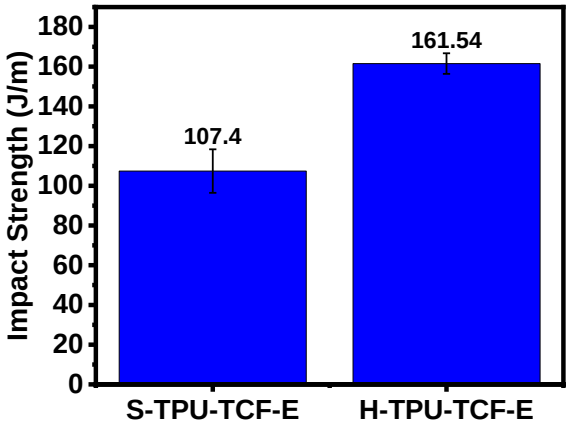

Figure 3.8: The Izod impact strength of S-TPU (161.50 J/m) and H-TPU (107.4 J/m) composites at room temperature

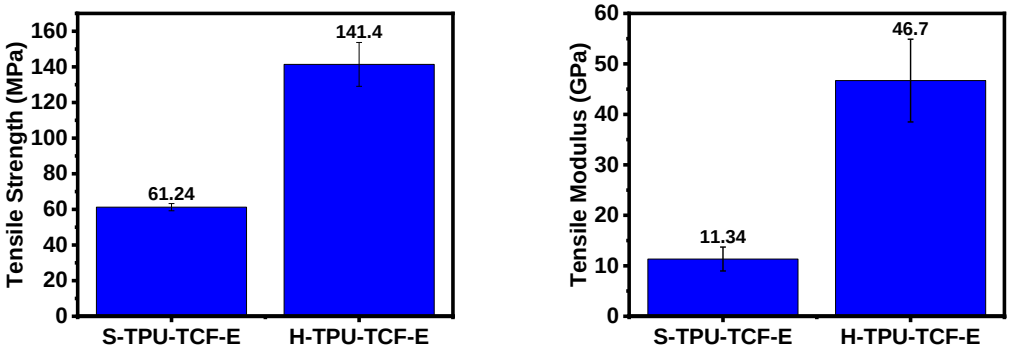

Figure 3.9: The ultimate tensile strength and modulus of TCF-S-TPU and TCF-H-TPU composites

3.4 (a) CONCLUSIONS

In this task, we have discussed the effect of unsized, epoxy, and urethane sized TCF on the interfacial bonding of soft and hard segmented polyurethane. The FTIR and DMA were performed on each composite, and the results showed that though there is similarity in the chemical structure, the urethane, and unsized TCF is not compatible with segmented TPU. The urethane sizing on the TCF surface requires 180 °C operating temperature to react with TPU. Due to the higher operating temperature, the control of the matrix and fiber flow becomes challenging, which causes a decrease in the storage modulus and tan delta values. However, epoxy sized TCF-TPU showed a significant difference in the DMA properties compared to other constituents. Hence, mechanical characterization was performed on epoxy sized TCF reinforced in S-TPU and H-TPU polymer. It was observed that the H-TPU composite possesses higher tensile, flexural, and impact resistance compared to S-TPU composites. Henceforth, TCF-H-TPU composite is used for a fusion bonding study [50]

b) Investigate the molecular interaction at the interface of TSU with unsized, epoxy and urethane sized TCF using hand-layup method followed by the compression molding technique.

3.5 (b) EXPERIMENTAL

3.2.1 Fabrication of TCF-TSU using hand-layup technique

TCF-E, TCF-U, and TCF-UN reinforced TSU laminates were fabricated using hand-layup method followed by a compression molding technique to achieve >60% fiber volume fraction in the consolidated panels. TSU (3:1 resin to hardener ratio) was stirred for 10 minutes to achieve a homogenous mixture. The resin was spread on fourteen layers of TCF fabrics. The TCF was either in a non-crimped fabric form referred to as 'C-ply' (TCF-E) and plate wrapped CF tow bundle (TCF-U and TCF-UN). The layup was designed in a symmetric laminate sequence $[0, 90]_{7S}$. A perforated release film (peel ply) was placed on the top of the fabric lay-up, and the entire setup was sealed with nylon 6 high temperature bagging material to evacuate trapped air. The assembly was placed in a Carver hot press (Model 3895-compression molding press) which has 305 mm × 305 mm (12" x12") heated platens operated at 180 °C, and 0.6 MPa (83 Psi) to achieve 50-60 wt. % fraction of TCF-TSU composite.

3.6 (b) RESULTS AND DISCUSSION

3.6.1 Contact angle measurement

The surface energy of TCF-Un, TCF-E, TCF-U, and TSU resin was calculated using Antonov's equation explained in the 3.2.6 section and the data presented in Table 3.3. TCF-Un showed the lowest surface energy (25.01 mN/m) due to

absence of functional groups on the TCF surface. Both epoxy and urethane-sized TCF showed 78% and 96% improvement in the surface energy. The difference in the data mainly contributed to the reactivity of epoxy (C=O) and urethane linkage (COONH) (as explained in the XPS section 2.3.2).

Jiao et al. [24] observed a similar trend, and stated that the polarity of the functional group enhances the surface energy of the CF due to the sizing chemistry. Their data coincided with the AFM results in that the polarity of sizing influences the surface roughness of TCF. The surface energy of TCF-U (49 mN/m) is similar to TSU resin (≈48 mN/m); hence it was concluded that the TSU provide strong wettability with TCF-U along with strong interfacial bonding. This enhances the mechanical properties of the TCF-U-TSU composites than unsized and epoxy sized TCF-TSU.

Table 3.3: Surface energy results of TCF fiber and TSU resin

Component	Contact angle (°)	Surface energy (mN/m)
TSU (resin)	60.88	47.57
TCF-UN	102.61	25.01
TCF-E	66.95	44.53
TCF-U	57.69	49.10

3.6.2 Thermogravimetric analysis (TGA)

Thermal stability, fiber content, and decomposition temperature have been analyzed using TGA under nitrogen atmosphere. Normalized TGA curves of epoxy, urethane and unsized TCF are presented in Figure. 3.10 and the percentage of weight loss data was studied. The unsized, epoxy, and urethane-sized TCF composites showed similar decomposition trends with one stage of weight loss, and the transition starts at the 215-300°C and the final transition observed at 600°C. During the thermal transition of TCF-TSU composites, three minor degradation steps were observed. The first step was observed at 305-358°C, indicating the separation of polyol and isocyanate. The second and third steps occurred in the range of 374-550°C which implies the formation of carbon dioxide [25]. The percentage weight loss for TCF-UN, TCF-E, and TCF-U composites is 59%, 68%, and 76%, respectively.

The difference in the fiber volume fraction is attributed to the difference in the sizing concentration. Wang et al. [26] stated that high fiber content enhances the mechanical strength and modulus of composite by restricting the molecular movement of the polymer through a strong hydrogen bonding network between fiber and matrix. It can be interpreted that the TCF-U can provide higher (due to an increase in 12% and 29% fiber content than TCF-E and TCF-UN, respectively) mechanical properties of the composites than TCF-E and TCF-UN.

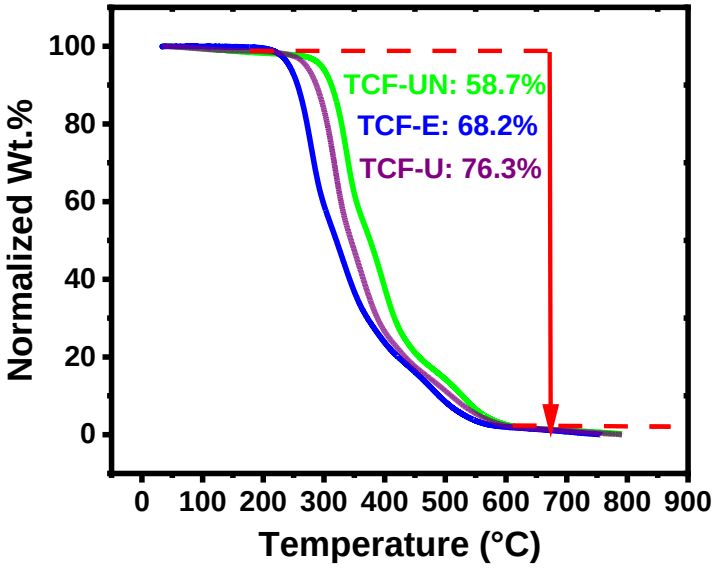

Figure 3.10: Normalized TGA curves of different sized TCF reinforced in TSU composites, (a) 59% fiber wt. fraction in TCF-UN, (b) 68% fiber wt. Fraction in TCF-E, (c) 76% fiber wt. Fraction in TCF-U

3.6.3 Dynamic mechanical analysis (DMA)

DMA was performed on unidirectional TCF-TSU composites specimens to evaluate the elastic stiffness and energy dissipation capacity through storage modulus (E') and tan δ of composites as a function of temperature, presented in Figure 3.11.

Keusch et al [27] stated that storage modulus is directly, and tan δ is inversely proportional to interfacial bonding of composites. The difference in the initial storage modulus (at –100 °C) after incorporating sized TCF indicates an improvement in the interfacial bonding of composites, Figure 3.11(a). As shown in Table.3.4, compared to TSU, the E' results of unsized, epoxy sized, and urethane sized TCF increases by 632.7%, 785.3%, and 800.0%, respectively. Edie et al. [28] reported that the fiber volume fraction (Vf) significantly affects the E' value.

Hence the damping factor curve was analyzed to understand molecular motion at the interface and quantifies the interfacial bonding of composite. The tan δ curve of TCF-UN, TCF-E, TCF-U reinforced TSU composites showed no remarkable difference in the T_g value, shown in Figure. 3.11(b). However, the damping behavior at the T_g of TCF-UN and TCF-E was observed to be higher than TCF-U. The differences in T_g indicates poor interfacial fiber-matrix bonding in TCF-E and TCF-UN composites. The tan δ values has decreased 2.2% from 0.2725 for TCF-UN to 0.2665 for TCF-E and 9.2% (0.2474) for TCF-U. A composite with strong interfacial bonding tends to restrict the motion of the molecular chain at the interface by providing less dissipation energy, which decreases the height of the tan δ peak [27]. Hence, urethane sized TCF composite has a strong interfacial bonding compared to epoxy and unsized TCF composite.

Table 3.4: Storage modulus (E'), tan δ and fiber volume fraction of TCF-TSU composites with epoxy and urethane sizing treatments

Material	E' MPa (at -100°C)	Tan δ	V_f
TSU	2704.1	0.4347	-
TCF-UN-TSU	19813.1	0.2725	50
TCF-E-TSU	23938.2	0.2665	60
TCF-U-TSU	24337.1	0.2474	69

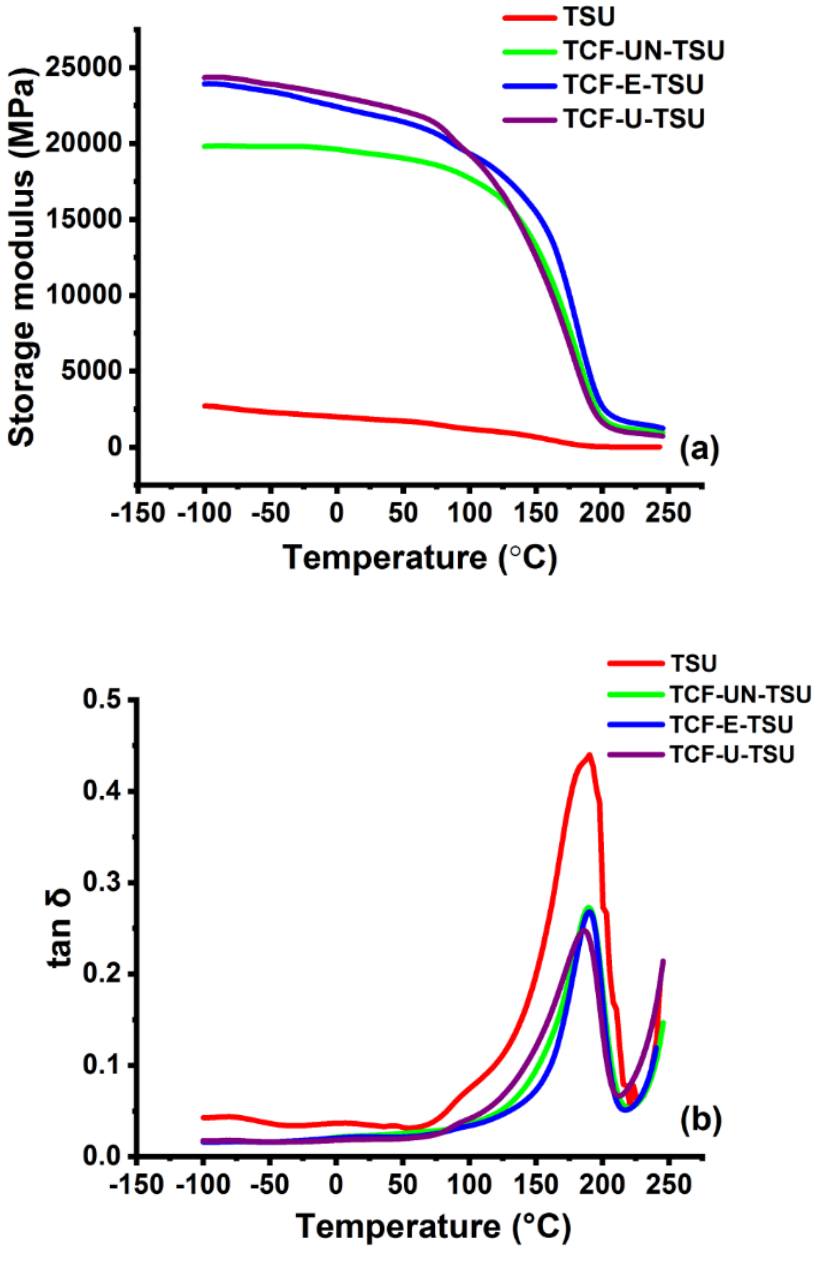

Figure 3.11: Dynamic mechanical characteristics of TSU (0.5 Hz) and TCF-TSU composites (at 1 Hz) with unsized, urethane and epoxy sizing on TCF surface: (a) the storage modulus, (b) damping factor (tan δ) as a function of temperature

3.6.4 Flexural properties

Flexural properties of unsized, epoxy, and urethane sized TCF reinforced TSU composites are presented in Figure 3.12. Based on the surface analysis of AFM and XPS, it can be inferred that the surface roughness in the urethane (polar groups) sizing enhanced the flexural strength of TCF-U composites compared to TCF-E and TCF-UN. The flexural strength increases by 24% and 7% from 482 ± 25 MPa of TCF-UN to 598 ± 77 MPa of TCF-U and 515 ± 66 MPa of TCF-E. The enhancement in flexural strength indicates excellent interfacial adhesion between fiber and matrix due to chemical interaction and reduces fiber pullout [29,30]. The strong interface between TCF-U and TSU might contributed to a hydrogen bond formation by a trans-urethanization reaction. In this reaction, the active functional group from sized TCF gets crosslinked with a reactive group of urethane polymer through intermolecular interaction. The hydrogen bond creates a bridge between fiber and matrix and enhances the flexural strength of the compounds [31,32]. Furthermore, the flexural strength of TCF-E is still higher than TCF-UN, either due to the mechanical interlocking or poor chemical interaction of epoxy and urethane linkages, which showed less increase in the properties. Flexural modulus is also presented in Figure. 3.12. The results showed a similar trend where TCF-U-TSU (58±6.2 GPa) has higher stiffness than TCF-E-TSU (50±1.2 GPa) and TCF-UN-TSU (38±1.2 GPa) composites. It can hence be inferred that that strong interfacial interaction increases failure resistance of TCF-U-TSU composites [5].

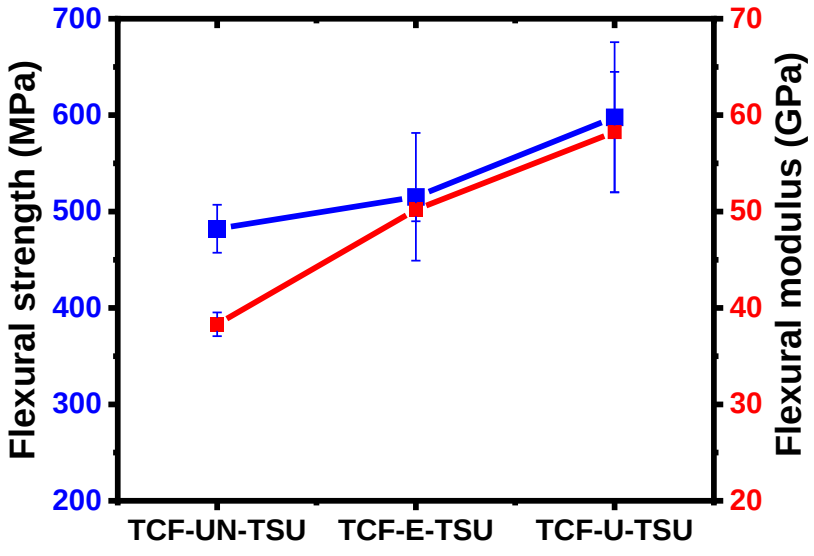

Figure 3.12: Flexural strength and modulus of unsized, epoxy and urethane sized TCF reinforced in TSU composites

3.6.5 Interlaminar shear strength (ILSS)

ILSS test was performed to understand the interfacial bonding between TCF-UN, TCF-E, and TCF-U with TSU polymer and the results compared with contact angle of each constituent presented in Figure 3.13. As shown in Figure 3.13, the ILSS results improved from 15 ± 0.9 MPa (TCF-UN) to 21.9 ± 3.7 MPa (TCF-E) (46%) due to epoxy sizing, which not only roughens the surface for mechanical interlocking, but also provides oxirane functional group to enhance the wettability between fiber and matrix. The TCF-U contributed largely to ILSS properties from 21.9 MPa to 32.09 ± 2.1 MPa with a 50% improvement. The data also showed an inversely proportional relation between contact angle and ILSS properties. Thus, the improvement in the strength confirms the presence of a chemical bridge between fiber and matrix that enhanced interfacial adhesion. This behavior of results correlated with the flexural properties of TCF-TSU composites. The obtained ILSS properties of TCF-U-TSU are higher in comparison to CF-epoxy composite [34] and glass fiber- MWNT-epoxy hybrid [35] composites.

The typical stress-strain curve reveals the different failure patterns of TSU composites. Two stages of failure were observed in ILSS for sized TCF composites. In the first stage, initial failure is attained with maximum stress at the interface and the failure transfer to the second stage. In the second stage, the crack induced with a slight decrease of load and propagated through the interface until it breaks completely. However, for unsized TCF, the ILSS curve breaks smoothly at the initial stage. Hence, the breakage illustrates that sizing protects crack transfer by enhancing fracture energy absorption capacity and effectively increasing interfacial bonding of urethane and epoxy sized composite.

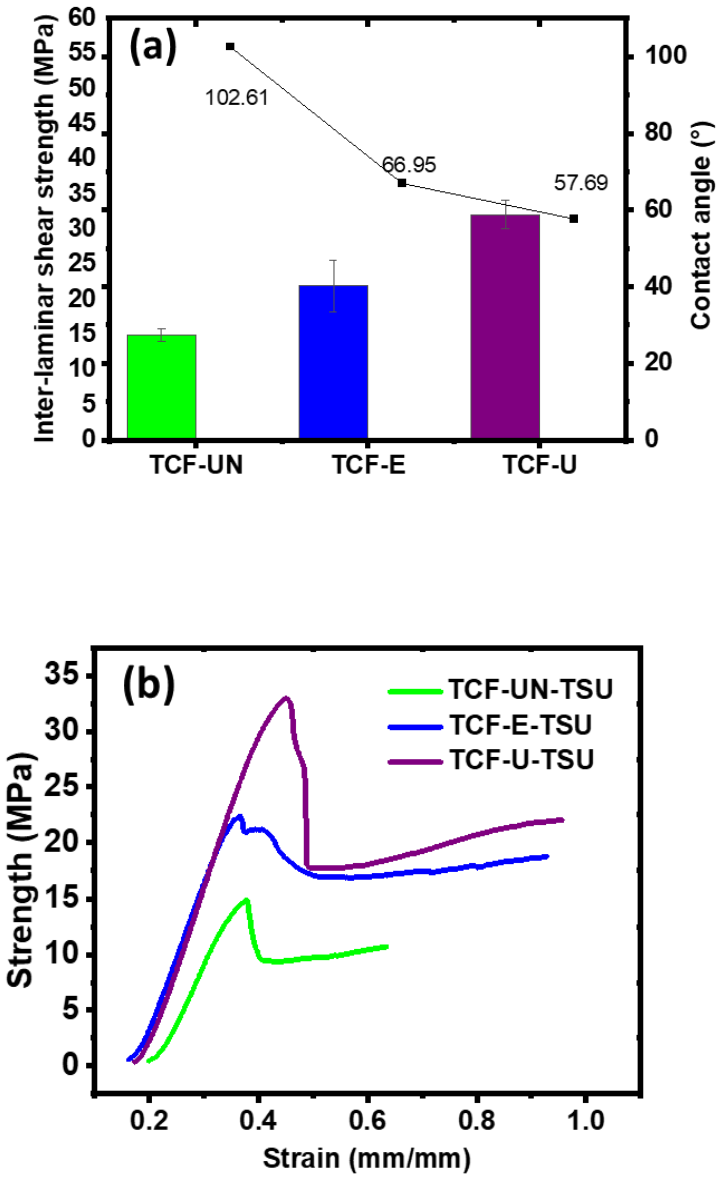

Figure 3.13: (a) Interlaminar shear strength and (b) typical stress strain curve of TCF-UN (15 MPa), TCF-E (21.9 MPa) and TCF-U (32.1 MPa) reinforced in TSU composites

3.6.6 Impact strength

Impact strength is the capacity of a material to dissipate the energy applied at high-rate loading [36]. Figure. 3.14 shows the impact strength of TCF-UN, TCF-E, and TCF-U reinforced TSU composites. The trend of impact strength is consistent with flexural and ILSS properties. As shown in Figure 3.14, the impact strength results improved from 29.1 ± 4.5 J/m (TCF-UN) to 63.1 ± 2.8 J/m (TCF-E) (116%) by epoxy sizing. Similarly, the impact strength of TCF-U improved by 170% from 29.1 J/m to 78.6 ± 14.8 J/m.

The urethane sizing significantly improved the toughness of the TCF reinforced composites by enhancing the interlocking efficiency at the fiber-matrix interface and allowed to increase the energy absorption capacity during impact loading [37]. Sizing provides efficient and effective resistance to crack propagation during impact loading due to strong interfacial adhesion in the composite.

The AFM findings suggest that the urethane sizing increases the groove's depth on the TCF surface compared to epoxy sizing and thus increases the surface roughness and surface energy (contact angle measurement) that enhances the wettability of TCF-U with TSU resin. The polar groups present on the TCF-U surface (XPS results) can have good interface adhesion with TSU than TCF-E due to similar molecular structure. Thus, the increase in the molecular interaction in the fiber and matrix can produce a strong hydrogen bond that enhances the interfacial strength. The strong interface helps to transfer stress uniformly from fiber to matrix and provides excellent mechanical strength of the composites. Therefore, all the characterization validated that TCF-U has higher mechanical properties than TCF-E and TCF-UN.

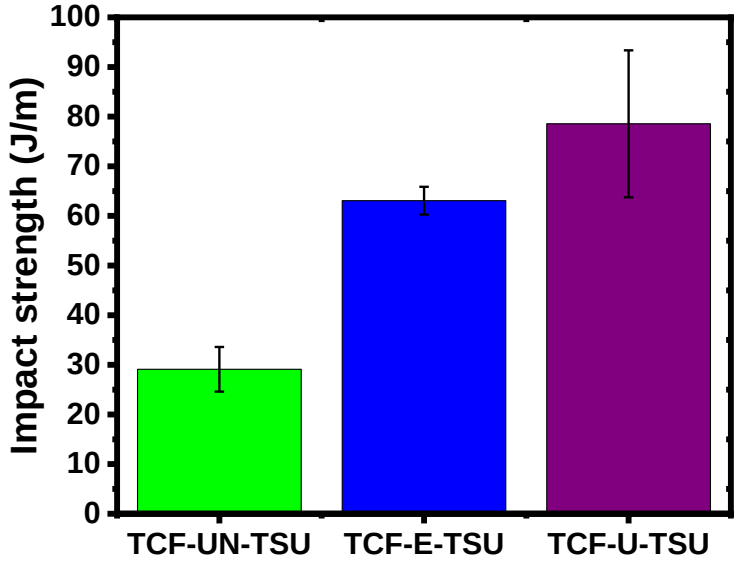

Figure 3.14: Izod impact strength of untreated (29.1 J/m), epoxy (63.1 J/m) and urethane sized (78.6 J/m) TCF-TSU composites

3.6.7 TCF's microstructure and surface morphology of fractured composites

The SEM micrographs are performed on untreated, epoxy and urethane sized TCF to understand the interfacial interaction of TCF with TSU. The fractured images of the flexural test are presented in Figure 3.15 (a-c), respectively. The unsized TCF (Figure 3.15 (a)) reveals a smooth surface with visible grooves parallel to the fiber axis. The micrographs also reveal less/no resin adhere to the TCF-UN surface, indicating the weak interface between fiber and matrix due to lower surface roughness (120 nm) that reduces the stress transfer from matrix to fiber, causing poor ILSS properties and eventually decreases the flex properties.

Figure 3.15 (b) shows the surface morphology of TCF-E, where a non-uniform coating of resin on the fiber was observed along with spindle size particles throughout the fiber length due to higher surface roughness (228.6 nm) compared to TCF-UN. This behavior is a result of chemical/mechanical interaction between urethane and epoxy groups that improves the mechanical properties of TCF-E-TSU composite. While in Figure 3.15 (c), superior fiber-matrix interaction was observed, and TCF-U had the highest surface roughness that is 457.6 nm, compared to other sized TCF, which may have contributed to improved bond strength. Furthermore, the micrograph of TCF-U shows a homogeneous distribution of polymer on the fiber surface that implies the crack induced during loading restrain the initial crack by absorbing intense energy. Additionally, sizing restricts the crack propagation and changes its direction by enhancing energy dissipation (DMA results) and provides the highest flexural and ILSS and impact properties in urethane sized TCF-TSU composite [38,39,46].

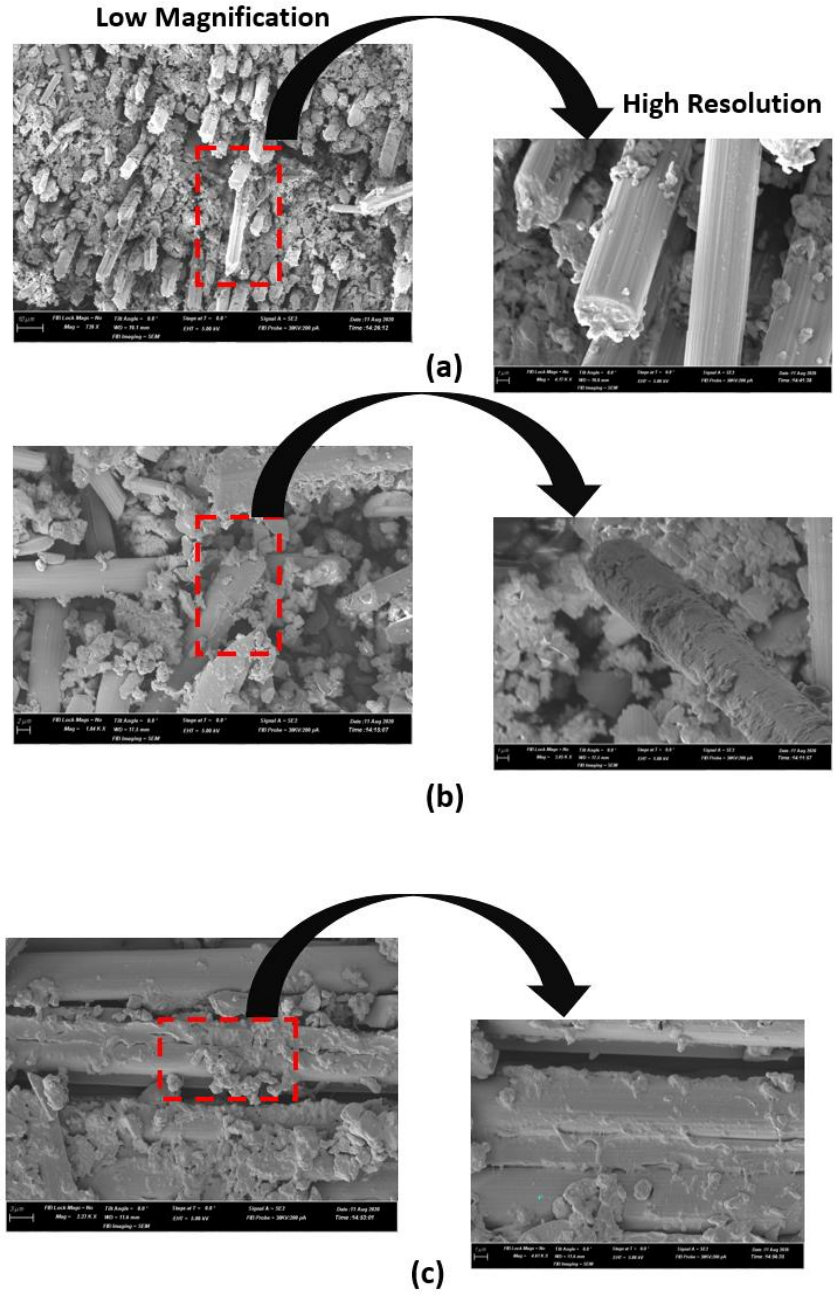

Figure 3.15: SEM micrographs of fracture surface morphologies for the TCF-TSU composites with epoxy, urethane and unsized surface sizing (a) TCF-UN-TSU, (b)TCF-E-TSU, (c) TCF-U-TSU at 4-10μm magnifications (left) and 1μm resolution (right). The matrix adherence increased for TCF-U than TCF-E and TCF-Un

3.7 (b) CONCLUSIONS

An efficient surface treatment method was used to enhance TCF-TSU composite interfacial bonding through epoxy and urethane sizing on the TCF surface to evaluate the mechanical properties of the composites. The surface energy results showed that TCF-U and TSU have similar surface energies, and capable of high degree of interfacial adhesion between fiber and matrix. Compared to unsized TCF, the damping factor of TCF-U-TSU and TCF-E-TSU decreased by 9.2% and 2.2 %, respectively. DMA results also reveal that TCF-U has a strong interface compared to TCF-E due to the similar molecular structure of TSU. Flexural and ILSS properties TCF-U-TSU composites enhanced by 24% (from 482±25 MPa to 515±66 MPa) and 50% (from 21.9±0.9 MPa to 32.09±2.1 MPa), for TCF-U and TCF-E, respectively, suggesting better interfacial adhesion between TCF-U-TSU respectively, compared to TCF-UN-TSU. AFM, XPS, DMA, contact angle, mechanical properties, and fractured micrographs correlated to each other, suggesting better interfacial adhesion of TCF-TSU composites using urethane sizing. TGA data reveals that the TCF-U-TSU composite can withstand up to 215°C, which can benefit high-temperature automotive and related applications. Hence, modifying the surfaces enhances the mechanical interlocking and chemical bonding and thereby improves mechanical properties of the TCF-TSU composites. The hypothesis proposed in Chapter 1 that urethane sized TCF is compatible with urethane system is validated through thermal and mechanical characterization. Hence for the fusion bonding study, TCF-U-TSU composite is used as a thermoset substrate to understand the bonding efficiency of thermoset composite to thermoplastic composites.

c) Evaluate the fusion bonding between TPU (TP) composites and TSU (TS) composites using Co-consolidation technique

3.8 (c) EXPERIMENTAL

3.8.1 Fabrication of fusion bonded TCF-TPU and TCF-TSU composites using compression molding technique

H-TPU-TCF-E and TCF-U-TSU composites were bonded through the co-consolidation method using the compression molding technique. During fabrication, no external adhesive has used because TPU film can act as an adhesive layer between TS and TP bonding. Pre consolidated TCF-TSU panels were placed in a 152 mm × 152 mm (6” × 6”) processing tool, and the eight layers of TCF mats were stacked in an alternate sequence, sandwiched between TPU films, presented in Figure 3.16. The assembly was placed in a Carver hot press (model 3895). This press uses 305 mm × 305 mm (12" x12") heated platens with a maximum temperature of 813 K (540°C) and a clamping force of 294.2 kN. The processing started at 180 °C at 0.19 MPa and was held for 90 mins to allow the resin to flow through the bond line and displace air and produce macromolecular chain entanglement at the interface. The pressure was ramped up gradually to 3.5 MPa at the rate of 0.15 MPa/min and held for 45 mins to improve the adhesion at the fiber-matrix interface.

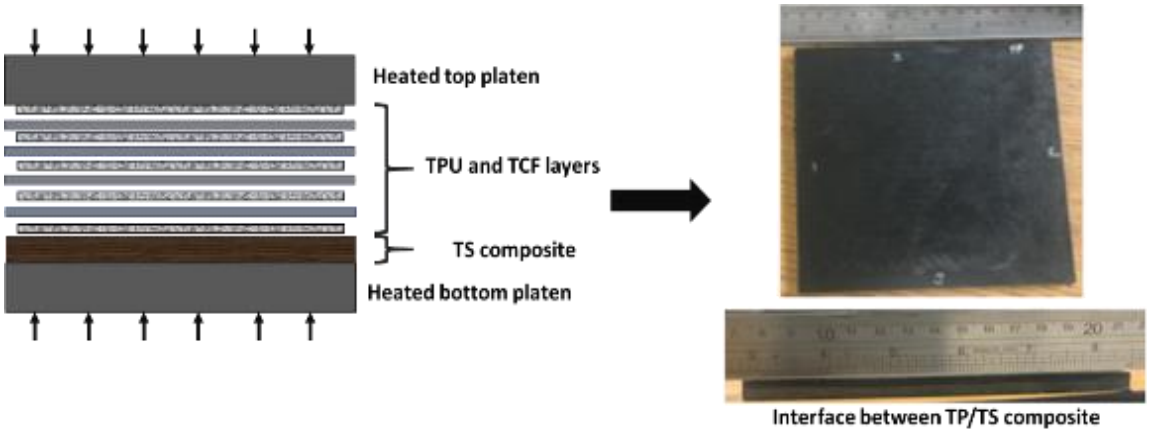

Figure 3.16: Schematic representation of TP and TS fusion bonding process using co-consolidation method

3.8.2 Sample preparation of fusion bonded TCF-TPU and TCF-TSU composites for lap shear test

The lap shear test specimens of TP and TS bonded composites were fabricated using a similar processing method as the co-consolidation process with slight modification in the technique. The top and bottom section of the TS composite panel were wrapped with Kapton tape. The center of the panel, i.e., 25.4 mm length, was unwrapped, and TP and TCF mats stacked alternatively using the same processing parameters as explained in section 3.8.1 (a) to produce a bond within 25.4 mm × 25.4 mm area with TP composite. The lap shear test specimens were prepared according to ASTM D5868-01 and tested using Test Resource frame ((Model 313 Series frame, MN) at crosshead speed of 13 mm/minute. The joined panel was cut into 152.4 mm × 25.4 mm, and three samples were tested.

Characterization techniques

3.8.3 Contact angle measurements:

The surface wettability of H-TPU-TCF-E and TCF-U-TSU was measured using Data Physics OCA 15 EC goniometer. Deionized (DI) water (γd = 19.9 mN/m, γp = 52.2 mN/m) and Diiodomethane (γd = 47.4 mN/m, γp = 2.6 mN/m) were selected as testing liquids. DI water is a highly polar solvent and Diiodomethane is a non-polar solvent used to measure the contact angle of TPU and TSU composites. The measurement was determined using a single direct dosing system SD-DM. The liquid dropping rate was 1 µL/sec up to 1.5 µL. The measurements were made on 25.4 × 25.4 mm^2 samples. For each specimen, a minimum of three drops were deposited using a microliter syringe, and the average value of contact angle is presented in Table 3.5. The contact angles of TPU and TSU composites was

measured using two testing liquids with known surface energies for the dispersive and polar components using Owens–Wendt method explained in equation 6 and 7 [40].

$$\gamma_L (1+\cos\Theta) = 2\sqrt{(\gamma_{Ld}\,\gamma_{cd})} + 2\sqrt{(\gamma_{Lp}\,\gamma_{cp})} \qquad [6]$$

$$\gamma_c = \gamma_{cd} + \gamma_{cp} \qquad [7]$$

where,

θ: the contact angle between composites and the testing liquid

γ: the surface tension (mN/m)

γ_d: the dispersive component (mN/m)

γ_p: the polar component (mN/m)

The subscript L and c stand for the liquids and composite respectively.

4.2.4 Mechanical characterization

All the mechanical testing performed as per the explanation provided in the section 3.2.1 (a)

3.9 RESULTS AND DISCUSSION

3.9.1 Contact angle measurement

The surface energy and the surface roughness of TSU and TPU composites were evaluated to understand the interfacial wettability between the materials. In both the samples, a large contact angle was observed with water that indicates the hydrophobicity, while low contact angle indicates the hydrophilicity of the surface. The surface energy values of TS are greater than TP composite, which illustrates the TS has a higher molecular attraction that can enhance the contact between TS and TP substrates.

For further understanding, the data is represented in Table 3.5. was used to quantify the binding strength at the interface of the composites. The Owens-Wendt method derived the following equations to determine the adhesion between two solids using a single liquid system [41].

$$\gamma_{TP/TS} = \gamma_{TP} + \gamma_{TS} - 2\,(\gamma_{TPd}\,\gamma_{TSd})^{0.5} - 2\,(\gamma_{TPp}\,\gamma_{TSp})^{0.5} \quad \ldots\ldots\ldots\ldots\ldots\ldots \quad (8)$$

$$\gamma_{TP/water} = \gamma_{TP} + \gamma_{water} - 2\,(\gamma_{TPd}\,\gamma_{waterd})^{0.5} - 2\,(\gamma_{TPp}\,\gamma_{waterp})^{0.5} \ldots\ldots\ldots \quad (9)$$

$$\gamma_{TS/water} = \gamma_{water} + \gamma_{TS} - 2\,(\gamma_{waterd}\,\gamma_{TSd})^{0.5} - 2\,(\gamma_{waterp}\,\gamma_{TSp})^{0.5} \ldots\ldots\ldots \quad (10)$$

$$W_{adh} = \gamma_{TP/water} + \gamma_{TS/water} - \gamma_{TP/TS} \quad \ldots\ldots\ldots\ldots\ldots\ldots\ldots\ldots\ldots\ldots\ldots\ldots \quad (11)$$

Where,

γ_{TP}: Surface energy of H-TPU-TCF-E composite

γ_{TS}: Surface energy of TCF-U-TSU composites

$\gamma_{TP/TS}$: Surface energy at the interface of TP and TS composite

$\gamma_{TP/water}$: Surface energy of H-TPU-TCF-E composite with water as a liquid system

W_{adh}: Work of adhesion of composite

The W_{adh} obtained for TP/TS bonding with water was 31.04 mN/m. Xiong et al. [42] explained that as the W_{adh} increases, the adhesive strength at the interface increases. Based on the author's findings, we can hypothesize that there is a strong interaction may present between TS and TP composites, which will provide a significant enhancement in the mechanical properties of the fusion bonded TP/TS composites. To support the given hypothesis, flexural, ILSS, and the lap-shear test is performed.

Table 3.5: Contact angle and surface energy of TPU

Specimens	Contact angle (Θ)		γ^d (mN/m)	γ^p (mN/m)	γ (mN/m)
	DI water	Diiodomethane			
H-TPU-TCF-E (TP)	81.7 ± 0.9	65.4±2.3	19.84	2.95	22.79
TCF-U-TSU (TS)	63.7 ± 0.5	58.0 ± 1.1	20.54	19.22	39.76

3.9.2 Flexural properties

The flexural behavior of TP/TS fusion-bonded composite specimens is presented in Figure 3.17. All the specimens were loaded from the TP side to achieve the appropriate load transfer within joined composites. The stress-strain curve of the fusion-bonded TP/TS composite is presented in Figure 3.18. The flexural strength of TP/TS composites is significantly increased by 295.3% (from 90.9 MPa to 359.3 MPa) than the TP composites and 40% lower (from 598 MPa to 359.3 MPa) than the TS composites. The decrease in the TS properties can be due to the processing temperature of fusion-bonded composites [43]. The increase in the flex strength of TP composites contributed to the higher surface energy of TS composites. During processing, the molten TPU interpenetrates across the TS surface and produces the molecular entanglement at the TP/TS interface; this molecular entanglement restricts the molecular motion by forming either a physical or chemical bond which enhances the strength of the TP composites [44]. Furthermore, the stress-strain showed the first laminate failure at 200 MPa on the TP side; that illustrates improved load absorption capacity of TP (from 90.9 MPa to 200 MPa) by 120% after the joining of the composites. The failure observed at the interface region shows the progressive behavior due to the ductility of TP composite and the crack transfer to TS. The first lamina in the TS region failed at 265 MPa, indicating brittle failure mode at 359 MPa. A similar failure behavior was observed with flexural modulus.

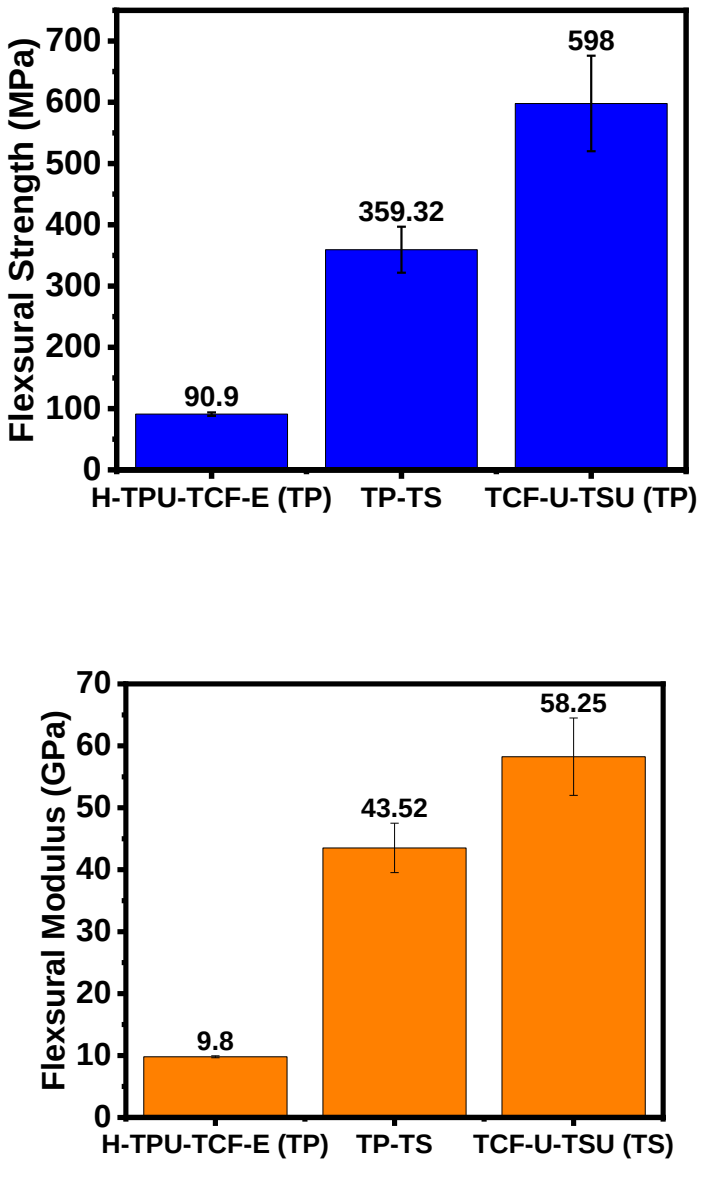

Figure 3.17: The flexural strength and modulus of TP/TS composite within comparison to TP and TS composites

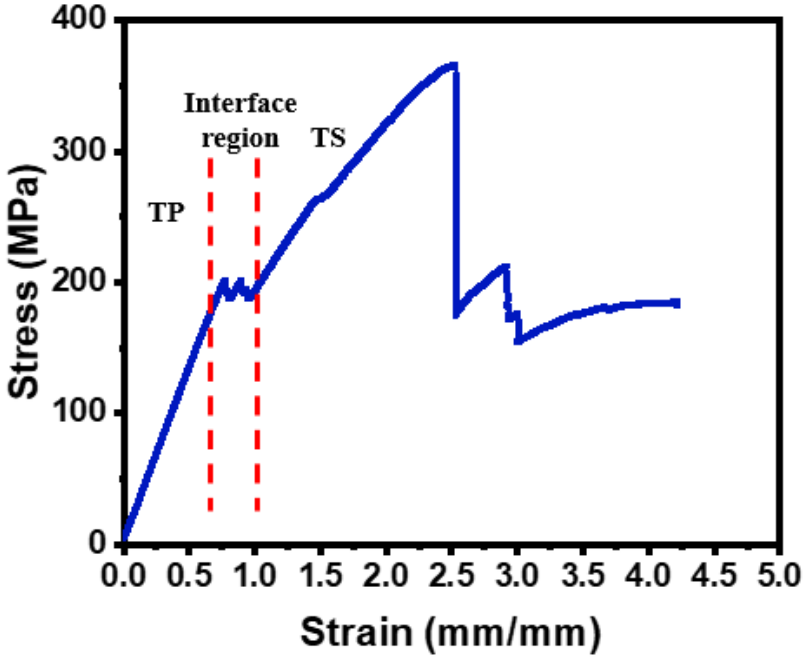

Figure 3.18: Typical stress-strain curve of fusion bonded TP/TS composites

3.9.3 ILSS properties

The ILSS properties are driven by the interaction at the interface of composites. The failure behavior of ILSS correlates to the flexural properties. The results showed an increase of 51% from 10.8 MPa to 16.3 MPa for TP composites, presented in Figure 3.19. Optical microscopy images were taken by a high-resolution optical digital microscope (Keyence VHX 7000). The fractured surface images of TP/TS bonded are presented in Figure 3.20. The micrograph showed that the delamination initiated from the TP side and propagated to the TS side, and a thin layer of TP is adhere to the TS layer. Hence, the results indicate that the adequate interfacial bonding presented between TP and TS contributed to the chemical interaction between TPU film and TS composites.

3.9.4 Lap shear strength properties

The lap shear strength was performed to understand the bonding strength between TP and TS substrates, presented in Figure 3.21. The resultant adhesion strength of joined composites is 7.6 ± 0.5 MPa. The results illustrate that with no external adhesive layer, the lap shear strength is enhanced by 21% compared to PA66/GF and epoxy/CF bonded composites with no treatment. The failure mode in TP/TS composite indicates good adhesion between bonded substrates [45]. The failure mode in TP/TS composite indicates good adhesion between bonded substrates. The high surface energy leads to a better spreading of the polymer at the interface and provides a more uniform contact with the substrate. Hence, the results correlate with the surface energy findings and state that the surface roughness and similar chemical groups enhanced the bond strength of the TP/TS composites by improving the mechanical properties of fusion-bonded composites.

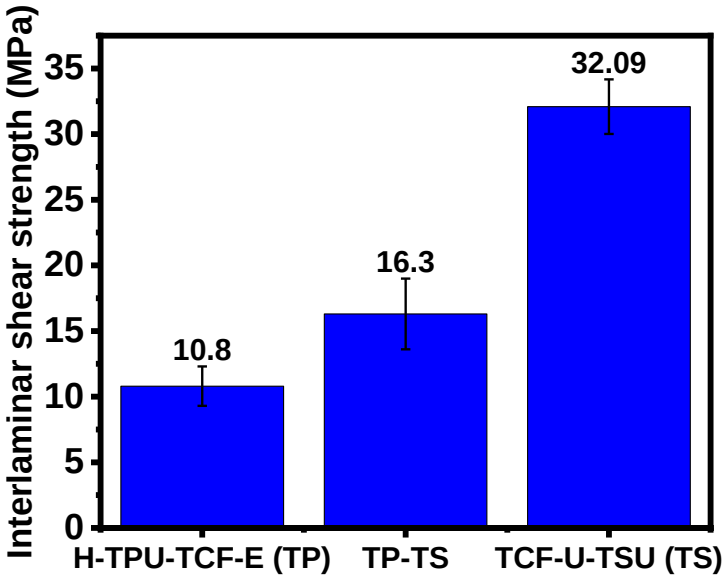

Figure 3.19: The ILSS properties of fusion bonded TP/TS composite in comparison with TP and TS composites

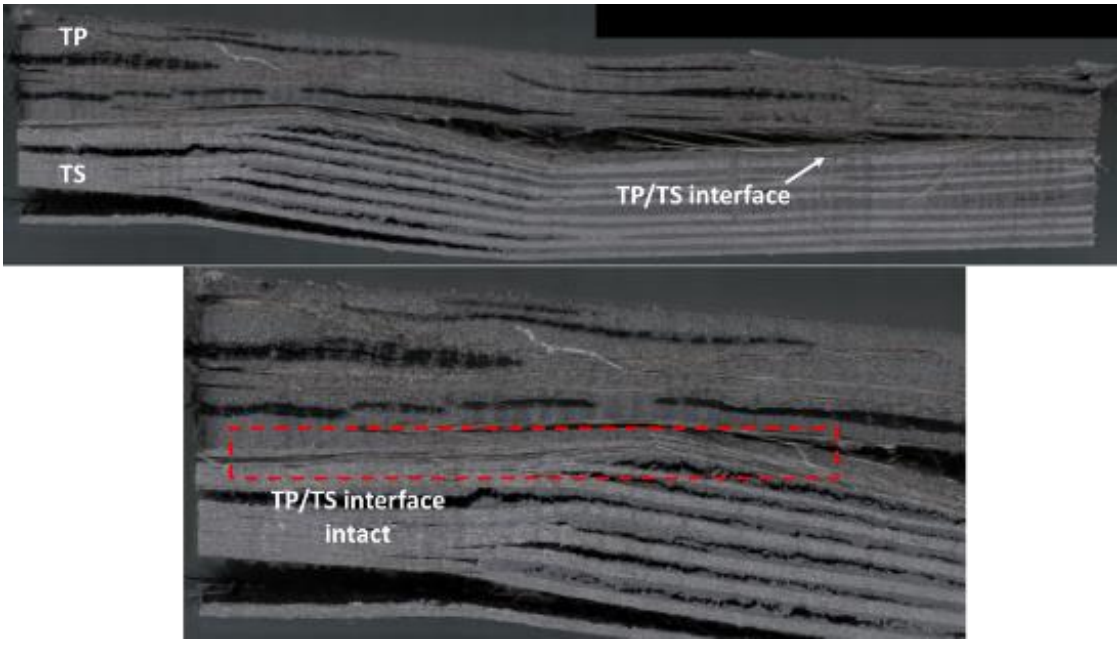

Figure 3.20: Optical micrographs of TP/TS composites at 200 µm magnification resolution

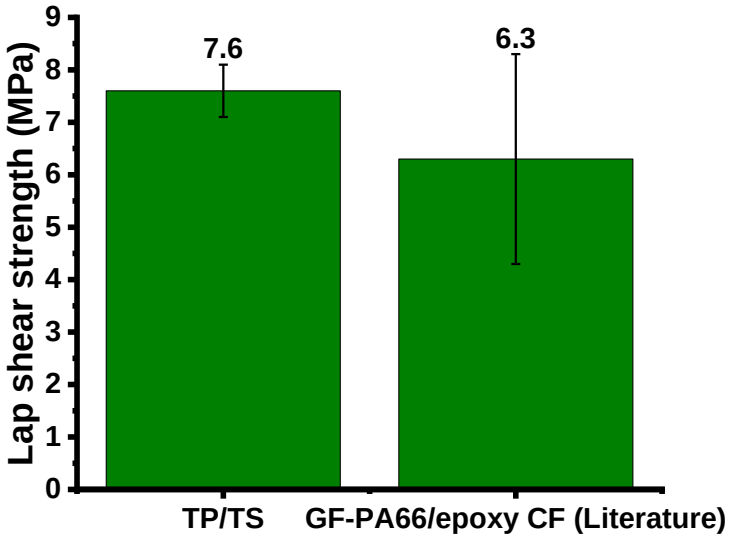

Figure 3.21: Comparison of lap shear strength of TP/TS composites with reported literature

3.10 (c) CONCLUSIONS

In this task, a co-consolidation method was explored to promote the adhesion between TP and TS composites without external adhesive. The surface energy achieved through contact angle measurement illustrates that TS has higher surface roughness than TP, which may enhance the bond strength of the composite. The work of adhesion at the interface of TP/TS composites ensures the strong bonding between two constituents. Thus, the surface analysis results confirm through flexural, ILSS, and lap shear strength. The data indicate that due to the increase in the surface energy, wettability between two dissimilar materials increases, improving the flexural and ILSS properties by 295% and 51%, respectively. Compared with the reported values, the lap shear strength was enhanced by 21%, confirming the strong interfacial bonding between TP and TS composites. The experimental data can be used in computational modeling (presented in Chapter 4) to understand the crack behavior at the micro and macro level.

REFERENCES

[1] R.L. Zhang, Y. Liu, Y.D. Huang, L. Liu, Effect of particle size and distribution of the sizing agent on the carbon fibers surface and interfacial shear strength (IFSS) of its composites, Appl Surf Sci. 287 (2013) 423–427.

[2] Y.D. Huang, R.L. Zhang, L. Liu, D. Su, A method of preparation the waterborne epoxy resin sizing agent for the carbon fiber, Pat CN 2010103001313. (2010).

[3] S.M. Goushegir, J.F. Dos Santos, S.T. Amancio-Filho, Friction spot joining of aluminum AA2024/carbon-fiber reinforced poly (phenylene sulfide) composite single lap joints: microstructure and mechanical performance, Mater Des. 54 (2014) 196–206.

[4] G. Zhao, T. Wang, Q. Wang, Surface modification of carbon fiber and its effects on the mechanical and tribological properties of the polyurethane composites, Polym Compos. 32 (2011) 1726–1733.

[5] F. Gnädinger, P. Middendorf, B. Fox, Interfacial shear strength studies of experimental carbon fibres, novel thermosetting polyurethane and epoxy matrices and bespoke sizing agents, Compos Sci Technol. 133 (2016) 104–110.

[6] C. Ageorges, L. Ye, M. Hou, Advances in fusion bonding techniques for joining thermoplastic matrix composites: a review, Compos Part A Appl Sci Manuf. 32 (2001) 839–857.

[7] J. Weber, J. Schlimbach, Co-consolidation of CF/PEEK tape-preforms and CF/PEEK organo sheets to manufacture reinforcements in stamp-forming process, Adv Manuf Polym Compos Sci. 5 (2019) 172–183.

[8] M. Hou, Thermoplastic adhesive for thermosetting composites, in: Mater Sci

Forum, 2012: pp. 2968–2973.

[9] C. Ageorges, L. Ye, Y.-W. Mai, M. Hou, Characteristics of resistance welding of lap shear coupons.: Part II. Consolidation, Compos Part A Appl Sci Manuf. 29 (1998) 911–919.

[10] C. Ageorges, L. Ye, M. Hou, Experimental investigation of the resistance welding of thermoplastic-matrix composites. Part II: optimum processing window and mechanical performance, Compos Sci Technol. 60 (2000) 1191–1202.

[11] C. Ageorges, L. Ye, Resistance welding of metal/thermoplastic composite joints, J Thermoplast Compos Mater. 14 (2001) 449–475.

[12] B. Harras, K.C. Cole, T. Vu-Khanh, Optimization of the ultrasonic welding of PEEK-carbon composites, J Reinf Plast Compos. 15 (1996) 174–182.

[13] S. Deng, L. Djukic, R. Paton, L. Ye, Thermoplastic--epoxy interactions and their potential applications in joining composite structures--A review, Compos Part A Appl Sci Manuf. 68 (2015) 121–132.

[14] I. ASTM, Standard test methods for flexural properties of unreinforced and reinforced plastics and electrical insulating materials, ASTM D790-07. (2007).

[15] A.A.S. for Testing, Materials, Standard test methods for determining the Izod pendulum impact resistance of plastics, ASTM international, 2010.

[16] D. ASTM, Standard test method for apparent interlaminar shear strength of parallel fiber composite by short beam method, Pennsylvania, USA. (2012).

[17] A. Alten, E. Erzi, Ö. Gürsoy, G.H. A\ugao\uglu, D. Dispinar, G. Orhan, Production and mechanical characterization of Ni-coated carbon fibers reinforced Al-6063 alloy matrix composites, J Alloys Compd. 787 (2019) 543–550.

[18] L.F.M. Da Silva, A. Öchsner, R.D. Adams, Handbook of adhesion technology, Springer Science \& Business Media, 2011.

[19] M. Dong, C. Wang, H. Liu, C. Liu, C. Shen, J. Zhang, C. Jia, T. Ding, Z. Guo, Enhanced solid particle erosion properties of thermoplastic polyurethane-carbon nanotube nanocomposites, Macromol Mater Eng. 304 (2019) 1900010.

[20] E.A.M. Hassan, L. Yang, T.H.H. Elagib, D. Ge, X. Lv, J. Zhou, M. Yu, S. Zhu, Synergistic effect of hydrogen bonding and $π$-$π$ stacking in interface of CF/PEEK composites, Compos Part B Eng. 171 (2019) 70–77.

[21] F.-L. Jin, S.-J. Park, Impact-strength improvement of epoxy resins reinforced with a biodegradable polymer, Mater Sci Eng A. 478 (2008) 402–405.

[22] J.-P. Yang, Z.-K. Chen, G. Yang, S.-Y. Fu, L. Ye, Simultaneous improvements in the cryogenic tensile strength, ductility and impact strength of epoxy resins by a hyperbranched polymer, Polymer (Guildf). 49 (2008) 3168–3175.

[23] B. Pukanszky, Influence of interface interaction on the ultimate tensile properties of polymer composites, Composites. 21 (1990) 255–262.

[24] W. Jiao, Y. Cai, W. Liu, F. Yang, L. Jiang, W. Jiao, R. Wang, Preparation of carbon fiber unsaturated sizing agent for enhancing interfacial strength of carbon fiber/vinyl ester resin composite, Appl Surf Sci. 439 (2018) 88–95.

[25] J.C.Q. Amado, Thermal Resistance Properties of Polyurethanes and Its Composites, in: Thermosoftening Plast, IntechOpen, 2019.

[26] F. Wang, M. Yang, S. Zhou, S. Ran, J. Zhang, Effect of fiber volume fraction on the thermal and mechanical behavior of polylactide-based composites incorporating bamboo fibers, J Appl Polym Sci. 135 (2018) 46148.

[27] S. Keusch, R. Haessler, Influence of surface treatment of glass fibres on the dynamic mechanical properties of epoxy resin composites, Compos Part A Appl Sci Manuf. 30 (1999) 997–1002.

[28] D.D. Edie, J.M. Kennedy, R.J. Cano, R.A. Ross, Evaluating surface treatment effects on interfacial bond strength using dynamic mechanical analysis, in: Compos Mater Fatigue Fract Fourth Vol, ASTM International, 1993.

[29] P. Kiss, W. Stadlbauer, C. Burgstaller, V.-M. Archodoulaki, Development of high-performance glass fibre-polypropylene composite laminates: Effect of fibre sizing type and coupling agent concentration on mechanical properties, Compos Part A Appl Sci Manuf. 138 (2020) 106056.

[30] C. Ozkan, N.G. Karsli, A. Aytac, V. Deniz, Short carbon fiber reinforced polycarbonate composites: Effects of different sizing materials, Compos Part B Eng. 62 (2014) 230–235.

[31] F. Schue, Transreactions in condensation polymers, Edited by Stoyko Fakirov. Wiley-VCH, 1999, pp 485, price£140 ISBN 3-527-29790-1, Polym Int. 49 (2000) 806–807.

[32] L.D. Agnol, H.L. Ceratti, D. Favero, S.P. Rempel, L. da S.A. Schiavo, J.R. Ernzen, F.T.G. Dias, O. Bianchi, Transurethanization reaction as an alternative for melt modification of polyamide 6, J Polym Res. 26 (2019) 112.

[33] K.S. Ahmed, S. Vijayarangan, Tensile, flexural and interlaminar shear properties of woven jute and jute-glass fabric reinforced polyester composites, J Mater Process Technol. 207 (2008) 330–335.

[34] Y. Wang, S.K. Raman Pillai, J. Che, M.B. Chan-Park, High interlaminar shear strength enhancement of carbon fiber/epoxy composite through fiber-and matrix-anchored carbon nanotube networks, ACS Appl Mater Interfaces. 9 (2017) 8960–8966.

[35] Z. Fan, M.H. Santare, S.G. Advani, Interlaminar shear strength of glass fiber reinforced epoxy composites enhanced with multi-walled carbon nanotubes,

Compos Part A Appl Sci Manuf. 39 (2008) 540–554.

[36] P.K. Mallick, Fiber-reinforced composites: materials, manufacturing, and design, CRC press, 2007.

[37] T. Yu, J. Ren, S. Li, H. Yuan, Y. Li, Effect of fiber surface-treatments on the properties of poly (lactic acid)/ramie composites, Compos Part A Appl Sci Manuf. 41 (2010) 499–505.

[38] M. Andideh, M. Esfandeh, Effect of surface modification of electrochemically oxidized carbon fibers by grafting hydroxyl and amine functionalized hyperbranched polyurethanes on interlaminar shear strength of epoxy composites, Carbon N Y. 123 (2017) 233–242.

[39] P.H. Thornton, Energy absorption in composite structures, J Compos Mater. 13 (1979) 247–262.

[40] W. Song, A. Gu, G. Liang, L. Yuan, Effect of the surface roughness on interfacial properties of carbon fibers reinforced epoxy resin composites, Appl Surf Sci. 257 (2011) 4069–4074.

[41] G.M. Kontogeorgis, S. Kiil, Introduction to applied colloid and surface chemistry, Wiley Online Library, 2016.

[42] H. Xiong, H. Zhang, J. Dong, Adhesion strength and stability of TiB2/TiC interface in composite coatings by first principles calculation, Comput Mater Sci. 127 (2017) 244–250.

[43] M. Abouhamzeh, J. Sinke, Effects of fusion bonding on the thermoset composite, Compos Part A Appl Sci Manuf. 118 (2019) 142–149.

[44] J.S.U. Schell, J. Guilleminot, C. Binetruy, P. Krawczak, Computational and experimental analysis of fusion bonding in thermoplastic composites: Influence of process parameters, J Mater Process Technol. 209 (2009) 5211–5219.

[45] J. Zhang, M. De Souza, C. Creighton, R.J. Varley, New approaches to bonding thermoplastic and thermoset polymer composites, Compos Part A Appl Sci Manuf. 133 (2020) 105870.

[46] S. Husić, I. Javni, Z.S. Petrović, Thermal and mechanical properties of glass reinforced soy-based polyurethane composites, Compos Sci Technol. 65 (2005) 19–25.

[47] S. Jiang, Q. Li, Y. Zhao, J. Wang, M. Kang, Effect of surface silanization of carbon fiber on mechanical properties of carbon fiber reinforced polyurethane composites, Compos Sci Technol. 110 (2015) 87–94.

[48] M.S. Sánchez-Adsuar, A. Linares-Solano, D. Cazorla-Amorós, L. Ibarra-Rueda, Influence of the nature and the content of carbon fiber on properties of thermoplastic polyurethane-carbon fiber composites, J Appl Polym Sci. 90 (2003) 2676–2683.

[49] Y. Zhang, Y. Zhang, Y. Liu, X. Wang, B. Yang, A novel surface modification of carbon fiber for high-performance thermoplastic polyurethane composites, Appl Surf Sci. 382 (2016) 144–154.

[50] S. Kore, M. Theodore, U. Vaidya, Effect of the Segmental Structure of Thermoplastic Polyurethane (Hardness) on the Interfacial Adhesion of Textile-Grade Carbon Fiber Composites, Applied Polymer Materials, 2021.

[51] Kore, S., Theodore, M., Pillai, R., Thomas, V., & Vaidya, U. (2021). Improvement of interfacial adhesion of unidirectional textile grade carbon fiber (TCF) with unsized, epoxy and urethane sizing reinforced in thermoset urethane composites. Materials Today Communications, 28, 102669.

Chapter 4.

THE EFFECT OF SIZING THICKNESS OF TEXTILE GRADE CARBON FIBER (TCF) ON THE INTERFACIAL PROPERTIES OF TCF-TSU COMPOSITE THROUGH FINITE ELEMENT ANALYSIS

ABSTRACT

The fiber-matrix properties are influenced by the structure of the polymer, surface treatment of the fiber, and interphase thickness. In chapters 2 and 3, the structural effect of S-TPU, H-TPU, and TSU with surface treatment of TCF is evaluated through the surface and thermal characterization. In this research, the effect of interface thickness on the interfacial strength and tensile properties of textile grade carbon fiber (TCF) reinforced thermoset laminate were examined through a combination of experimental and numerical simulation. Unsized, epoxy, and urethane-sized TCF with thermoset urethane (TSU) system were tested for tensile, compression, and in-plane shear according to ASTM D3039, ASTM D 3410, ASTM D 3518, respectively, in longitudinal and transverse directions. The experimental laminate properties were simulated through computational micromechanics theory using the Dehomogenized approach, which accounted for the fiber, matrix, and interface properties. The correlation of TCF-TSU interface thickness with fiber-matrix shear and tensile properties with respect to the matrix was assessed. The experimental and simulated results were compared to understand the interfacial adhesion behavior at the laminate level. The results showed that increasing interface thickness from 0.07 μm to 0.53 μm reduces the interfacial shear stress and improves the tensile strength and modulus by 1200% between interface and matrix.

Keywords: Interface thickness of TCF-TSU, Dehomogenized method, reverse engineering

4.1 INTRODUCTION

Chapters 2 and 3 explained the structural integrity of polymer composites and the three primary factors influencing the interfacial bonding - matrix, fiber, and interface [1]. The results showed that the chemical groups on the textile grade carbon fiber (TCF) surface (unsized (TCF-Un), epoxy (TCF-E), and urethane (TCF-U) sizing) reacts adversely with TPU and TSU polymer; where TPU showed higher compatibility with TCF-E and TSU showed good chemical interaction with TCF-U. Thus, in the overall studies, the chemical interaction at the interface of TCF-PU has been investigated.

After evaluating the two factors: structure of the polymer and the surface treatment of TCF on the interface; the third important factor that needs to be examined is the sizing thickness on TCF and its effect on the mechanical properties. Yao et al. [2] studied the optimization of interfacial microstructure and mechanical properties of carbon fiber-epoxy composites via carbon nanotube sizing. In this, work the authors applied multiple sizing layers on the carbon fiber surface and observed 13.45% and 20.31% improvement in interlaminar shear strength and flexure strength respectively of the composites than those with unsized fibers [2]. Braginsky et al. [3] studied the alteration of the interphase thickness effect on the crack propagation of fiber-reinforced ceramic composites using the extended finite element model (FEA) method.

There are various analytical approaches (using finite element modeling (FEM) tools) related to interface tailoring, which are based on single fiber pullout, fiber push out, single fiber fragmentation method, and micro-indentation method [1,4–6]. Mishnaevsky [7] studied the effect of the nanostructured interface on the

mechanical properties of the composites through a computational micromechanical approach. The author observed that the fiber sizing controls the local deformation and damage initiation at the interface and enhances material stiffness. Wang et al. [8] examined the effect of heterogenous interphase on the mechanical properties of unidirectional fiber composites. The authors studied the relationship of fiber volume fraction and interphase properties distribution on the failure mechanism of composites at a constant interphase thickness (5 μm). The results showed a strong interaction at 5 μm thickness compared to zero interphase thickness. Singh et al. [4] designed a finite element model using cohesive zone modeling (CZM) to study the fiber-matrix interface using glass fiber. The results showed that the continuous coating on the fiber surface exhibited 300% higher load-bearing than the discontinuous coating.

For the micromechanical analysis, researchers have used the Asymptotic Homogenization Method (AHM), Equivalent Inclusion Method (EIM) followed by finite element analysis (FEA) model, homogenization-based continuum damage mechanics (HCDM), and parametrically homogenized continuum damage mechanics (PDCDM) [9–11]. Thus, there are two fundamental challenges while considering these analytical techniques – 1) conducting a microscale and nanoscale experiment, and 2) designing a model for anisotropic composite materials [9,12]. An unique technique is explained by Minnetyan et al. to overcome the challenges, where the authors evaluated the fiber-matrix interface of the composites using a dehomogenization approach through Hierarchical progressive failure analysis (HPFA) [13]. In this approach, the HPFA model automatically generates a new finite element mesh at the unit cell to predict the deformation and

damages in the composite using laminate properties for continuous and discontinuous reinforcements [14].

Hence, in this work, the dehomogenized approach is used to evaluate the effect of the sizing thickness on the interface of TCF reinforced composites using GENeral Optimization Analyzer (GENOA) software. The work compared the simulated results with experimental findings on the laminate level. The fiber and matrix properties are extracted from unsized TCF-TSU laminates by performing tensile, compression, and in-plane shear testing. The simulated TCF and TSU properties obtained from the reverse engineering concept were used to investigate the relationship between sizing thickness and the adherence between interface and TSU.

4.2 Mechanism of Dehomogenized method

In this method, fiber, matrix, and interface properties are extracted by incorporating the mechanical properties of composite laminates using the reverse engineering method from Material Characterization and Qualification (MCQ) software [15] as explained in Figure 4.1. The MCQ method generates FEA analysis by creating a model of stress-strain behavior using the macroscale properties and subdividing into a unit cell approach where the matrix surrounds the fiber. The mechanism behind the approach is that GENOA creates a new mesh to replicate the failure mode of the input data at each time of load increment [16]. The stresses and strains at the micro-level are obtained from the lamina scale using micro-stress theory. There are various steps involved to perform the simulations, which are as follows: 1) fiber-matrix calibration using laminate properties; 2) micro stress determination designing a damage/ failure criteria for linear and non-linear failure mode; 3) ply

mechanics using two anisotropic laminae, where the fiber and matrix crack is examined under tensile (0° and 90°), compression (0° and 90°), and in-plane shear mode (±45°) (the significance of the each test method is presented in Table 4.1) The fiber and matrix properties obtained from previous steps are incorporated into the progressive failure mode (PFA), and the data is altered using interphase properties. The overall outcome of the work is to input the effective fiber-matrix properties to determine the stress, strain, damage, and failure modes in the ply at the laminate level.

4.2.1 Failure mechanism in the PFA

The failure mechanism is conducted considering the local coordinate orientation in the loading direction to capture failure within the unit sub-volume. Thus, several failure criteria were investigated in tension, compression, and in-plane shear direction through micromechanical analysis using the following equations used from [14], where m and f represent matrix and fiber, and S, V, and E stands for strength, volume fraction, and modulus, respectively.

For longitudinal tensile strength (S_{11T})

$$S_{11T} = S_{f11} (E_{f11} V_f + V_m E_m) \quad [12]$$

For transverse tensile strength (S_{22})

$$S_{22T} = [1- ((V_f)^{0.5} - V_f) (1- E_m/ E_{f22})] S_m [1- (4 V_v / 3.14 (1- V_f))^{0.5}] \quad [13]$$

For longitudinal compressive strength (S_{11C})

1) Fiber crushing mode (c):

$$S_{11cc} = S_{f11c} (E_{f11} V_f + V_m E_m) \quad [14]$$

2) Fiber delamination mode (d)

$$S_{11cd} = 10 S_{12} + 2.5 S_m [1- (4 V_v / 3.14 (1- V_f))^{0.5}] \quad [15]$$

3) Fiber buckling mode (b)

$$S_{11cb} = [Gm (1- (4 V_v / 3.14 (1- V_f))^{0.5})]/ [(1- V_f (Gm (1- (4 V_v / 3.14 (1- V_f)/ G_{f12})^{0.5} \quad [16]$$

For transverse compressive strength (S_{22C})

$$S_{22C} = [1- ((V_f)^{0.5} - V_f) (1- E_m/ E_{f22})] S_m [1- (4 V_v / 3.14 (1- V_f))^{0.5}] \quad [17]$$

For in-plane shear strength (S_{12})

$$S_{12} = [1- ((V_f)^{0.5} - V_f) (1- G_m/ G_{f12})] S_m [1- (4 V_v / 3.14 (1- V_f))^{0.5}] \quad [18]$$

This approach examines five mechanical properties, such as tensile, compression, and in-plane shear according to ASTM D3039, ASTM D 3410, ASTM D 3518, respectively. The experimental mechanical characterization of TCF-TSU for unsized, epoxy, and urethane sizing are presented in Table 4.2. The results showed a 30% higher tensile strength of TFC-Un than TCF-E and TCF-U composites. Madhukar et al. [17] studied the adhesion between graphite/ epoxy composites through tensile and flexural properties in longitudinal and transverse direction. The author stated that fiber dominates the longitudinal tensile strength, whereas fiber-matrix adhesion strongly influences the transverse direction. TCF-TSU mechanical properties correlate with the authors' findings stating that TCF-E and TCF-U showed comparable transverse tensile (700% higher) strength than TCF-Un. The longitudinal tensile strength of TCF-TSU showed no influence of sizing and the interface of the composites. Thus, to understand the micromechanics at the interface of TCF-TSU composites.

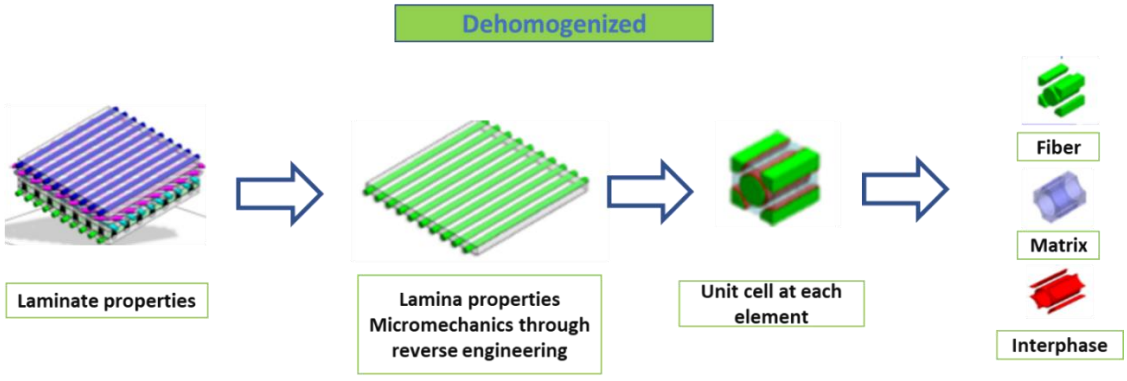

Figure 4.1:De-homogenized microscale method for fiber-matrix interphase (a) experimental mechanical properties of laminates; (b) extract lamina properties using reverse engineering; (c) convert lamina properties to representative volume element (RVE) model (d) slice unit cell to produce fiber, matrix and interphase properties [16]

Table 4.1: Purpose of performing mechanical characterization on unsized, epoxy and urethane sized TCF composites [16]

Mechanical Test	Purpose
Longitudinal tensile	Failure mode is controlled by fiber properties
Transverse tensile	Failure is controlled by matrix properties
Longitudinal compression	Fiber matrix delamination under fiber micro-buckling and fiber crushing failure behavior
Transverse compression	Failure behavior is controlled by matrix cracking, matrix tensile strength, matrix modulus and fiber volume ratio
In plane shear	Failure occurs at the fiber matrix interface sue to shearing

Table 4.2: The experimental mechanical properties unsized, epoxy and urethane sized TCF composites

Specimens	Tensile (0°) (MPa/GPa)	Tensile (90°) (MPa/GPa)	Compression (0°) (MPa/GPa)	Compression (90°) (MPa/GPa)	In-plane shear (MPa)
TCF-Un	636.37/114.77	1.76/1.95	439.18/267.9	39.66/15	28.45
TCF-E	448.69/118.85	13.86/3.51	-	-	49.86
TCF-U	561.92/101.29	14.5/4.28	-	-	40.8

4.2.2 Effective TCF and TSU properties using reverse engineering mechanism

Five ASTM standard tests were conducted for unsized TCF-TSU data for fiber-matrix calibration, presented in Table 4.2. The volume fraction of unsized TCF-TSU, TCF, and TSU properties was used to predict the results. The fiber, matrix, and void content values are modified from the input section to improve the correlation between calibrated and experimental results. The calibrated properties are presented in Table 4.3, and the stress-strain curve with each ASTM standard is presented in Figure 4.2. The effective properties achieved through the reverse engineering method showed less variation (0.1-2%) in the tensile and compression properties. Thus, the properties obtained through simulation provided Poissions ratio (v_{12}) in planes 1 and 2 and shear modulus data with greater accuracy. The effective stress-strain curve is further validated and adjusted using linear and non-linear failure mode by tailoring the damage/fracture criteria. In this criteria, the failure mode is evaluated using lamina and laminates properties. Hence, the effective fiber and matrix properties are presented in Table 4.4. The interface is modeled for 0.07 μm interface thickness to represent the zero-thickness at the interface to improve the accuracy of the effective properties. Thus, effective fiber-matrix properties are used to tailor the interface thickness and understand its effect on the mechanical properties.

Table 4.3: Comparative properties of calibrated unsized TCF-TPU composite generated using experimental results

Properties	Units	Experimental	Effective	% difference
Fiber vol. fraction	%	63.48	64.05	0.9
E11 (longitudinal modulus of fiber)	GPa	182	182.49	0.27
Em (Youngs modulus of matrix)	GPa	0.616	0.6288	2.08
E11	GPa	114.77	114.78	0.01
E22	GPa	2.87	2.87	0.0
G12	GPa	0.5213	0.5213	0.0
Nu12		0.28	0.2799	-0.0
S11T	MPa	636.37	636.37	0.0
S11C	MPa	396.9	396.9	0.0
S22T	MPa	2.2	2.2	0.0
S22C	MPa	39.66	39.66	0.0
S12S	MPa	28.45	28.45	0.0

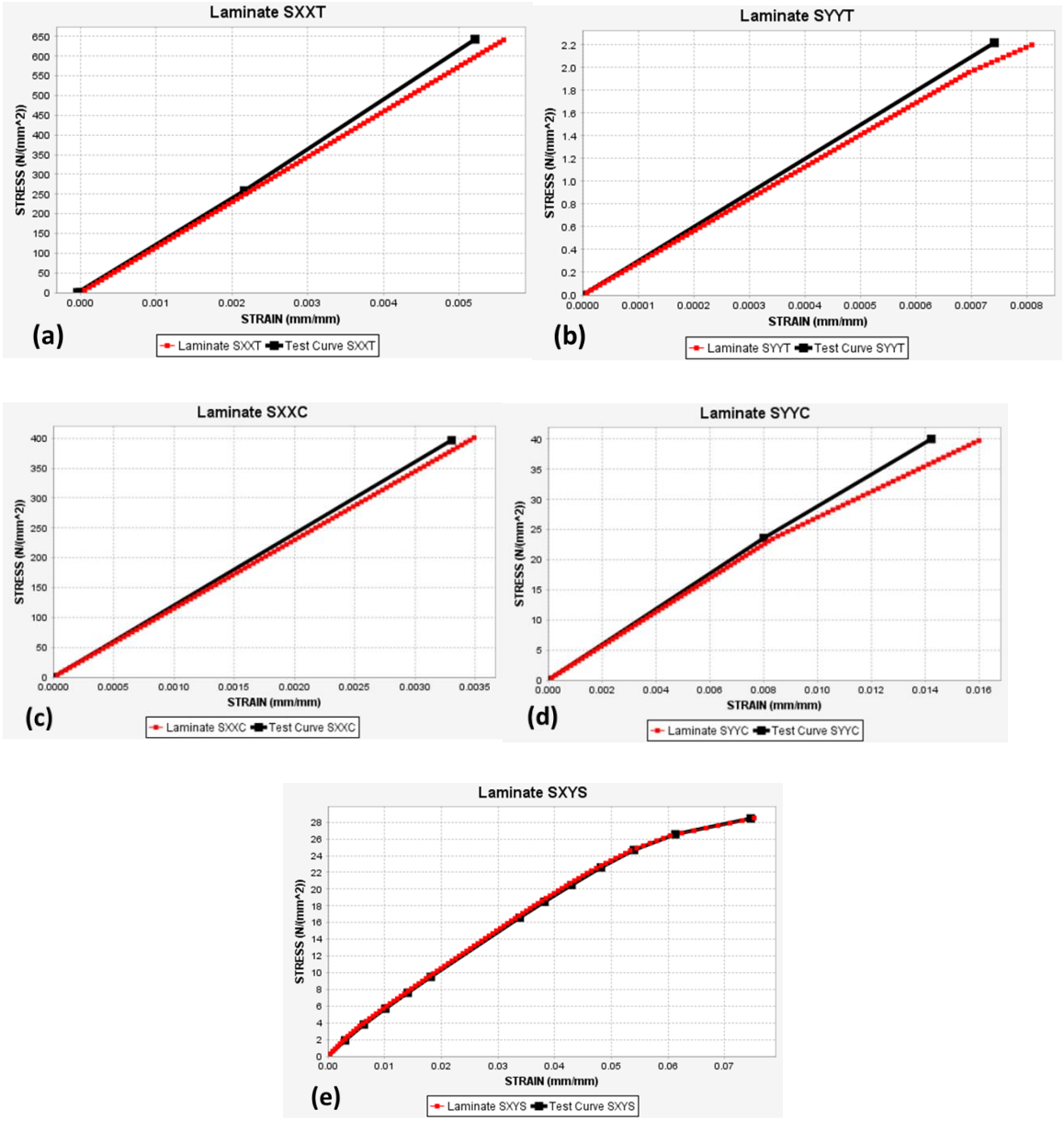

Figure 4.2: Reverse engineering of unsized TCF-PU composites produced through linear and non-linear failure mode (a) longitudinal tensile test (b) transverse tensile test (c) longitudinal compression (d) transverse compression (e) in-plane shear. The laminate analysis showed no difference between simulated (red color) and experimental (black color) failure mode

Table 4.4: Effective fiber and matrix properties obtained using Dehomogenization method at zero interface thickness using PFA equation presented in section 4.2.1

Fiber properties	Effective
E11 (GPa)	182.46
E22 (GPa)	18.51
G12 (GPa)	1.073
G23 (GPa)	7.061
NU12	0.194
NU23	0.31
S11T (MPa)	1011.72
S11C (MPa)	596.51

Matrix properties	Effective
E (GPa)	1.0719
NU	0.4250
ST (MPa)	18.0
SC (MPa)	63.6
SS (MPa)	56.04

4.3 RESULTS AND DISCUSSION

In the fiber-matrix interface study, using effective fiber-matrix properties (presented in Table 4.4), five factors at the interphase were adjusted to correlate the simulated results with experimental findings, which are as follows:1) shear strength between interface and matrix, 2) axial loading between interface and matrix, 3) interface thickness, 4) modulus effect between interface and matrix, 5) Poisson's ratio effect between interface and matrix. The stress-strain curve obtained from simulated results for epoxy-sized TCF (1% sizing concentration) and urethane-sized TCF (1.5% sizing concentration) is presented in Figure 4.3 and Figure 4.4.

The interphase properties obtained through a stress-strain curve are presented in Table 4.5 and Figure 4.5. The epoxy-sized TCF showed 72% increase in shear strength than unsized TCF. Whereas urethane-sized TCF showed a 19% decrease in shear strength than epoxy-sized TCF at the interphase, shearing is related to the matrix and independent of fiber properties. The results further showed that increasing interface thickness by 7% (from epoxy sized TCF to urethane sized TCF) enhances the tensile strength by 1.5% and modulus by 36% of TSU matrix bonded with the interface. Furthermore, to validate the interphase properties, the effective fiber and matrix properties are used to design a similar cross-ply laminate structure of TCF-TSU laminate, presented in chapter 3 (b). The comparative results are shown in Figure 4.6. The results showed less than 10% difference between experimental and simulated properties.

In an anisotropic laminate, the strength between matrix and interface illustrates that though there is poor interfacial strength at higher interface thickness; however, it does not compromise the tensile properties of TCF-TSU composites. The

interphase properties obtained through simulation depict the exact behavior of the interface at the cross-ply laminates. Hence, interface thickness is an important aspect that directly correlates with the strength of the composites. The results correlate with Yao et al. findings, where the author stated that increasing the sizing treatments enhances the interface thickness and improves the flexural strength of the composites [2].

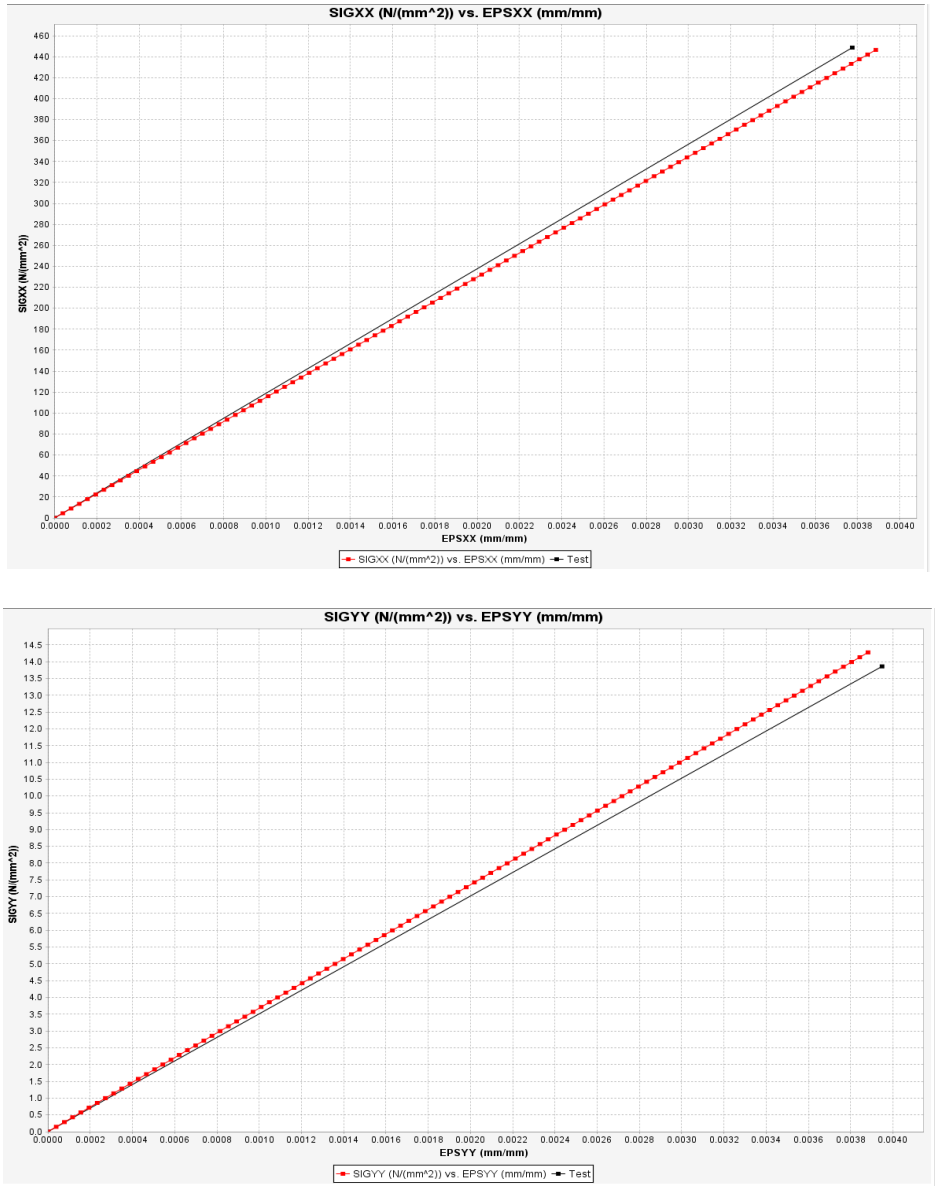

Figure 4.3: A correlation between the tensile strength of epoxy sized TCF-TSU composites in longitudinal (SIG XX) and transverse (SIG YY) direction: simulation (red color) vs. experimental (black color) results at 0.49 µm interface thickness

Figure 4.4: A correlation between the tensile strength of epoxy sized TCF-TSU composites in longitudinal (SIG XX) and transverse (SIG YY) direction: simulation (red color) vs. experimental (black color) results at 0.53 μm interface thickness

Table 4.5: Interphase properties of TCF-E and TCF-U composites obtained using Dehomogenization method

Interphase parameters	TCF-Un	TCF-E	TCF-U	Interphase properties of TCF-Un	Interphase properties of TCF-E	Interphase properties of TCF-U
Ratio of Interface shear strength to matrix shear strength	0.75	1.3	1.05	0.86 MPa	1.48 MPa	1.197 MPa
Ratio of Interface tensile strength to Matrix tensile strength	0.1	1.3	1.32	8.98 MPa	116.74 MPa	118.53 MPa
Ratio of Interface Thickness to fiber radius	0.01	0.14	0.15	0.07 μm	0.49 μm	0.525 μm
Ratio of Interface modulus to Matrix modulus	0.5	0.8	1.03	1.57 GPa	2.52 GPa	3.245 GPa

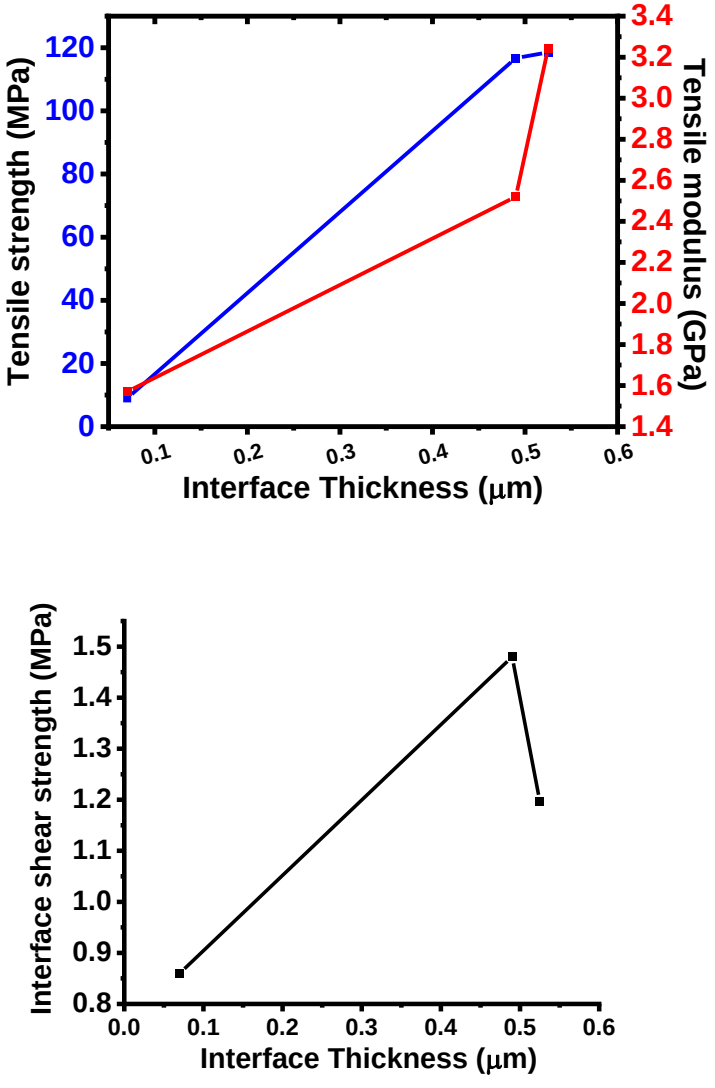

Figure 4.5: A representative plots of tensile strength and modulus and interfacial shear strength of TCF-TSU composites at various interface thickness with respect to matrix

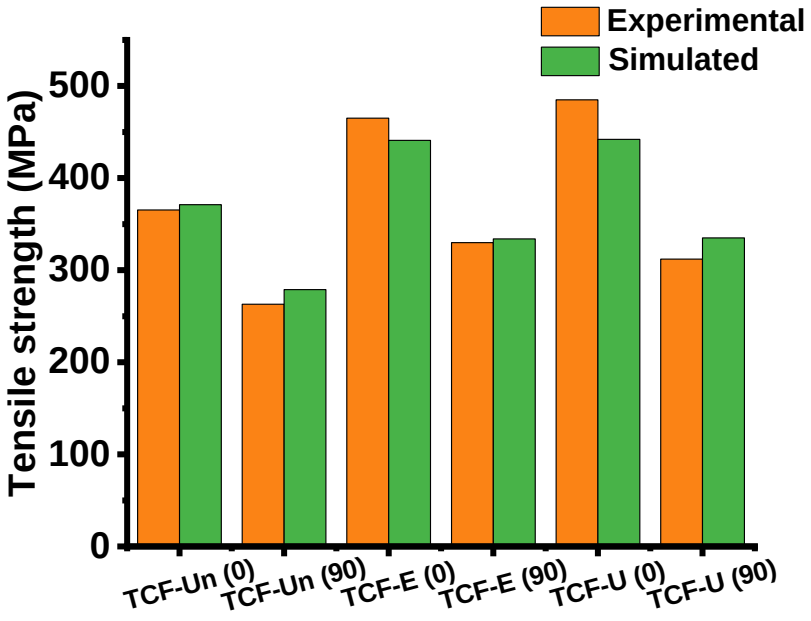

Figure 4.6: Tensile strength of unsized, epoxy and urethane sized TCF-TSU cross-ply composites experimental (orange color) and simulation (green color) result comparison using effective fiber- matrix properties

4.4 CONCLUSIONS

In the overall investigation, the essential factors affecting fiber, matrix, and interface of unsized, epoxy, and urethane-sized TCF-TSU were studied using surface, thermal and mechanical properties. In this study, the sizing thickness effect on the mechanical properties of TCF-TSU composites, was examined using the dehomogenized approach and reverse engineering mechanism. The key findings are as follows:

- The experimental tensile strength in the longitudinal direction of TCF-Un-TSU showed higher strength than TCF-E and TCF-U. The results confirm that the longitudinal properties are independent of the interface properties.
- The effective fiber matrix properties obtained through simulation showed that increasing interface thickness from 0.49 μm to 0.523 μm reduces the interfacial strength between interface and matrix; however, it increases the tensile strength and modulus.
- The simulation designed for cross-ply laminates layup of TCF-TSU for unsized, epoxy, and urethane sized (from Chapter 3: section b) showed less than 10% variation in the tensile properties than experimental results.

REFERENCES

[1] S. Sockalingam, M. Dey, J.W. Gillespie Jr, M. Keefe, Finite element analysis of the microdroplet test method using cohesive zone model of the fiber/matrix interface, Compos Part A Appl Sci Manuf. 56 (2014) 239–247.

[2] H. Yao, X. Sui, Z. Zhao, Z. Xu, L. Chen, H. Deng, Y. Liu, X. Qian, Optimization of interfacial microstructure and mechanical properties of carbon fiber/epoxy composites via carbon nanotube sizing, Appl Surf Sci. 347 (2015) 583–590.

[3] M. Braginsky, C.P. Przybyla, Simulation of crack propagation/deflection in ceramic matrix continuous fiber reinforced composites with weak interphase via the extended finite element method, Compos Struct. 136 (2016) 538–545.

[4] D.K. Singh, A. Vaidya, V. Thomas, M. Theodore, S. Kore, U. Vaidya, Finite Element Modeling of the Fiber-Matrix Interface in Polymer Composites, J Compos Sci. 4 (2020) 58.

[5] D. Esqué-de Los Ojos, R. Ghisleni, A. Battisti, G. Mohanty, J. Michler, J. Sort, A.J. Brunner, Understanding the mechanical behavior of fiber/matrix interfaces during push-in tests by means of finite element simulations and a cohesive zone model, Comput Mater Sci. 117 (2016) 330–337.

[6] S.-H. Lee, S. Wang, G.M. Pharr, H. Xu, Evaluation of interphase properties in a cellulose fiber-reinforced polypropylene composite by nanoindentation and finite element analysis, Compos Part A Appl Sci Manuf. 38 (2007) 1517–1524.

[7] L. Mishnaevsky Jr, Nanostructured interfaces for enhancing mechanical properties of composites: Computational micromechanical studies, Compos Part B Eng. 68 (2015) 75–84.

[8] B. Wang, G. Fang, S. Liu, J. Liang, Effect of heterogeneous interphase on the mechanical properties of unidirectional fiber composites studied by FFT-based method, Compos Struct. 220 (2019) 642–651.

[9] P. Pitchai, H. Berger, P.J. Guruprasad, Investigating the influence of interface in a three phase composite using variational asymptotic method based homogenization technique, Compos Struct. 233 (2020) 111562.

[10] X. Zhang, D.J. O'Brien, S. Ghosh, Parametrically homogenized continuum damage mechanics (PHCDM) models for composites from micromechanical analysis, Comput Methods Appl Mech Eng. 346 (2019) 456–485.

[11] P. Raghavan, S. Ghosh, A continuum damage mechanics model for unidirectional composites undergoing interfacial debonding, Mech Mater. 37 (2005) 955–979.

[12] Q. Sun, Z. Meng, G. Zhou, S.-P. Lin, H. Kang, S. Keten, H. Guo, X. Su, Multi-scale computational analysis of unidirectional carbon fiber reinforced polymer composites under various loading conditions, Compos Struct. 196 (2018) 30–43.

[13] P. Kim, H. Baid, A. Hassen, A. Kumar, J. Lindahl, D. Hoskins, C. Ajinjeru, C. Duty, P. Yeole, U. Vaidya, others, Analysis on part distortion and residual stress in big area additive manufacturing with carbon fiber-reinforced thermoplastic using dehomogenization technique, 2019.

[14] L. Minnetyan, X. Su, F. Abdi, Fiber--Matrix Interphase Effects on Damage Progression in Composite Structures, in: Charact Nanocomposites, Jenny Stanford Publishing, 2017: pp. 61–73.

[15] F. Abdi, C. Godines, S. DorMohammadi, L. Minnetyan, Fatigue Validation of Composite Open Hole Analysis Technique for Standard and Nonstandard

Laminate-Part 2, in: 57th AIAA/ASCE/AHS/ASC Struct Struct Dyn Mater Conf, 2016: p. 978.

[16] S. DorMohammdi, C. Godines, F. Abdi, D. Huang, M. Repupilli, L. Minnetyan, Damage-tolerant composite design principles for aircraft components under fatigue service loading using multi-scale progressive failure analysis, J Compos Mater. 51 (2017) 2181–2202.

[17] M.S. Madhukar, L.T. Drzal, Fiber-matrix adhesion and its effect on composite mechanical properties: II. Longitudinal (0) and transverse (90) tensile and flexure behavior of graphite/epoxy composites, J Compos Mater. 25 (1991) 958–991.

VITA

Surbhi Kore was born and raised in Thane, India. She completed her bachelor's degree in Polymer Engineering from the Institute of Chemical Technology (formerly known as UDCT). In 2017, she started the Ph.D. program in Mechanical, Aerospace, and Biomedical Engineering Department at the University of Tennessee, Knoxville, concentrating in polymer composites interfacial adhesion theory. Her research interest includes examining the structure-property relationships of polymer and its impact on the interfacial adhesion between polymer and carbon fibers. Surbhi's research was in collaboration with Institute for Advanced Composites Manufacturing Innovation (IACMI) – the Composites Institute, and Carbon Fiber Technology Facility (CFTF) at Oak Ridge National Laboratory (ORNL). Surbhi is graduating with a Doctor of Philosophy program in Mechanical Engineering in December 2021 and intends to continue her career in the polymer composites field.